UNIVERSIDAD AUTONOMA DE MADRID

New insights into anthracycline-induced cardiotoxicity

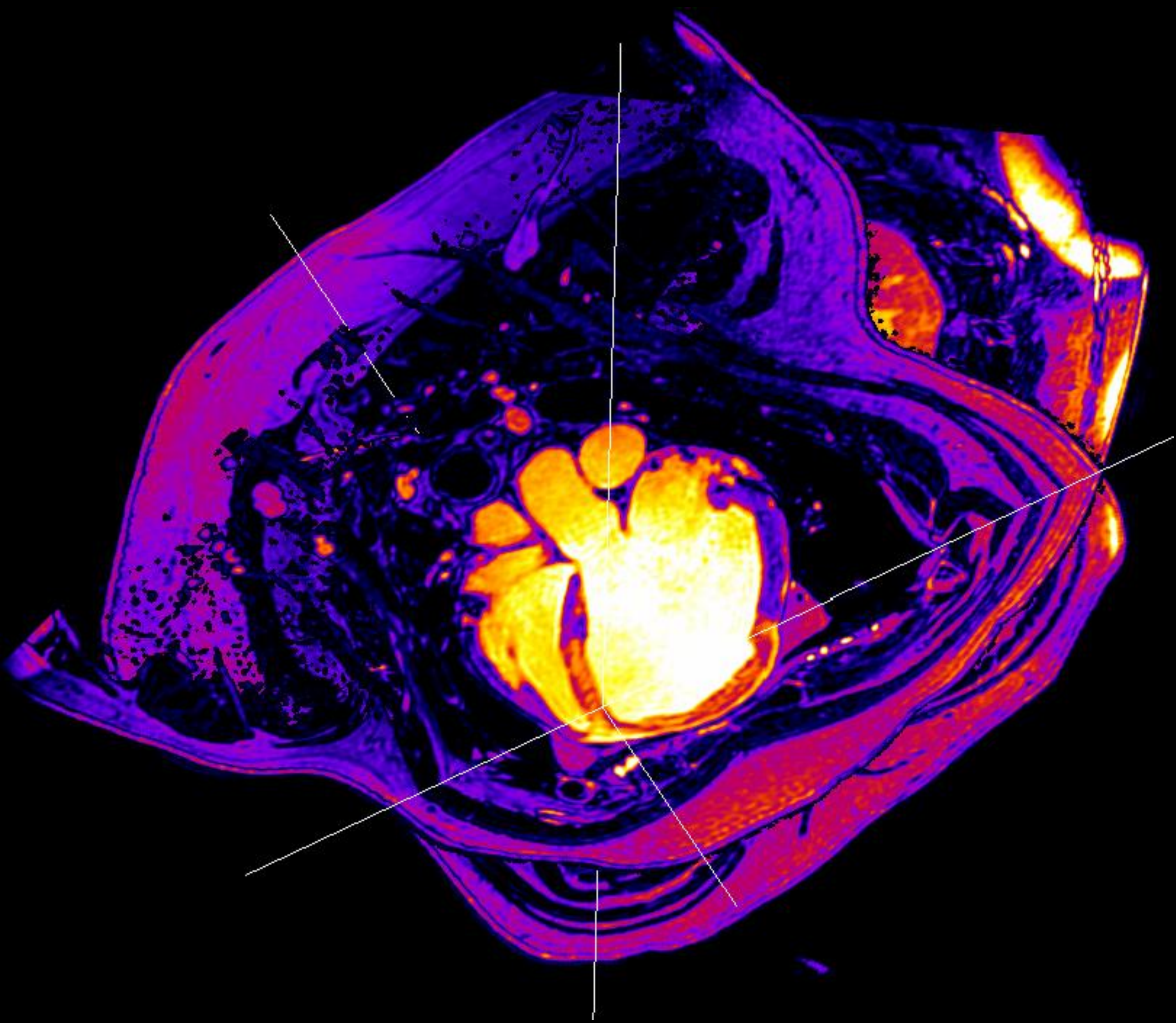

Carlos Galán Arriola

Supervisors: Dr. Borja Ibáñez and Dr. Javier Sánchez González

Doctoral Thesis Madrid, 2020

Universidad Autónoma de Madrid

Programa de Doctorado en Biociencias Moleculares

"New insights into anthracycline-induced cardiotoxicity"

Carlos Galán Arriola

Madrid, 2019

Universidad Autónoma de Madrid.

Facultad de Medicina.

Departamento de Bioquímica

Título de la Tesis: “New insights into anthracycline-induced cardiotoxicity”.

Doctorando: Carlos Galán Arriola, licenciado en Veterinaria por la Universidad de Madrid.

Director de Tesis: Borja Ibáñez Cabeza.

Codirector de Tesis: Javier Sánchez González.

Lugar de realización: Centro Nacional de Investigaciones Cardiovasculares Carlos III (CNIC), Madrid.

Borja Ibáñez Cabeza, doctor en Medicina y director del Departamento de Investigación Clínica del Centro Nacional de Investigaciones Cardiovasculares Carlos III (CNIC), Javier Sánchez González, doctor en Física,

Informan: Que D. Carlos Galán Arriola ha realizado durante los últimos cinco años bajo nuestra dirección la Tesis Doctoral “New insights into antrhacycline-induced cardiotoxicity”. De este modo valorados que dicha tesis contribuye de forma original al campo de la investigación cardiovascular traslacional.

BORJA IBAÑEZ y JAVIER SÁNCHEZ GONZÁLEZ

"Ideas are like fish. If you want to catch little fish, you can stay in the shallow water. But if you want to catch the big fish, you've got to go deeper. Down deep, the fish are more powerful and more pure. They're huge and abstract. And they're very beautiful."

David Lynch

Acknowledgements

Sin duda esta tesis es la culminación de un largo camino del que mucha gente ha tomado parte a lo largo de los años; y sin la cual no habría y tenido lugar. Agradecer tanto al Dr. Borja Ibáñez como al Dr. Javier Sánchez haber depositado no sólo la confianza en mí, sino haber puesto ante mí todas las herramientas disponibles para poder desarrollarme como investigador y poner a prueba mis capacidades a unos límites a los que era incapaz de imaginar que pudiera llegar cuando empecé a recorrer este camino. Por su mentoring y a la vez la libertad de dejarme crecer libre y darme cuenta de mis errores. Gracias por darme los años más estimulantes y a la vez los más duros; he aprendido como nunca.

A Rodri y a Jaume, por tutelarme en mis primeros pasos y ser partícipes de toda esta evolución. Espero haberme convertido en alguien de quién sentiros orgullosos. Gran parte de lo que soy os lo debo a vosotros. Rodri, gracias por enseñarme a ser metódico, ordenado y dudar de todo. Jaume gracias por enseñarme lo multidisciplinar que tiene que ser un científico y por abrirme al mundo de R y ggplot2; desde luego esta tesis no sería lo mismo sin estas dos cosas.

A Gonzalo, porque el casi infinito número de estudios de imagen que lleva esta tesis no ha salido de la nada. Gracias por tu capacidad de trabajo y por poner cabeza y buen juicio donde a veces sólo reina el sinsentido. Eres más del 50% de esta tesis. Gracias también al resto de técnicos: Marta, Ángel y Brai.

Al personal de animalario – gran parte del otro 50% os pertenece a vosotras -, gracias por preparar, cuidar, alimentar, tratar y curar a todos los cerdos que forman (y los que no forman) parte de estos estudios. Gracias Tamara por coordinar toda esta vorágine de experimentos; Inés por intentar poner coto a nuestra locura colectiva y por preocuparte de nuestro estado de salud mental en las horas más bajas; Nuria por estar siempre ahí y por ayudarnos y por el esfuerzo a pesar de que la experimentación con animales no es nada agradable; Óscar por su sentido del humor; Lorena, por dar un toque diferente a la zona y ser confidente de todo lo que acontece; Antonio, porque pese a ser el último en llegar, has arrimado el hombro desde el primer día. Gracias también a todos los cuidadores de la zona, a Revillo, Cristian, Attila, Javi y Gustavo.

A Josema, porque tu sentido del humor me ha salvado más de una vez de una muerte segura en la -3. Por ser una persona infatigable y un amigo con el que no contaba que a estas alturas pudiera encontrar en un sitio como este. Gracias por ser el compañero de celda perfecto.

A Manu, por todo su apoyo durante estos años y por ser un compañero de viaje infatigable. A Jean Paul, por su ayuda y paciencia en el escabroso terreno de la hiperemia miocárdica. A Jorge, por enseñarme a no perder nunca la perspectiva clínica de lo que hago y por ser un ejemplo de esfuerzo y actitud ante las dificultades. A Austin, por enseñarme a ser inconformista y a pensar fuera de toda caja posible, gracias por mostrarme que hay muchos más caminos de los que imaginamos para dar solución a un problema. A Xavi, por aportar orden y cabeza y poner contrapeso a la deriva hacia el caos en el que a veces se convierte este trabajo.

Especial mención a Antonio y Claudia, sin vuestro ojo experto y el enorme esfuerzo que le habéis echado no habríamos podido elucidar todo lo que vemos en la reso. Muchas gracias también a Marisa, Iván y Rodrigo por este último empujón y, por lo que espero, sean muchos más años de proyectos juntos.

A los chicos de “bench”, por enseñarme que hay vida más allá de los cerdos y por desaturarme de tanto cardiólogo. A Edu, por la pasión y el cuidado que le pones a todo lo que haces, eres el ejemplo de científico al que me gustaría parecerme algún día. Rocío, porque no sé cómo puedes ponerle tanta motivación a todo sin perder nunca el fuelle, gracias por tener paciencia con un naive de lo biomolecular como yo. Y a Agus, porque eres un auténtico crack y ya me hubiese gustado parecerme a ti la mitad de la mitad cuando empecé.

Gracias y mención especial a todo el personal administrativo y managers. Gracias Anabel, por ser la primera cara con la que me crucé por aquí cuando aún no sabía lo que se venía encima; gracias por quedarte hasta casi medianoche rellenando la PFIS, sin ti hoy no habría podido hacer la tesis. Gracias a Eeva por estar siempre ahí y lanzar una sonrisa a tiempo (que sirve más de lo que crees), gracias a Edu (Bieger) y a Sonia por su apoyo logístico y no tan logístico. Gracias a Víctor Bautista y a Ali Ayaon, por su apoyo al realizar los modelos quirúrgicos de esta tesis, sin los cuales se habría quedado a medio gas.

Gracias al Dr. James McCully y a todos mis compañeros del laboratorio del Boston Children’s Hospital: Arzoo, Alvise, Giovanna, Kamila, Caytlin, David y Dimitri. Gracias por enseñarme sobre el trasplante mitocondrial, así como formas diferentes de trabajar y por acompañarme durante mi estancia en una de las mejores experiencias de mi vida. Gracias a todos los que habéis pasado por aquí que, aunque lo creáis o no, habéis hecho mella y me habéis aportado algún granito de arena que otro: David, Juan, Dani, Chusa, Ramón y el inestimable número de cardiólogos del programa Res@CNIC, alumnos de prácticas, etc.

Gracias a Manu y a José, por ayudar a abstraerme del estrés que supone una empresa de este calibre. Gracias por vuestra amistad. Si no he muerto en el intento es gracias a vosotros.

Gracias a mi familia, a vosotros os dedico en especial esta tesis porque sois de los que más habéis sufrido sus consecuencias. A mis padres Estela y José Carlos y a mis hermanas Rebeca y Paloma: gracias por apoyarme en todas mis decisiones y por vuestro apoyo y amor incondicionales.

Contents

List of Figures

List of Tables

1 Summary / Resumen

El incremento de la esperanza de vida en la población así como el desarrollo de nuevas terapias efectivas contra el cáncer han dado lugar a un aumento en la población de supervivientes de cáncer en edad avanzada; los cuales, frecuentemente presentan comorbilidades que predisponen al desarrolo de insuficiencia cardiaca. Las antraciclinas son una primera opción para numerosos tipos de cánceres, pero cerca del 10 % de los pacientes que las reciben desarrollan alguna forma de cardiotoxicidad y posterior desarrollo de insuficiencia cardíaca. El "intercambio" del cáncer a la insuficiencia cardíaca supone una pesada carga psicológica para los pacientes y tiene consecuencias económicas devastadoras para los sistemas de salud. A pesar de que las antraciclinas se han utilizado desde la década de 1960, y sus efectos cardiotóxicos se conocieron poco después de convertirse en el estándar de muchos protocolos de quimioterapia, todavía hay varias lagunas y preguntas abiertas con respecto a este efecto secundario tan frecuente.

En particular, es necesario obtener conocimiento científico sobre la detección temprana de la cardiotoxicidad inducida por antraciclinas, para comprender mejor los mecanismos que conducen a este daño así como las señales sobre la vulnerabilidad inter-individual y la identificación de terapias que puedan prevenir o tratar esta forma de daño miocárdico. La presente tesis se enfoca en estos 4 aspectos críticos no resueltos, abordando para ello los siguientes objetivos:

1) Indentificar el marcador más temprano de cardiotoxicidad mediante técnicas de imagen no invasivas; 2) estudiar el papel del daño en la microcirculación como parte de esta cardiotoxicidad; 3) estudiar la interacción entre la hipertrofia cardiaca y la exposición a antraciclinas; y 4) evaluar el efecto del precondicionamiento remoto isquémico como terapia para prevenir la cardiotoxicidad inducida por antraciclinas. Para lograr estos objetivos, desarrollamos diferentes modelos porcinos de cardiotoxicidad y utilizamos la tecnología de la resonancia magnética cardiaca.

———-

The increasing life expectancy of the population and the development of effective anticancer therapies result in a growing population of aged cancer survivors, which frequently have comorbidities for developing heart failure (HF). Anthracyclines are still first line treatment for many cancer types, but up to 10% of patients who received them develop some form of cardiotoxicity and subsequent HF. The trade-off between cancer and chronic HF is of massive psychological burden for patients, and of devastating economic consequences for healthcare systems.. Despite anthracyclines have been used since the 1960s, and their cardiotoxic effects known very early since they became standard of care, there are still several gaps and open questions regarding this frequent side effect.

In particular, there is a need to gain scientific knowledge about early detection of anthracycline-induced cardiotoxicity, to better understand mechanisms leading to toxicity and cues about inter-individual vulnerability, and the identification of therapies that can prevent or treat this form of myocardial damage. The present thesis focuses on these 4 critical unresolved aspects by addressing the following objectives:

1) To identify the earliest non-invasive marker of anthracycline-induced cardiotoxicity; 2) to study the role of microcirculation damage as part of the cardiotoxicity effect of anthracyclines; 3) to study the interplay between cardiac hypertrophy and exposure to anthracyclines to induce cardiotoxicity; and 4) to test the effect of remote ischemic conditioning as a therapy to prevent anthracycline-induced cardiotoxicity. To reach these aims, we developed different swine models of anthracycline-induced cardiotoxicity and hypertrophy, and we used state of the art cardiac magnetic resonance imaging.

2 Abreviations

ACT – Anthracycline-induced Cardiotoxicity

BCA – Bicinchoninic Acid kit for protein determination

CAD – Coronary Artery Disease

CFR – Coronary Flow Reserve

CMR – Cardiac Magnetic Resonance

CT – Cardiotoxicity

CVD – Cardiovascular Disease

ECG – Electrocardiogram

ECV – Extracellular Volume

EDTA - Ethylenediaminetetraacetic acid

FDA – Food and Drug Administration

FOV – Field of View

GraSE - Gradient-Spin-Echo

HE – Hematoxylin and eosin

HF – Heart Failure

IC – Ischemic Conditioning

i.c – Intracoronary

i.v - Intravenously

IPC – Ischemic Preconditioning

LAD – Left Anterior Descending coronary artery

LGE – Late Gadolinium Enhancement

LIPC – Local Ischemic Preconditioning

LV – Left Ventricle/Ventricular

LVEF – Left ventricular Ejection Fraction

M – Masson’s Trichrome

MOLLI - Modified Look-Locker Inversion recovery

PET – Positron Emission Tomography

PFA - Paraformaldehyde

SSFP – segmented cine Steady-State Free-Precession

SR – Sirius Red

RIPC – Remote Ischemic Preconditioning

ROI – Region of Interest

ROS – Reactive Oxygen Species

TBST – Tris-buffered saline + polysorbate 20

TEM – Transmission Electron Microscopy

Top2 – Topoisomerase 2

3 Introduction

3.1 Chemotherapy-induced cardiotoxicity

Advances in new anticancer drugs have improved survival rates in cancer patients. Among their side effects, cardiovascular diseases (CVDs) are one of the more common undesirable consequences of chemotherapy, being the main cause of non-related neoplasm death in cancer patient survivors [1, 2]. The risk of cardiovascular events in a long-term perspective in these patients can triplicate the risk in the rest of the population [3–5]. These CVD can be explained as the result of cardiotoxicity, which is the harmful effect that some of these chemotherapy drugs exert on cardiovascular system, resulting in direct or accelerated development of CVDs, especially in the presence of different risk factors [6]. The complexity of cardiovascular complications derived from anticancer drug use includes a wide range of diseases such as myocardial dysfunction, heart failure (HF), coronary artery disease (CAD), valvular disease, arrhythmias, arterial hypertension, thromboembolic disease, peripheral vascular disease, stroke, pulmonary hypertension and pericarditis [7]. Given the clinical importance of LV dysfunction and HF, we focus on the chemotherapy affecting cardiovascular system in that way; being the most concerning complication in cardiotoxicity, (**Table 1** represents a summary list of these agents). HF secondary to cancer treatment drugs has been deeply described as a severe side effect of anthracyclines – the major cause of chemotherapy-induced cardiotoxicity [8] –. HF development have been recorded in 1-5% of patient cancer survivors [9, 10].

Chemotherapy-cardiotoxicity definition is not exempt from controversy, in most of the cases its explanation is diffuse and only include “LV dysfunction” or “HF development” as concept terms. Modern guideline definitions included more specific explanations [11, 12], being the most common used the loss of 10% points in LVEF or values under 53% measured by echocardiography [12]. The problem with all these definition is that they do not include any subclinical damage, which can take place at early stages of cardiotoxicity, having become one of the cornerstones in cardiotoxicity conceptualization [7].

3.2 Anthracyclines

Anthracyclines are highly effective and frequently used chemotherapy drugs, with the most commonly familiy member used being doxorubicin, alone or in combination with other anti-cancer agents [13]. Their main side effects include undesirable reactions such as hair loss, erosions, gastrointestinal complications or immunosuppression, - and as previously commented -; prominent undesired effect of anthracycline therapy is CT (ACT) and subsequent HF **(Figure 1, A)**.

Chemotherapy agent	Frequency of use	Incidence (%)
Anthracyclines (dose dependent)		
Doxorubicin	++++	3-25
Epirubicin	+	0.9-11.4
Idarubicin	++	5-18
Mitoxanthone		2.6
Liposomal anthracyclines		2
Alkylating agents		
Cyclophosphamide	++++	7-28
Ifosfamide	+++	0.5-17
Antimebatolites		
Decitabine	++	5
Clofarabine	+	27
Antimicrotubule agents		
Docetaxel	++	2.3-13
Paclitaxel		<1
Monoclonal antibodies		
Trastuzumab	+++	2-28
Bevacizumab	++	1-10.9
Adotrastuzumab emtansine	+	1.8
Pertuzumab	+	0.9-16

Chemotherapy agent	Frequency of use	Incidence (%)
Small molecule tyrosine kinase inhibitors		
Pazopanib	++++	0.6-11
Ponatinib	+	3-15
Sorafenib	++++	1.9-11
Dabrafenib	++++	8-9
Sunitinib	++++	1-27
Dasatinib	++++	8-9
Lapatinib	++++	0.9-4.9
Trametanib	++++	7-11
Proteasome inhibitors		
Carfilzomib	++	7
Bortezomib	++	1-5
Miscellaneous		
Tretinoin	++++	6
Everolimus		<1
Temsironimus		<1

Table 1: List of chemotherapy agents that cause LV dysfunction and HF.

Their frequency use and their incidence values (adapted from Zamorano, Lancellotti et al [7] and Chang et al [14].

Among them, doxorubicin is the most common member of the group. It was discovered as a metabolite deriving from some strains of *Streptomyces peucetius*, discovered in Italy during the 60's. Its chemical structure consisted in a tetracyclic ring with adjacent quinone-hydroquinone groups, being the side chain ending with a primary alcohol **(Figure 1, B)**. This structural difference has critical consequences on the spectrum of the doxorubicin activity, compared with the other members of the group (daunorubicin, epirubicin or idarubicin); making it the most powerful for the treatment of several malignancies such as breast cancer, childhood solid tumors, lymphomas and aggressive carcinomas. Depending on the accumulated dose, the incidence of severe ACT resulting in overt systolic heart failure can be as high as 25% [14]. The trade-off between cancer and chronic heart failure places an immense personal burden on patients, with physical and psychological consequences.

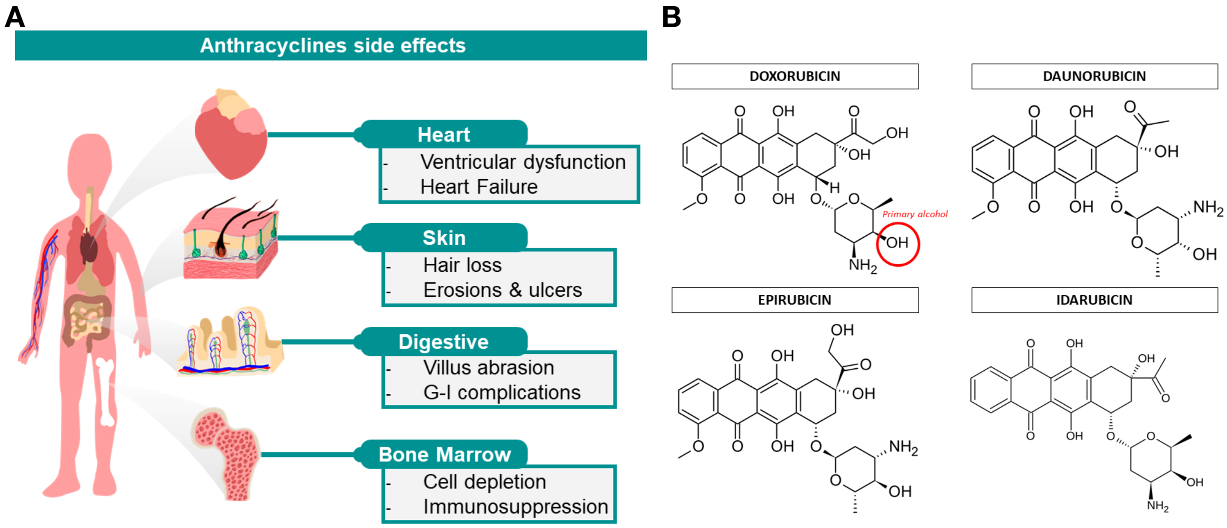

Figure 1: General properties of anthracyclines

(A) List of different side effect of anthracycline usage.

(B) Structures of doxorubicin, daunorubicin, epirubicin and idarubicin. Primary alcohol from the side chain termination in doxorubicin determinates its efficacy for a wide range of neoplasia (Images merged from their Wikipedia articles in www.wikipedia.org).

Given the high cardiotoxicity reported for all anthracycline family members, in recent times several efforts have been performed to identify new derived compounds (up to 2000 analogs) with the same or superior effectiveness and less myocardial toxicity with weak success. Only liposomal doxorubicin have been proved to have less ACT incidence in animal models and human clinical trials [13]. Both, systemic and cardiovascular complications, make these patients very special to clinically handle; for what cardio-oncology-hematology have been raised as an emerging specialty aimed at minimizing CVD in cancer patients [15].

3.3 Molecular mechanisms of anthracycline-induced cardiotoxicity

Doxorubicin effect based on the direct targeting of topoisomerase 2 (Top2) to cause DNA double-strand break and demise of the highly proliferative cancer cells. In mammalian cells, there are two different Top2 isozymes: Top2a and Top2B. Top2a is only expressed in proliferating and tumor cells and plays important roles in cell cycle events, such as DNA replication [16]. The high efficacy of doxorubicin chemotherapy is due to the highly elevated expression of Top2a in cancer cells. The heart is a post-mitotic organ, and proliferation of adult cardiomyocytes is a very rare phenomenon. Adult cardiomyocytes do not express Top2a but only Top2B [17].

The main mechanism of ACT is mediated through Top2B, leading to a mitochondrial-damaging effect. Anthracyclines bind to Top2B creating double-strand DNA breaks and dysregulating gene transcription, resulting in increased reactive oxygen species (ROS) generation, iron deposition, and defective mitochondrial biogenesis [18, 19]. In fact, genetically deleting topoisomerase 2b would prevent doxorubicin cardiotoxicity in mice and FDA approved drugs as dexrazoxane can degrade Top2B in the heart mitigating cardiotoxicity [20]. Doxorubicin-Top2B complexes bind promoters of antioxidative and electron-transport genes to reduce their transcripts and protein expression [18, 21].

Doxorubicin being a cationic compound readily enters mitochondria binds to cardiolipin, in the inner mitochondrial membrane, and inhibits the respiratory chain. Indeed, the electron–transport chain proteins require cardiolipin to function properly, and it has been proposed that because doxorubicin disrupts the cardiolipin–respiratory chain protein interface, more superoxide (O2-) formation occurs [22]. Finally, mitochondrial DNA could be a direct target of doxorubicin [23], as mtDNA lesions and free radical-associated mitochondrial dysfunction have been found in the hearts of patients treated with doxorubicin [22]. To date, three topoisomerases have been identified in vertebrate mitochondria: Top1mt [24] Top2B [25] and Top3a [26]. Top3a and Top2B both function in mitochondria and the nucleus, and the only specific mitochondrial topoisomerase in vertebrates is Top1mt [24]. Mitochondrial topoisomerase 1 (Top1mt) specifically controls mtDNA homeostasis, and it has been shown that Top1mt, which is conserved across vertebrates, is critical for cardiac tolerance to doxorubicin and adaptive response to doxorubicin cardiotoxicity [27].

Apart of their effect on Top2B, other mechanisms contributing ACT development are ROS production by several pathways like directly interfering electron transport chain, intercalating DNA or intracellular and mitochondrial iron overload [13]. Have been also describe in the last years, the direct effect of ACT in the endothelial cells, arterial smooth muscle cells and microcirculation(28), contributing to the multifactorial final damage of doxorubicin to myocardial tissue. These phenomena lead to mitochondrial swelling, intra-cardiomyocyte vacuolization, and ultimately cell death and replacement of cardiomyocytes by fibrotic tissue [28–30]. **(Figure 2)**.

The microvasculature compartment in ACT: Damage to the microcirculation is a well-known cardiotoxic side effect of radiotherapy [14]; however, the effect of other anti-cancer agents on the microvasculature is less well described. In the case of anthracyclines -one of the most widely prescribed chemotherapy agents- there is scarce evidence showing a damage to the microcirculation as part of its cardiotoxic effect. In vitro, doxorubicin has demonstrated to induce injury to endothelial cells, which seems to be mediated by ROS production [31–33]. Doxorubicin has been shown to induce apoptosis [34] and a premature senescent phenotype [35] in smooth muscle cells in vitro. The effect of doxorubicin on the cardiac vascular compartment has only been experimentally studied in small animals (mainly mice and rats) [36, 37], but only by evaluation at the time of sacrifice (once functional ACT is already present). Observational studies in patients undergoing chemotherapy regime including anthracyclines have suggested that myocardial perfusion in these might be reduced even in the absence of LV systolic dysfunction [38, 39]. Overall, despite there is indirect evidence suggesting that anthracyclines might exert a cardiotoxic effect in the myocardial vasculature, there is a lack of a comprehensive prospective study evaluating microcirculation from the anatomical and functional perspectives across all stages of cardiotoxicity (ranging from pre-exposure to subclinical to overt cardiac dysfunction).

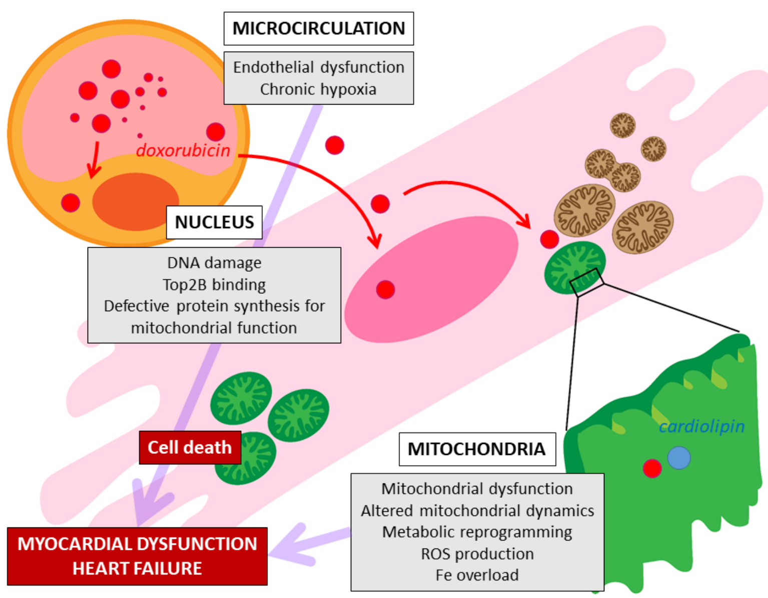

Figure 2: Multifactorial mechanisms leading to ACT

Microcirculation, mitochondria and nucleus are three role-players in the development of ACT.

3.4 Risk factors for anthracycline-induced cardiotoxicity

Patients receiving potential cardiotoxic chemotherapy should undergo deeply clinical and CV risk assessment before the treatment. Since the discovery of ACT, the pursuit of relevant risk factors have been a priority in cardio-oncology. In the literature, there are several prospective and retrospective reports describing potential candidate risk factors to be considered:

1 – *Cumulative dose*: cumulative dosage of anthracyclines have been very well described as the main risk factor for ACT development in several studies [7, 14, 15]. It is considered that cumulative doses of doxorubicin up to 400 mg/m2 has an ACT incidence of 3-5%; the increment is exponential for 550 mg/m2 (7-26%) and 700 mg/m2 (up to 48%), **(Figure 3)**. Fortunately, current chemotherapeutic regimes including anthracyclines have been adjusted their cumulative dose using the minimum for being therapeutic and effective against the tumor .

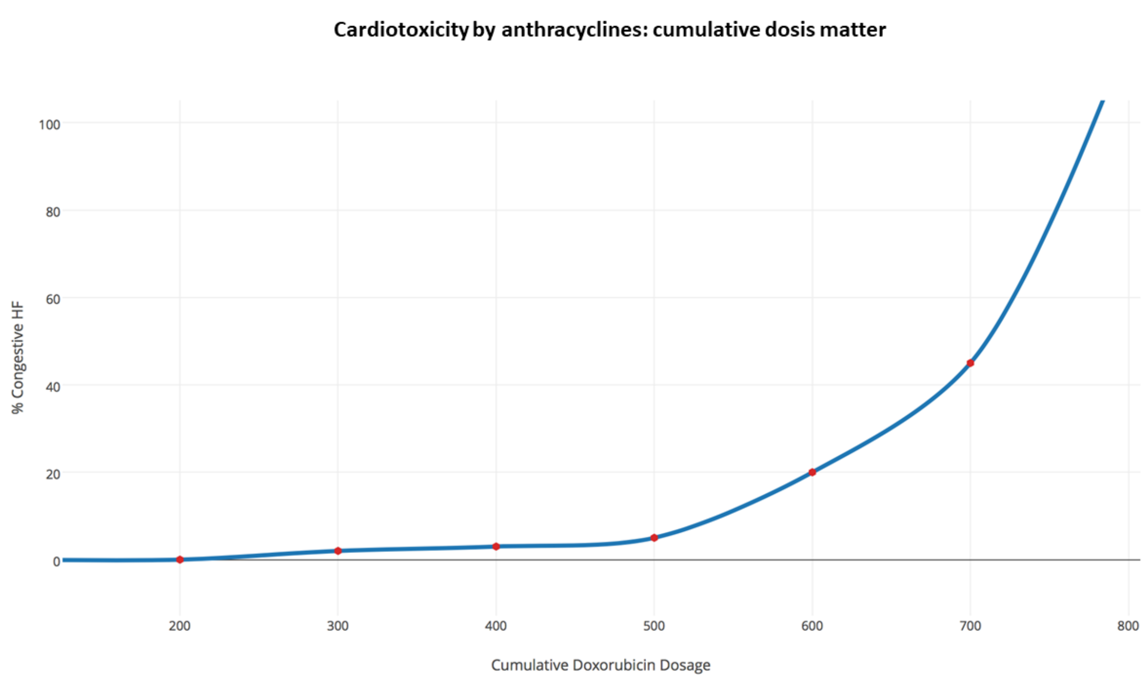

Figure 3: Correlation between anthracycline cummulative doses and HF incidence

2 – *CV comorbidities*: seems logic that previously affected myocardium is more sensitive to ACT than a healthy one. However, as we discuss later, there is a lack of clinical and mechanistic evidence of casualty between the

presence of CV comorbidities and ACT predisposition. However, a huge number of retrospective and prospective observational studies have been performed in order to identify this relationship. As a result, systemic arterial hypertension have been identify as one of the CV subjacent conditions with more correlation evidence with risk of ACT development in patients receiving anthracycline regimes. It is described that patients with hypertension have more possibilities to develop ACT than patients without this condition. Cardiac diseases concurring with high ventricular wall stress or genetic-base diseases have been also point as risk factors for ACT [7]. Most of the experimental animal studies have been performed in spontaneous hypertensive rats [40–44]; mainly describing an exacerbated acute and chronic cardiotoxic phenotype compared with wild type animals. However, in all the cases both anthracycline regimes (for hypertensive and normal rats) were indeed cardiotoxic and these studies did not explored the effect of subtle doses of doxorubicin in the hypertensive heart compared with healthy ones.

3 – *Co-administration of other cardiotoxic drugs*: the presence in the chemotherapeutic protocol of other cardiotoxic drugs also increments the impact of ACT due to the synergetic effect of both treatments. Thus, the combination of doxorubicin with radiotherapy - one of the most comment concomitant therapies with anthracyclines – and other drugs such as Trastuzumab (mainly in breast cancer patients) or alkylating agents, augment the incidence of ACT developing [15].

4 – *Others*: patients aged over 65 years old increase their risk factor for ACT development, but also very young people (less than 18 years old) are in risk by its age for ACT due to its developing heart is more vulnerable to the damage. Female sex, alcohol consumption and diabetes have been also pointed out as potential risk factors [7, 15].

3.5 Diagnosis of anthracycline-induced cardiotoxicity

When a patient is enrolled to receive anthracycline-based chemotherapy, basal cardiac function is evaluated in order to discard myocardial dysfunction prior to the treatment. If there is a decline in cardiac function, the case should be discussed with the onco-hematology team in other to consider other therapeutic options non-based in anthracycline administration. For this purpose, echocardiography is the major option due to its wide availability, cost-effectiveness and its facility. However, its evaluation is just functional, which does not allow identifying subclinical phases of the disease [45].

Current algorithms to identify early stages of anthracycline-induced cardiotoxicity are far from optimal. Diagnosis generally occurs once left ventricular (LV) functional deterioration becomes manifest, either as a decline in LV ejection fraction (LVEF) or longitudinal LV strain abnormalities [7, 15]. By this stage, the damage to the myocardium is often irreversible. The lack of a validated early damage marker limits the development of preventive strategies. Cardiac magnetic resonance (CMR) is the gold standard technique for anatomical and functional evaluation of the heart, and the advent of multiparametric algorithms allows accurate characterization of myocardial tissue **(Figure 4)**. CMR is thus suitable for the detection of myocardial edema [46–50] and diffuse myocardial fibrosis [51–53] , which are present at different stages of anthracycline-induced cardiotoxicity [54–58]. To date, there has been a lack of comprehensive serial multiparametric CMR tissue studies characterizing the full anthracycline treatment cycle from pre-treatment through treatment to overt LV systolic dysfunction and heart failure.

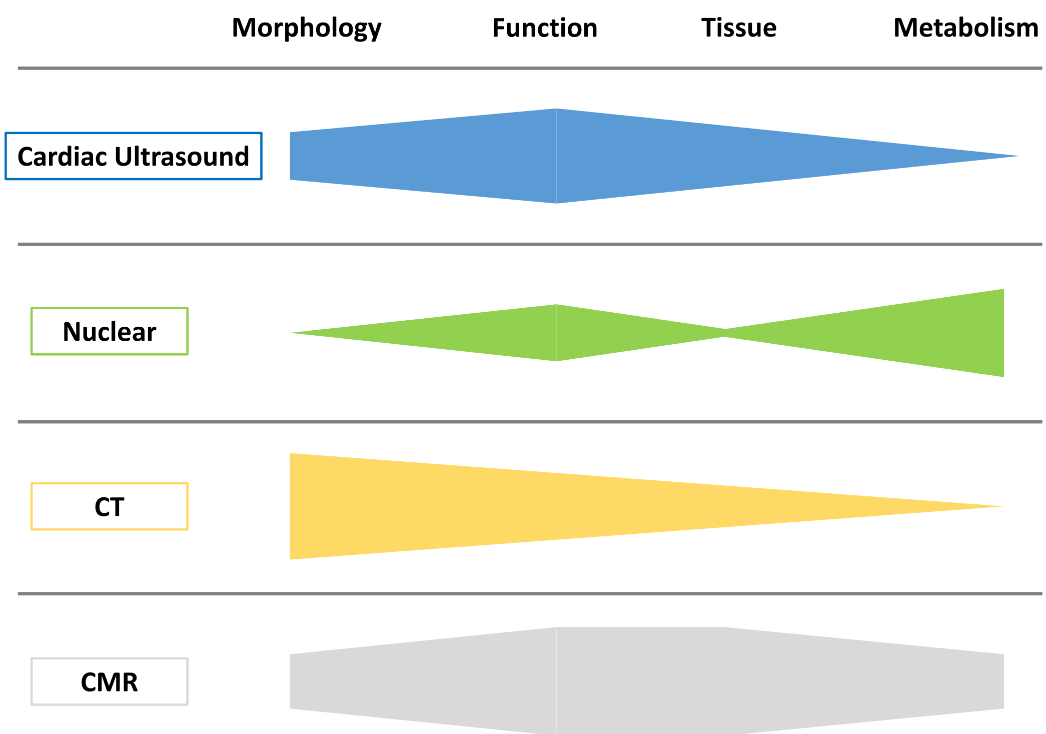

Figure 4: Strengths and weaknesses of different multimodality in-vivo imaging techniques in cardiology.

New imaging modalities that could unmask subclinical cardiotoxicity include PET/CT scan. It has been recently reported an increase in 18-fluorodeoxyglucose (FDG) uptake in Hodgkin lymphoma patients developing ACT and in wild type mice receiving increasing cumulative doses of doxorubicin. Other modalities such as SPETC have been used in some patient records in order to test if breast cancer woman present subclinical defects in myocardial quantitative perfusion [59].

3.6 Clinical management of anthracycline-induced cardiotoxicity

Therapeutic approach for ATC includes the use of standard Heart Failure therapy (Beta-blockers and ACEs inhibitors among others); and have been demonstrated clinical benefit in early-detected patients. However, specific-targeted ATC therapies are limited and only dexrazoxane – a FDA approved drug – have been demonstrated efficacy in animal models and human clinical trials [20,60]. But nevertheless, last evidence pointed that its usefulness is limited to certain kind of patients and its effect is indeed so mild, whence more clinical data is needed. Other drugs such as antioxidants, iron chelators and cell therapy have not search translational effectiveness despite their promising preclinical results. In the last years, PRADA trial [61] - a factorial, randomized, placebo-controlled and double blind study in cancer patients - tested the efficacy of metoprolol and candesartan or combination of both in women with breast cancer, demonstrating that co-treatment with candesartan improves the decline in LV function.

However, there is a lack of evidence testing specific targeted therapies for ACT in both, translational preclinical and clinical studies.

3.7 Animal models of anthracycline-induced cardiotoxicity

Since the finding of anthracyclines cardiotoxic properties, animal models in which evaluate and elucidate the mechanism underlying this have been hardly pursued. Most of the research in ACT have been carried out in small animal models, including mice and rats [22, 36, 41, 62–64]. In these individuals, anthracyclines are usually administrated intraperitoneal or intravenously (i.v) through the tail vein. Despite of its popularity, a vast quantity of the studies cannot show a clear manifestation of functional ACT. Thus, they revolve around molecular and structural changes in myocardium (such as oxidative stress, apoptosis or fibrosis) with rarely cardiac functional correlation.

Rabbits are also used for ACT preclinical research [34, 65, 66]. In this case, many groups take advantage of the animal size in order to conduct advance-imaging evaluation (primarily echocardiography, CT scans or CMR). Rabbits start to present more dramatic myelosuppresion as side effect secondary to anthracyclines treatment, increasing their morbidity and mortality. Even so, their usage in ACT is increasing nowadays.

Regarding pig models, during the 70's, Van Vleet et al [67] tested different dose regimes of doxorubicin in pigs in order to characterized the pathological features of its systemic administration. Unfortunately, they could not search enough cardiotoxic cumulative doses and all the piglets died before ACT development. Thus, in large animals, only i.c models (both, in pigs and dogs) have been able to show overt ACT but they did not characterized in deep using non-invasive multimodality imaging. Researchers also have used other species like calves and sheep (both, i.v and i.c approaches), but its deployment is straight uncommon.

3.8 Cardio-oncology gap challenges

In view of the foregoing, there are several clinical and preclinical loopholes regarding ACT. These gaps can be summarized with the following **(Figure 5)**.:

1 – Lack of a reliable translational models of ACT.

2 – Subclinical early markers of ACT development.

3 – Impact of ACT in other cellular compartments.

4 – Better understanding of ACT pathological mechanisms.

5 – Absence of effective targeted therapies for ACT.

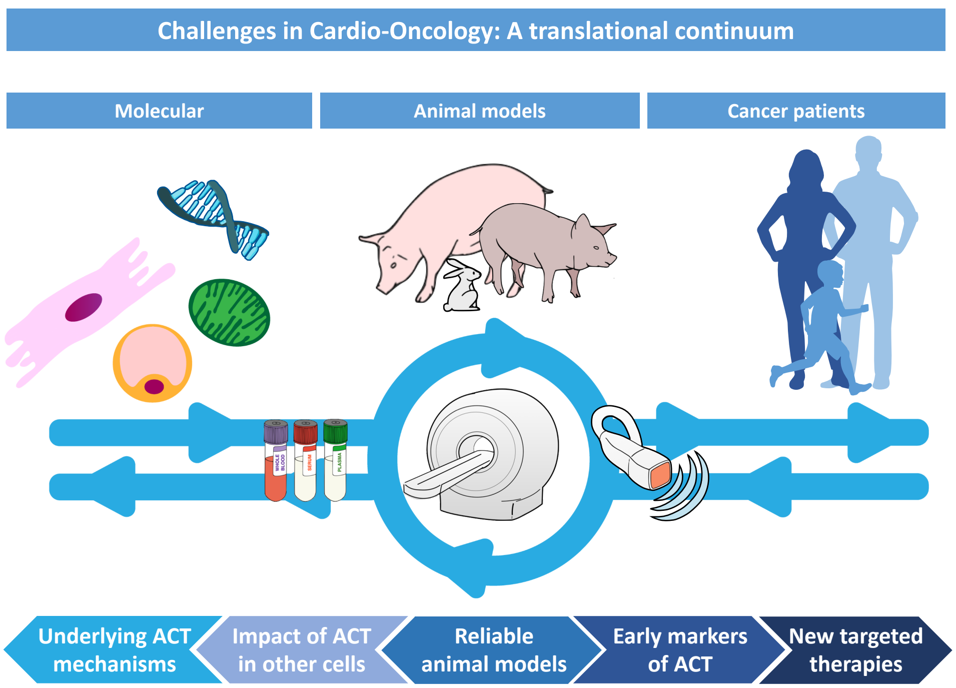

Figure 5: Current research gaps in the Cardio-Oncology field.

4 Objectives / Objetivos

We focused on previously mentioned research gaps regarding cardio-oncology and proposed 4 different main aims:

Objective 1: *Serial cardiac magnetic resonance (CMR) for early detection of anthracycline-induced cardiotoxicity (ACT)*

We used a large animal model (pig) of doxorubicin-induced cardiotoxicity to identify the earliest CMR marker of myocardial damage and its pathological correlates. We also studied the reversibility of cardiotoxicity upon detection of the early CMR marker.

Objective 2: *Effect of doxorubicin on cardiac microcirculation*

In this study, we studied the trajectories of microcirculation status across all stages of the pig anthracycline-induced cardiotoxicity model.

Objective 3: *Vulnerability of the hypertrophied heart to anthracycline-induced cardiotoxicity (ACT)*

The purpose of this work was to elucidate the impact of low cumulative i.v doxorubicin doses in pigs with LV pressure overload. A secondary endpoint of the study was to characterize with CMR the progression of the possible cardiotoxicity in both groups under doxorubicin regime.

Objective 4: *Remote ischemic preconditioning (RIPC) and anthracycline-induced cardiotoxicity (ACT)*

The purpose of this study was to elucidate the cardioprotective capability of repeated RIPC cycles before each doxorubicin administration in the i.c large-animal model.

Nosotros nos hemos centrado en las carencias en cardio-oncología anteriormente mencionadas y hemos propuesto 4 objetivos principales diferentes:

Objetivo 1: *Detección temprana de cardiotoxicidad por antraciclinas empleando la resonancia magnética cardiaca seriada*

Usamos un modelo de animal grande (cerdo) de cardiotoxicidad inducida por antraciclinas para identificar el marcador de daño miocárdico por resonancia magnética más temprano y correlacionarlo con su anatomía patológica. También estudiamos la reversibilidad de la cardiotoxicidad a partir de estos cambios tempranos.

Objetivo 2: *Efecto de la doxorrubicina en la microcirculación cardiaca*

En este estudio, evaluamos los cambios en la microcirculación a través de todas las etapas de nuestro modelo de cerdo de cardiotoxicidad por antraciclinas.

Objetivo 3: *Vulnerabilidad del corazón hipertrófico a la cardiotoxicidad por antraciclinas*

El propósito de este trabajo es dilucidar el impacto de dosis bajas y sistémicas (i.v) acumulativas en animales con sobrecarga de presión del ventrículo izquierdo. Un objetivo secundario es caracterizar mediante resonancia magnética cardiaca la progresión de la posible cardiotoxicidad en ambos grupos que reciben la doxorrubicina.

Objetivo 4: *Precondicionamiento isquémico remoto y cardiotoxicidad inducida por antraciclinas*

El propósito de este estudio es evaluar el potencial efecto cardioprotector de la aplicación repetida de precondicionamiento isquémico remoto antes de cada inyección de doxorubicina en el modelo i.c.

5 Material and methods

5.1 Study designs

All the studies were approved by the Institutional Animal Research Committee and conducted in accordance with recommendations of the Guide for the Care and Use of Laboratory Animals.

5.1.1 Objective 1: *Serial cardiac magnetic resonance for early detection of anthracycline-induced cardiotoxicity*

The study design is summarized in **Figure 6**. The study population consisted of 20 castrated male Large-White pigs (25-35 kg). Pigs in group 1 received five biweekly i.c doxorubicin injections (final injection at week 8) and were followed up until sacrifice at week 16 by i.v injection of pentobarbital sodium in overdose. In Group 2, pigs underwent three biweekly doxorubicin injections (final injection at week 4) and were similarly followed up until sacrifice at week 16. Group 3 pigs underwent the same doxorubicin protocol as Group 2 (three biweekly injections) but were sacrificed earlier, at week 6 (2 weeks after the final doxorubicin injection). Group 4 was a control group sacrificed after baseline CMR without doxorubicin exposure. In all groups, weekly comprehensive multi-parametric CMR exams were performed until sacrifice. During the treatment weeks, CMR scans were performed immediately before doxorubicin injections.

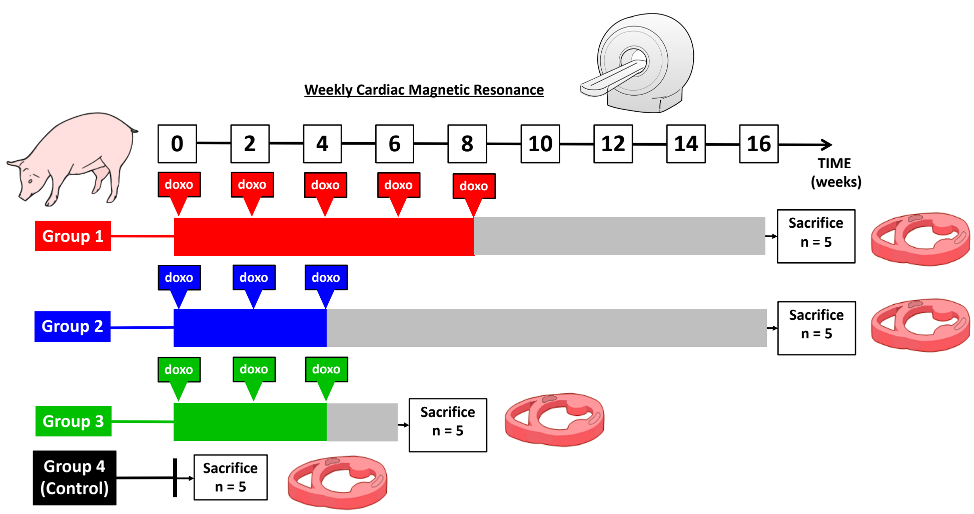

Figure 6: Study design for Objective 1.

5.1.2 Objective 2: *Effect of doxorubicin on cardiac microcirculation*

For studying microvascular damage, all groups from Objective 1 were use and two additional groups were performed ad hoc for this aim **(Figure 7)**. A total of 10 castrated male Large-White pigs (30-35 kg) were included in 2 different additional groups (N=5 per group): 1) “Acute 48h” (pigs received one single i.c injection (0.45mg/Kg) of doxorubicin and were sacrificed at 48 hours). 2) “Acute 2w” (pigs received one single i.c injection (0.45mg/Kg) of doxorubicin and were sacrificed 2 weeks later). Serial invasive coronary physiology studies with flow-pressure combo wires were performed in all animals at time-points noted in Figure 2 to obtain measures of coronary flow reserve (CFR). In the “acute 48h” group, CRF was also evaluated 10 min after the end of i.c doxorubicin injection. Serial non-invasive CMR studies were performed at timepoints noted in **Figure 7** to obtain measures of quantitative perfusion following a protocol previously reported by our group [68].

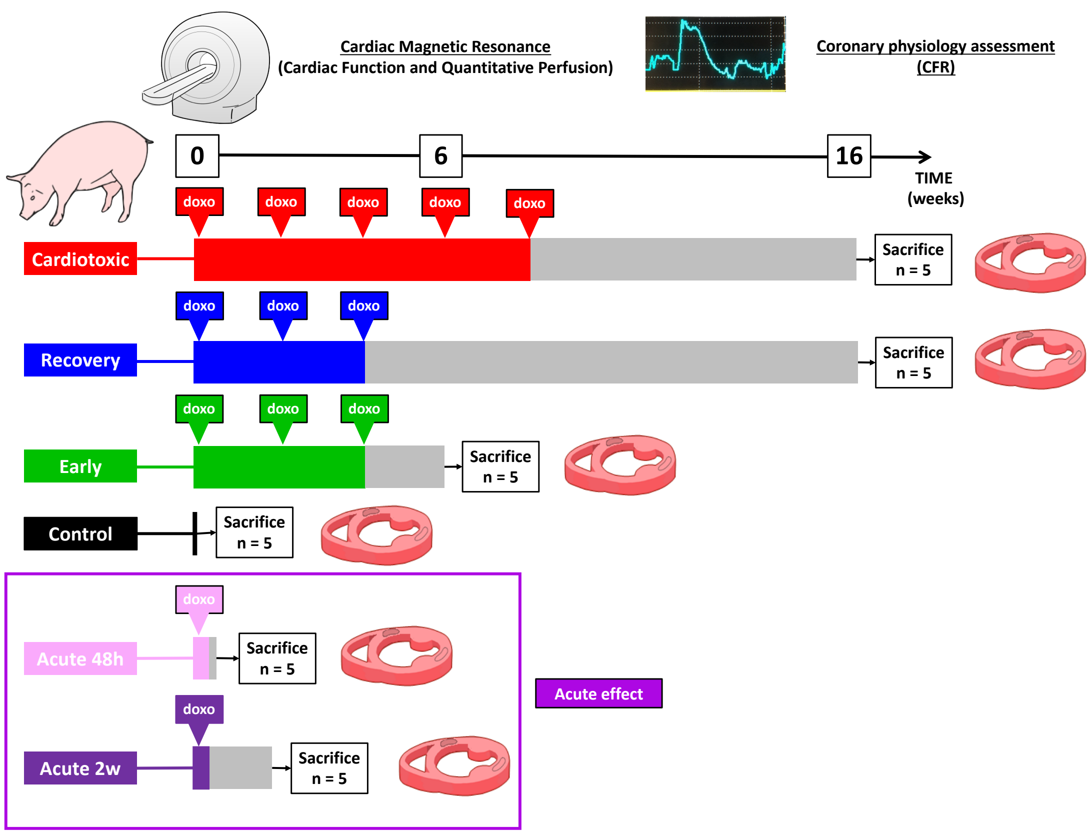

Figure 7: Study design for Objective 2.

5.1.3 Objective 3: *Vulnerability of the hypertrophied heart to anthracycline-induced cardiotoxicity*

A scheme of the study design is summarized in **Figure 8**. 28 Yucatan minipigs were included in the study. We divided the animals in the following branches: 1) 14 pigs underwent to aortic banding surgery at 2-3 months of age (time -4); and kept until 4 months of pressure afterload evolution (time 0). Then, they were divided to receive 5 weekly i.v injections of 1 mg/kg of doxorubicin (7 Banding + doxo group) or as controls (7 Banding control group). Afterwards, pigs were followed for 4 additional months and sacrificed at end of the study (time 4). 2) 14 additional non-operated pigs of 6-7 months old (time 0) were divided to receive 5 weekly intravenous injections of 1 mg/kg of doxorubicin (7 No Banding + doxo group) or as controls (7 No Banding control group). They were kept as well until sacrifice at 4 months (time 4). Serial multiparametric CMR scans were performed at time -4 and -3 in the Banding groups and at 0, 1, 2, 3 and 4 months in all groups. At the end of the study, all the animals were sacrificed with pentobarbital administration in overdose and cardiac tissue were harvested for ex vivo characterization.

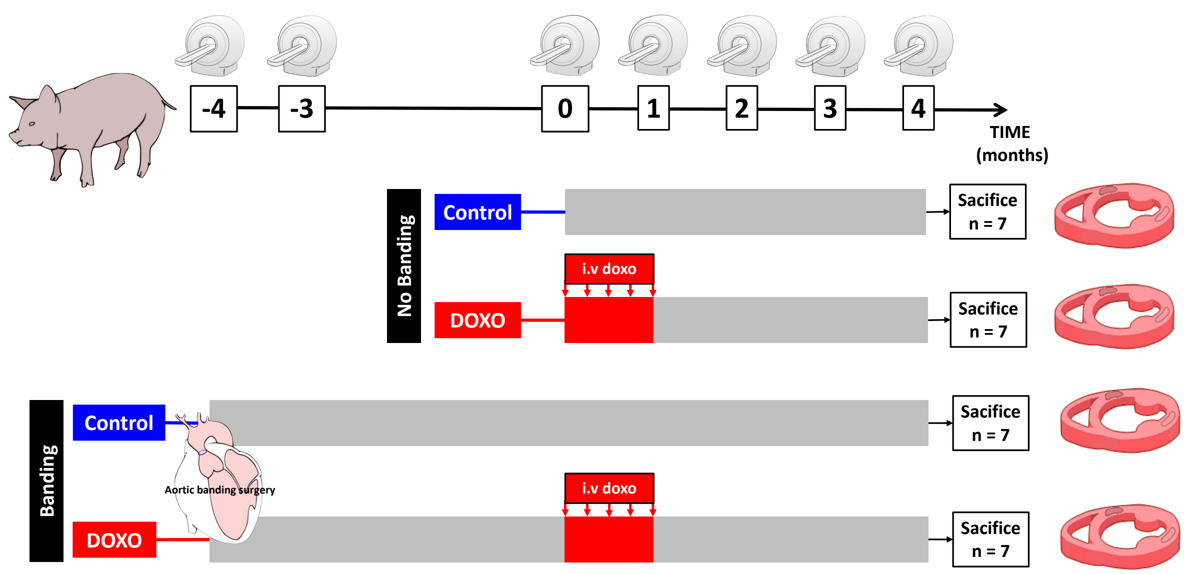

Figure 8: Study design for Objective 3.

5.1.4 Objective 4: *Remote ischemic preconditioning and anthracycline-induced cardiotoxicity*

A scheme of the study design is summarized in **Figure 9**. 20 healthy Large-White castrated male pigs (weighted around 30 kg), underwent to serial i.c doxorubicin administration in order to create a model of anthracycline-induced cardiomyopathy. As in the previous Objectives 1 and 2, the model consisted in an i.c injection of doxorubicin every 2 weeks up to 5 (weeks 0, 2, 4, 6 and 8). At the beginning of the study, animals were randomized 1:1 to receive (RIPC group) or not (No RIPC Group) 3 cycles of RIPC before each doxorubicin administration. Then, animals were kept for follow-ups at week 12 and sacrifice at week 16. CMR scans were performed at week 0, 6, 8, 12 and 16.

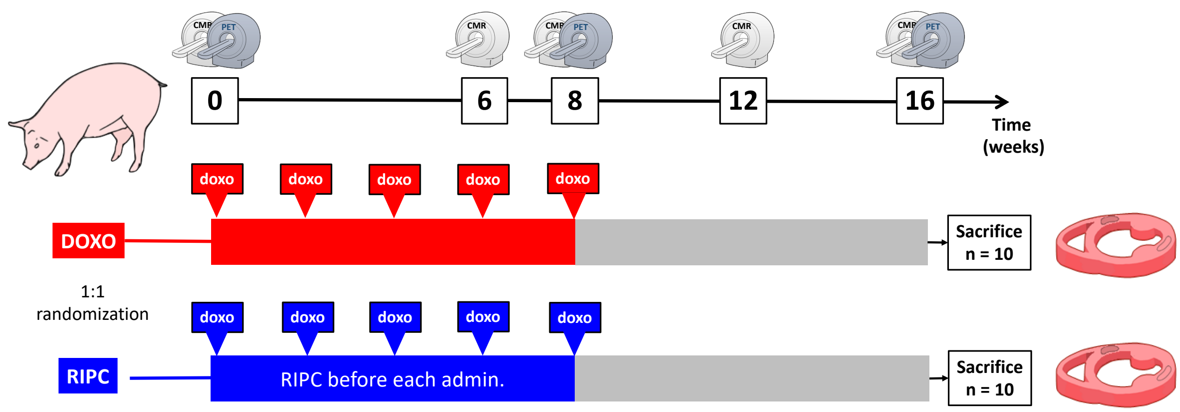

Figure 9: Study design for Objective 4.

5.2 Doxorubicin intracoronary administration procedure

For Objectives 1, 2 and 4, we used a modification of a previously described approach [69, 70]. Animals were anesthetized and endotracheally intubated. The femoral artery was then accessed by the Seldinger technique and a 7F sheath was inserted. Pigs were anticoagulated with 150 UI/kg of intravenous heparin, and a 5F coronary diagnostic catheter was inserted via a femoral sheath and placed at the origin of the left coronary artery. Under angiography guidance, a 0.014 mm coronary guide wire was positioned distally in the left anterior descending (LAD) coronary artery. The catheter was docked selectively in the LAD, and a 0.45 mg/kg dose of doxorubicin (Farmiblastina®, Pfizer) diluted in 30 ml saline was given as a slow bolus injection over 3 minutes. Electrocardiographic and hemodynamic monitoring was maintained during doxorubicin administration. Once the infusion was completed, coronary angiography was performed to document normal coronary flow, the catheter material was removed, and the animal allowed to recover.

5.3 Systemic doxorubicin administration procedure

All animals from doxo subgroups (banding and no banding) in the Objective 3, received the same chemotherapy regime, consisted in 1 mg/kg of intravenous doxorubicin diluted in 20 mL of saline solution during 3 minutes through the ear vein. After infusion, the catheter was wash out with 10 additional mL of saline to avoid caustic lesions secondary to anthracycline remnants in the distal vessel. The protocol was repeated weekly during a whole month, being 5 injections in total per animal. We decided this low-regime protocol after performing multiple proof of concept approaches resulting in high mortality with no cardiotoxicity development as it was previously reported [67] **(Figure 10)**.

5.4 Aortic banding surgery

For Objective 3. Supravalvular aortic stenosis was induced by emplacing a surgical banding on the ascending aorta, as was previously described [71–73]. Sedation was induced by intramuscular injection of ketamine (20 mg/kg), xylazine (2 mg/ kg) and midazolam (0.5 mg/kg), and then maintained with inhaled sevoflurane at 3% of concentration. Continuous i.v fentanyl solution was infused as analgesia during surgery, and perisurgical antibiotherapy prophylaxis consisted in a single dose of cefuroxime. A respirator, as well as ECG controlled mechanical endotracheal ventilation and oxygen saturation were controlled and monitored during the surgery. A minimally invasive right lateral thoracotomy was performed in the fourth intercostal space. Ascending aorta was identified after a pericardiectomy and constricted 3 cm above the aortic valve with a 10 mm Dacron band, adjusted to 70% of the perimeter. Pericardiectomy was left open, the pneumothorax evacuated with a chest tube and the thoracic wall and skin incisions were sutured. Then, animals were recovered from the anesthesia **(Figure 11)**.

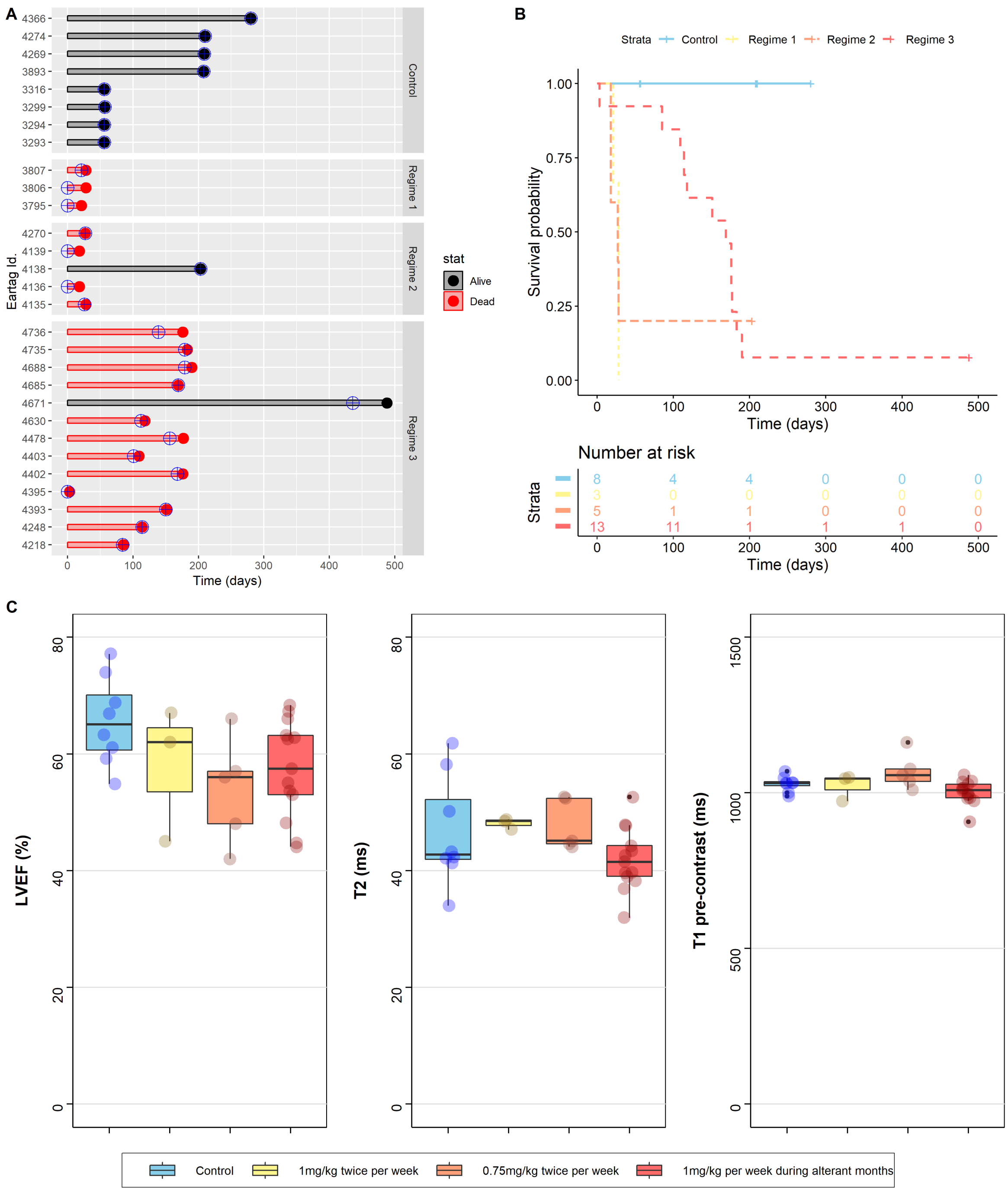

Figure 10: Proof of concept of different i.v doxorubicin regimes

(A) Event table for each regime and control groups indicating dead (red) or alive (black) animals and the last CMR scan performed (blue circled cross).

(B) Descriptive Kaplan-Meier curve for each group.

(C) CMR functional and mapping values from the last scan before the dead of the animal for each group.

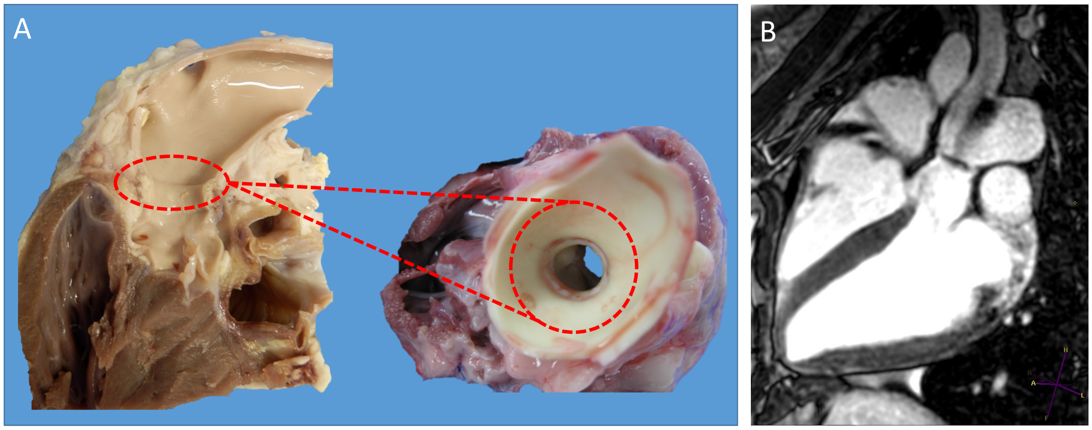

Figure 11: Aortic banding surgery

(A) Explant of a heart from a pig at 4 months of study in 3 chambers and transversal views. Red dashed circles indicate banding location at supravalvular level with a 30% of restriction.

(B) CMR 3D late gadolinium enhancement sequence of the same animal segmented at 3 chambers view. Post banding jet can be observed in black.

5.5 Remote ischemic preconditioning protocol

For Objective 4, animals randomized to RIPC group were subjected to 3 cycles of RIPC before doxorubicin administration. RIPC were performed using a homemade tourniquet to produce transient ischemia in the right leg. Total ischemia was assured by sight - checking the congestive reaction at the lower extremity -; and by doppler echography.I

5.6 Invasive Coronary Flow Reserve assessment

For Objective 3, a coronary pressure/flow guide wire (VOLCANO Combowire®) was advanced through the guiding catheter and placed distal in the LAD (for evaluation of the doxorubicin-infused territory) or distal in the left circumflex coronary artery (LCx) (for evaluation of the remote myocardium). CFR was assessed before each doxorubicin infusion and calculated by the ratio between basal and maximum hyperemia. The hyperemia protocol consisted in the intracoronary administration of 0.5 mg/kg of papaverine selective to the LAD or LCx coronary arteries, as previously described [74].

5.7 Cardiac Magnetic Resonance protocol

All studies were performed with a Philips 3-T Achieva Tx whole body scanner (Philips Healthcare, Best, The Netherlands) equipped with a 32-element phased-array cardiac coil. The CMR protocol included a standard segmented cine steady-state free-precession (SSFP) sequence to provide high-quality anatomical references, a T2 gradient-spin-echo (T2-GraSE) mapping sequence, and native and post-contrast T1-mapping and late gadolinium enhancement (LGE) sequences. The imaging parameters for the cine SSFP sequence were as follows: field of view (FOV) of 280*280 mm, slice thickness 6 mm with no gaps, repetition time (TR) 2.8 ms, echo time (TE) 1.4 ms, flip angle 45^o, cardiac phases = 30, voxel size 1.8*1.8 mm, and number of excitations (NEX) = 3. The imaging parameters for the T2-GraSE mapping were FOV 300 300 with an acquisition voxel size of 1.8*2.0 mm2 and slice thickness 8 mm, and eight echo times ranging from 6.7 to 53.6 ms. To reduce T1 effects, a two-heartbeat interval was used between excitations. The T1-mapping sequence (Modified Look-Locker Inversion recovery [MOLLI]) was acquired before and 10 min after contrast administration. All MOLLI sequences were based on a 5(3)3 scheme using a single shot steady-state free precession readout sequence (TR/TE/Flip angle= 2.1ms/1.05ms/350) with an in-plane acquisition resolution of 1.5*1.8 mm2 and an 8 mm slice thickness. T2 and T1 mapping sequences were both triggered at mid-diastole and acquired from a single short-axis mid-apical slice. LGE imaging was performed 15 min after intravenous administration of 0.2 mM/kg gadopentetate dimeglumine contrast agent using an 3D inversion-recovery spoiled turbo field echo sequence (TR/TE/Flip angle= 2.4ms/1.13ms/100) with an isotropic resolution of 1.5*1.5*1.5 mm3 on a FOV of 340*340*320 mm3 in the FH, LR, and AP directions. Data were acquired in mid-diastole with a 151.2 ms acquisition window. Acquisition was accelerated using a net SENSE factor of 2.25 (1.5*1.5 in the AP and LR directions) with a bandwidth of 853Hz per-pixel. Inversion time was adjusted before acquisition using a look-locker scout sequence with different inversion times to ensure proper nulling of the healthy myocardium signal. For the analysis, 3D volume was reconstructed in short axis, 2 chamber, and 4 chamber views with a slice thickness of 6mm. Cardiac quantitative perfusion was estimated using dynamic acquisition with dual-saturation recovery (TS=20, 80 ms) technique during gadolinium-based contrast administration (0.2 mmol) as previously described [74].

CMR studies were analyzed by 2 experienced and independent observers using dedicated software (IntelliSpace Portal, Philips Healthcare, Best, The Netherlands). T2 maps were automatically generated on the acquisition scanner by fitting the signal intensity of all echo times to a monoexponential decay curve at each pixel with a maximum likelihood expectation maximization algorithm. T1 maps were generated using a maximum-likelihood expectation-maximization algorithm and fitting the MR to a T1 inversion recovery with 3 independent model parameters. T2 and T1 relaxation maps were quantitatively analyzed by placing a wide transmural region of interest (ROI) at the anterior myocardial area (irrigated by the LAD) of the corresponding slice in all studies. Delayed gadolinium-enhanced regions were defined as >50% of maximum myocardial signal intensity (full width at half maximum) and qualitatively analyzed. Extracellular volume (ECV) was estimated with native T1-MOLLI values and 10 minutes post-contrast T1-MOLLI values corrected by hematocrit, as described elsewhere [51].

5.8 Positron Emission Tomography – Computed Tomography (PET-CT) protocol

All studies were performed with a Philips PET scan. Animals were fasted 24 hours before the exams, having free access to water consumption. Glucose levels were normalized to 100-150 mg/dL; to do that, blood drops were collected, and glucose was quantified using a CONTOURTM PLUS Blood Glucose Monitoring System. If glucose levels were under 100 mg/dL, we proceeded to administrate an i.v bolus of serum with glucose to 50% (5 mL for each range of 10 mg/dL of glucose levels under the limit – e.g. 5 mL from 90 to 100 mg/dL, 10 mL from 80 to 90 and so on). If glucose levels were over 150 ml/dL, we let the animal and repeated the measurement after 10-15 minutes until levels normalized. For extremely high levels (e.g. over 200 mg/dL), we protocolled insulin injections, but this scenario did not take place in any pig. In all the cases, glucose levels were to be maintained at least 30 minutes, with measurements every 10 minutes. Afterwards, fluorodeoxyglucose (FDG) radiotracer was i.v injected (10 mCi per study). Once administrated, biodistribution was waited for 40 minutes and then, the acquisition started. After that, a contrast enhanced cardiac CT scan was performed to superpose the anatomical structures to FDG distribution. PET studies were analyzed using dedicated software (IntelliSpace Portal, Philips Healthcare, Best, The Netherlands) by placing a ROI in the infused area and the remote area and normalizing with muscle values.

5.9 Necropsy and sample collection

At the end of their respective studies, animals were sedated and euthanatized by i.v pentobarbital in overdose. Then, heart was excised, and blood removed using abundant saline at room temperature. For water content quantification, harvested tissue samples were immediately blotted to remove surface moisture and then introduced into laboratory crystal containers previously weighed on a high-precision weighing machine. The tissue-loaded containers were weighed before and after drying for 48 h at 100ºC in a desiccating oven. Tissue water content (% dry weight) was calculated using the following formula: water content = ([wet weight - dry weight]/dry weight) x100. An empty container was weighed before and after desiccation as an additional calibration control.

5.10 Histology

For histological studies, samples were fixed in 4% formalin and then transferred to 70% ethanol. After paraffin embedding, 4 micron sections were cut and stained with hematoxylin and eosin (HE), Masson trichrome (M), and Sirius Red (SR). H-E and M staining sections were analyzed by two experienced independent blinded anatomopathologists for evaluating cardiomyocyte doxorubicin lesions and microcirculation damage using a previously reported scores explained bellow.

Stained sections were scanned and 20x20 magnification images were taken for collagen quantification using a modified macro [75].

For Objective 2, the arterial/arteriolar pathology evaluation was performed in every artery in the slice of each sample blinded to study group. Large, medium and small arteries, as well as arterioles were independently scored. Arterial damage was evaluated integrating all these parameters and a Damage Score created ad hoc for the study **(Figure 12)** with the following criteria:

- *Grade 0*: No lesions;
- *Grade 1*: Minimal tunica intima hyperplasia. No tunica media lesion;
- *Grade 2*: Slight to moderate tunica intima hyperplasia by myofibroblast proliferation and extracellular matrix accumulation. Disorganization of the tunica media with only isolated occasional smooth muscle cell loss;
- *Grade 3*: Moderate tunica intima hyperplasia with occasional luminal stenosis. Tunica media degeneration with moderate loss of smooth muscle cells replaced by extracellular matrix and/or collagen;
- *Grade 4*: Moderate to severe tunica intima hyperplasia with marked luminal stenosis. Tunica media degeneration with severe loss of smooth muscle cells replaced by extracellular matrix and/or collagen.

For cardiotoxicity damage evaluation in the Objective 4, an adaptation of Billingham score was used in H-E stained sections as previously reported [76].

5.11 Capillary bed evaluation

For objective 2, capillary density was checked by CD31 immunohistochemistry, using 4 micron slices from paraffin embedded samples. A specified macro-based analysis was performed to calculate the number of capillaries per mm2. 10 images of 10x magnification were taken and analyzed using FIJI (ImageJ) software [77]. A summary of the macro' running is showed in **Figure 13**.

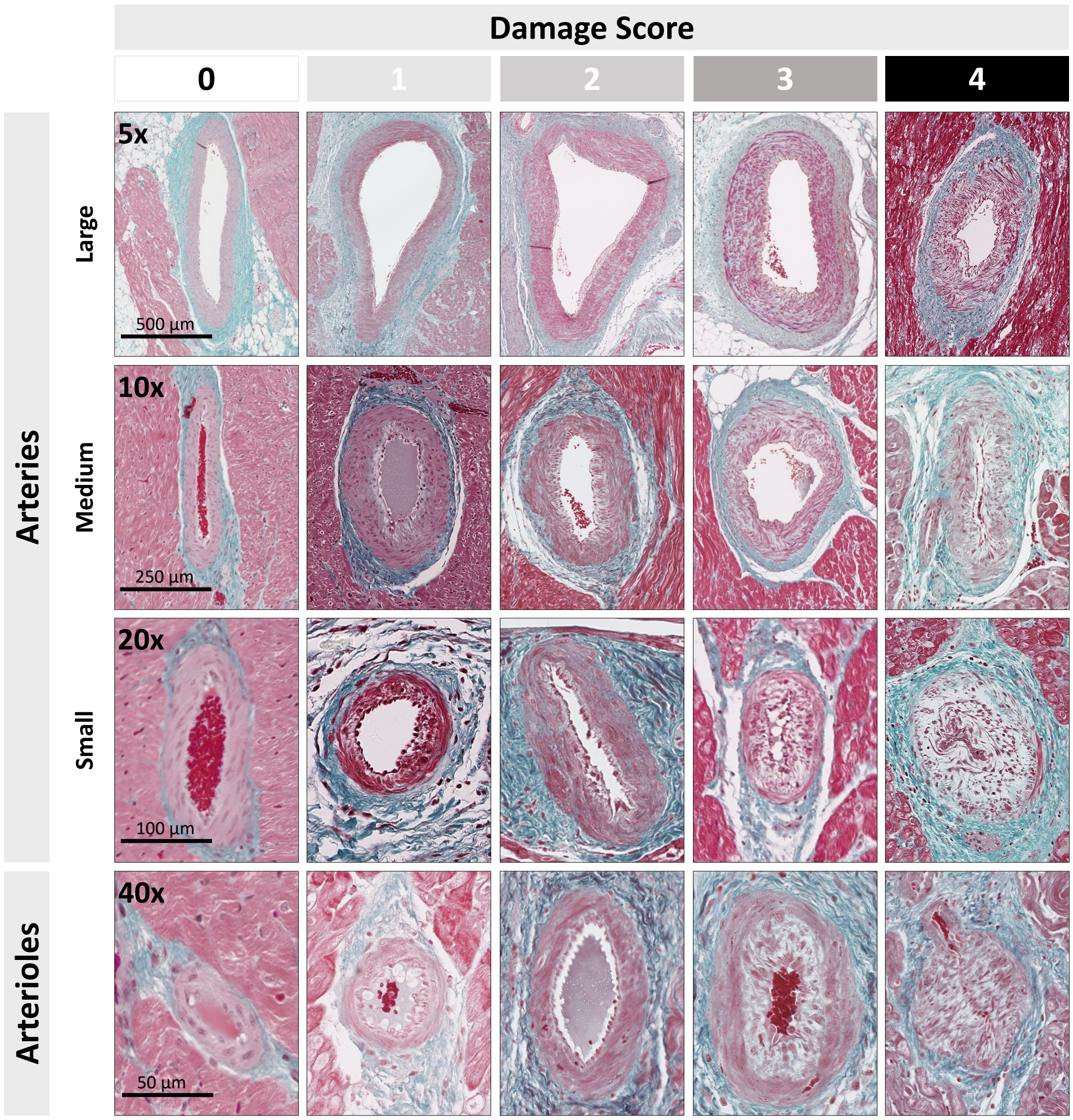

Figure 12: Damage Score for microvascular histopathological evaluation.

From 0 (normal) to 4 (maximum damage), for each size of artery and arterioles.

5.12 Transmission Electron Microscopy

Samples from infused area were maintained in 4% glutaraldehyde in 10% PFA solution for 24-48 hours. Afterwards, tissue was post-fixed in 1% osmium tetroxide water solution for 1 hour at room temperature. Then, samples were washed with water and underwent to block staining by 0.5% uracil acetate water solution for 10 minutes. Following this, tissue samples were dehydrated in alcohol water solutions in ascendant graduation

(30%, 50%, 70%, 95%, and 100%) and a last passage through acetone. After that, were included in Durcupan epoxy resin by steps in resin-acetone mixture in ascendant concentrations (1:3, 3:1) and, finally, pure resin. Resin-included samples were polymerized in an oven at 60ºC for 48 hours. Then, were ultrathin sliced using an ultramicrotome Leica Ultracut S (60 nm) and were deposited in 200 mesh copper grids. Grids were counterstained by uranyl acetate and lead citrate. Images were obtained by a Jeol Jem1010 (100 KV) transmission electron microscope, using a Gatan camera (Orius 200 SC model); and acquired and subsequently treated with the Digital Micrograph software. Individual images were acquired at 6000, 10000 and 4000X magnifications for: tissue evaluation (6000X), mitochondrial quantification (10000X) and mitochondrial cristae assessment (40000X), using ImageJ software 1.52p Wayne Rasband from USA National Institute of Health (NIH).

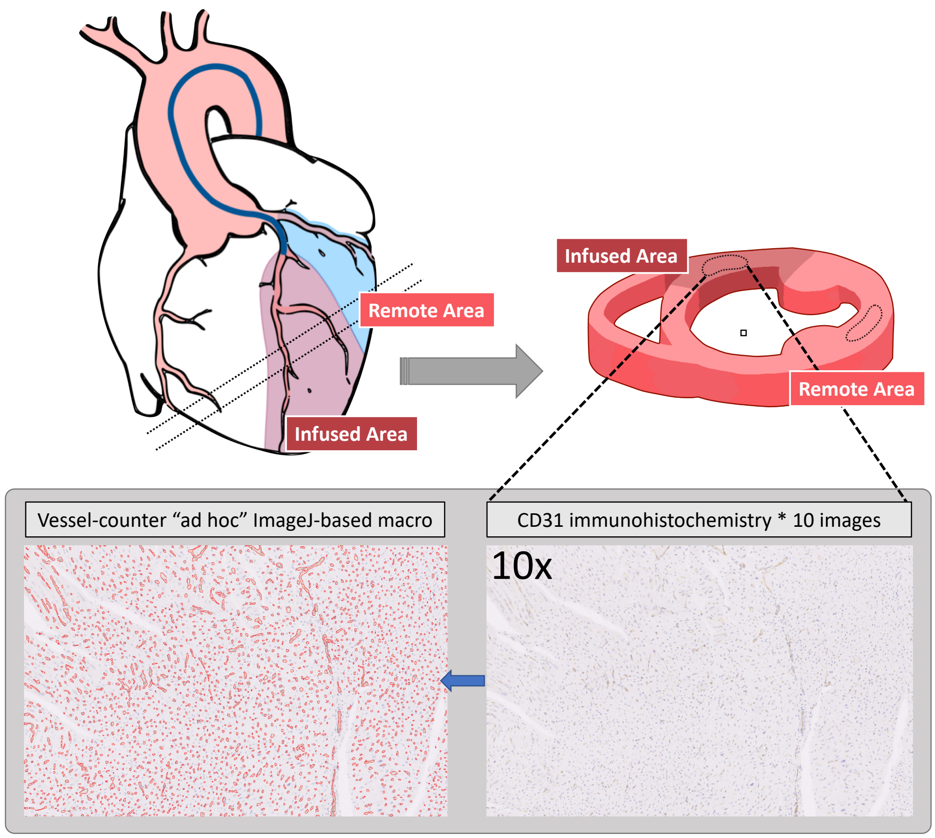

Figure 13: Scheme of CD31-capillary counter “ad hoc” macro running for endothelial quantification.

5.13 Statistical analysis

According to the data distribution, continuous variables were calculated as $mean \pm SD$ or $median \pm IQR$. Data normality was assessed with the Saphiro-Wilk test. Differences were considered statistically significant at $p<0.05$. All data were analyzed with RStudio (RStudio Team (2015): Integrated Development for RStudio, Inc., Boston, MA), and graphics were created with ggplot2.

Objective 1: *Sample size estimation*: Being this objective a "hypothesis generator" study (to explore CMR early markers in cardiotoxicity), we chose an arbitrary size of 5 animals per group. Once the early marker was defined (T2 mapping values), the rest of the groups were calculated taking in account relative changes in T2 relaxation times of 5 ms. Considering a SD of 3 ms and multiple comparisons between all the timepoints, we stablished also a sample size of 5 for the other groups with 80% of power to detect differences. The t-test was used for two-group comparisons and the changes of each imaging variable were assessed using one-way repeated measures analysis of the variance (ANOVA) test. To identify the timepoints showing statistically significant changes compared to the baseline values, pairwise paired t-test were performed considering p value adjustment for multiple comparisons (Bonferroni method).

Objective 2: *Sample size estimation*: from Objective 1. The t-test was used for two-group comparisons and the changes of each imaging variable were assessed using one-way repeated measures analysis of the variance (ANOVA) test. To identify the timepoints showing statistically significant changes compared to the baseline values, pairwise paired t-test were performed considering p value adjustment for multiple comparisons (Bonferroni method). For CFR and quantitative perfusion analyses in the grouped early analysis, only individuals from Cardiotoxic and Recovery groups were used because their values were complete in all the timepoints. For the histopathological analysis of the vessel injury, an ordinal multinomial regression nested by individual animal were performed to detect differences in damage score between groups. Chi-square analysis between each group and control group were performed as post-hoc analysis.

Objective 3: *Sample size estimation*: For stablishing i.v doxorubicin administration protocol, sample size was also arbitrary in order to test the best regime for the study. For the main experiment, LVEF was chosen as response variable between for evaluating effect of doxorubicin administration and aortic banding surgery itself. Taking in account differences in LVEF of 10% (definition of cardiotoxicity), with a SD of 6.5%, 0% of casualties and 80% of power and 0.05 of bilateral significance level; 7 pigs per group was the final sample size. Inasmuch as we found unexpected mortality of 30% in Banding + doxo group we performed more animals until reach a size of 7 at the end of the study. In order to discriminate between doxorubicin effect in banding / no banding groups but also the potential effect of banding in low doxorubicin protocols, t-test was used for two-group comparisons taking in account doxorubicin exposure and aortic banding presence using two-way factorial analysis of the variance (ANOVA) test. For Billingham score analysis Chi-square analysis between each group and control group were performed.

Objective 4: *Sample size estimation*: for calculating sample size in each group (RIPC and No RIPC), the purpose was to detect 8% of difference in LVEF- similar to other cardioprotection studies- between treated and no treated groups; with a SD of 6.5%, and 0% of casualties (previously defined in the animal model), a power of 0.8 and 0.05 of bilateral signification level. This resulted in 10 animals per group. T-test was used for two-group comparisons taking in account RIPC exposure at the end of the study (16 weeks).

6 Results

All CMR grouped data are detailed in **Supplementary Table 1** (for objective 1), **Supplementary Table 4** (for Objective 3) and **Supplementary Table 5** (for objective 4). CMR and CFR grouped data is detailed in **Supplementary Tables 3** and **3** for objective 2 at **Supplementary Material** chapter.

6.1 Objective 1: *Serial cardiac magnetic resonance for early detection of anthracycline-induced cardiotoxicity*

None of the pigs showed adverse events during doxorubicin administration at any time point (i.e. no changes were noted in ECG or systolic arterial pressure during injections). None of the pigs died during the study.

6.1.1 Serial cardiac magnetic resonance tissue characterization of anthracycline-induced cardiotoxicity

Five pigs received 5 biweekly doxorubicin injections (weeks 0, 2, 4, 6, and 8). Multiparametric CMR was performed weekly until week 16, when animals were sacrificed, and hearts harvested for pathology evaluation.

Left ventricular ejection fraction: Weekly CMR exams revealed no changes in LVEF until week 9 (one week after the fifth and final doxorubicin injection). From week 9 onwards, LVEF declined progressively, the decline becoming significant at week 12 ($55 \pm 4\%$ at baseline vs 43 ± 6 at week 12; p=0.01). The lowest LVEF value was recorded at the 16-week time point ($30 \pm 8\%$; p=0.01 vs baseline). Group and individual LVEF trajectories are presented in Figures 2A and 2B. In agreement with the LVEF data, no regional contractile abnormalities were documented until week 10, when the doxorubicin-infused myocardium showed regional wall motion defects (data not shown).

T2 relaxation times: Weekly CMR exams revealed no changes in T2 relaxation times on CMR exams performed at weeks 0 through 5. At week 6, T2 relaxation times were significantly longer than at baseline ($45.2 \pm 0.5ms$ and 52.0 ± 1.4 ms at baseline and week 6 respectively, p=0.007). T2 relaxation times subsequently increased, reaching a maximum at end follow-up ($73.0 \pm 4.6ms$ and 72.8 ± 4.6 on weeks 12 and 16; p=0.005 and p=0.001 vs baseline, respectively). Group and individual T2 trajectories are presented in **Figure 14, A** and **B**.

T1 relaxation times: Native T1 relaxation times showed no change from baseline until week 10 (2 weeks after the fifth and final doxorubicin dose). A non-significant increase was noted at week 10, followed by a progressive increase to end follow-up at week 16. Native T1 values were significantly longer than at baseline only from week 12 onwards ($1087 \pm 101ms$ and 1220 ± 59 at baseline and week 12 respectively, p=0.02).

Extracellular volume (ECV): ECV expansion was tracked using a validated formula that includes pre- and post-contrast T1 values and hematocrit [51]. In parallel with the native T1 trajectory, ECV did not differ from baseline until week 10 (2 weeks after the fifth and final doxorubicin dose). ECV subsequently expanded progressively, but with no statistically significant difference from baseline until week 14 ($26.03 \pm 5.8\%$ and 41 ± 1.34 at baseline and week 14 respectively, p=0.006). Group and individual ECV trajectories are presented in **Figure 14, A** and **B**.

Late gadolinium enhancement (LGE): Positive LGE areas first appeared in the doxorubicin-infused area from week 10 onwards. The enhanced areas formed a patchy pattern at week 12, becoming more evident at 16 weeks follow-up (**Figure 15, D**.)

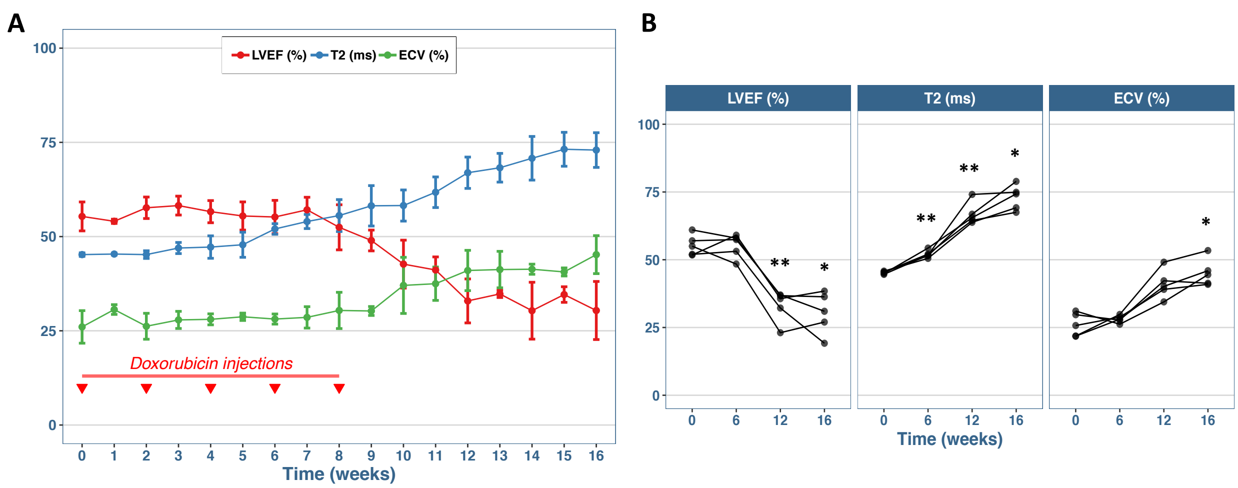

Figure 14: Animal model of anthracycline cardiotoxicity (Group 1).

(A) Time course of CMR imaging studies. Data are represented as $mean \pm SD$ (bars).

(B) Individual animal data at selected time points for LVEF, T2, and ECV. Asterisks indicate statistically significant differences compared with week 0.

* p <0.05, ** p <0.01 and ns (no significant).

(Picture adapted from Galán-Arriola et al [68]).

6.1.2 T2-driven strategy for the prevention of anthracycline-induced cardiotoxicity

Having documented T2 mapping abnormalities preceding systolic function deterioration, we next explored whether T2 relaxation time prolongation occurred at a reversible stage of anthracycline-induced cardiotoxicity.

To address this question, we studied a group of 5 pigs (Group 2) in which doxorubicin treatment was stopped upon detection of T2 prolongation. As in Group 1, T2 relaxation times in Group-2 pigs were non-significantly prolonged at week 5 and this prolongation became significant at week 6 (i.e. immediately before the scheduled fourth doxorubicin dose). Group 2 pigs therefore received only 3 doxorubicin doses (weeks 0, 2, and 4) and were followed-up until week 16. T2 relaxation times in Group 2 pigs were significantly prolonged at week 6 ($45.6 \pm 0.6ms$ and 51.6 ± 0.8 at baseline and week 6 respectively, p=0.004) but returned to baseline levels at week 8 ($45.5 \pm 1.3ms$; p=1 vs baseline), and these levels were maintained until end follow-up ($44.8 \pm 1.4ms$ at week 16; p=1 vs baseline) (Figure R.2B and E, blue lines). LVEF in Group 2 showed no deterioration during follow-up (**(Figure 15, A**), and regional LV wall motion was similarly unaffected. All other evaluated parameters in Group 2 remained within normal ranges throughout follow-up (**Figure 15, D**, blue lines).

6.1.3 Pathological correlates of early T2 mapping changes

The underlying tissue composition changes leading to early T2 relaxation-time prolongation in the presence of normal T1 and ECV readings was investigated in another group of five pigs (Group 3). Group 3 animals received 3 doxorubicin doses, at weeks 0, 2, and 4, and were sacrificed immediately after detection of T2 prolongation (at week 6). Like the other groups, these animals underwent a weekly CMR exam. Tissue samples from Group 3 animals were compared with samples from Group 1 and 2 animals, which were sacrificed at the end of the 16-week protocol.

Myocardial water content: As expected, T2 relaxation-time prolongation was associated with an increase in myocardial water content [46]. At week 6, after 3 doxorubicin doses, T2 relaxation times were significantly prolonged in Group-3 animals ($45.8 \pm 2.52ms$ and 52.6 ± 2.2 at baseline and week 6 respectively, p=0.01) (**Figure 15, B and E**, green lines). Myocardial water content was significantly elevated in samples harvested at this time point ($396 \pm 12\%$ of dry weight and 375 ± 0.7 in Group 3 and control respectively, p=0.014, **Figure 16, C**). ECV CMR data for Group 3 revealed no expansion of the extracellular space at week 6 (**Figure 15, C and F**, green line), indicating that the increased myocardial water content and T2 prolongation likely corresponds to intracellular edema.

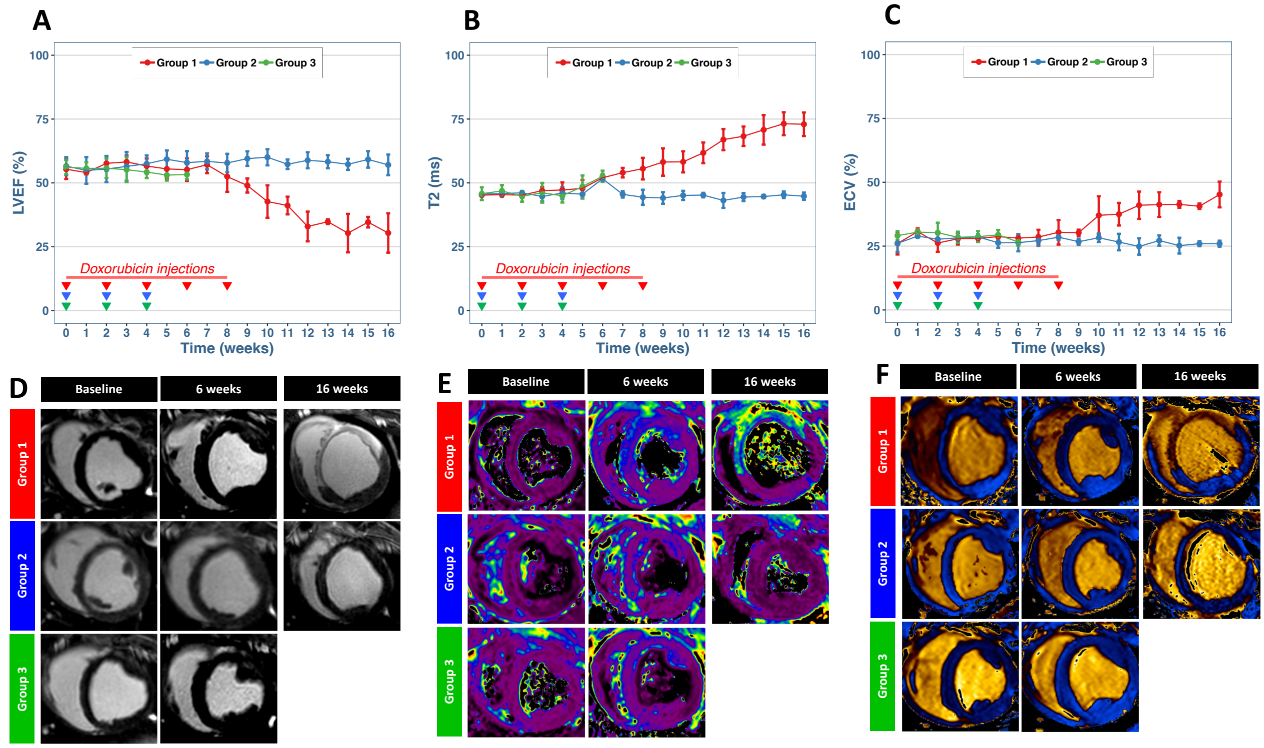

Figure 15: Time course CMR comparison between Group 1 and Group 2.

(A) LVEF (%).

(B) T2-GraSE mapping in the infused area (in ms).

(C) ECV in the infused area (%).

(D) Representative images of LGE sequences for selected time points and groups.

(E) Representative images of T2-Grase mapping for selected time points and groups, represented with a mask range (20-120 ms).

(F) Representative images of native T1-MOLLI mapping for selected time points and groups, represented with a ranged masked (550-1750 ms).

(Picture adapted from Galán-Arriola et al [68]).

At end follow-up in Group 1 (5 biweekly doxorubicin doses followed by sacrifice at week 16), myocardial water content was also significantly increased ($500 \pm 39\%$ of dry weight; p<0.001 vs control). At this time point, ECV CMR data revealed an overt increase in extracellular space (**Figure 15, C and F**, red line), a finding compatible with extracellular edema formation. This is consistent with the positive LGE at this disease stage (**Figure 15, D**). Interestingly, myocardial end follow-up water content in Group 2 (3 biweekly doxorubicin doses and follow-up to week 16) did not differ from controls ($365 \pm 0.5\%$; p=0.13 vs. control). Myocardial water content in all groups is shown in **Figure 16, C**.

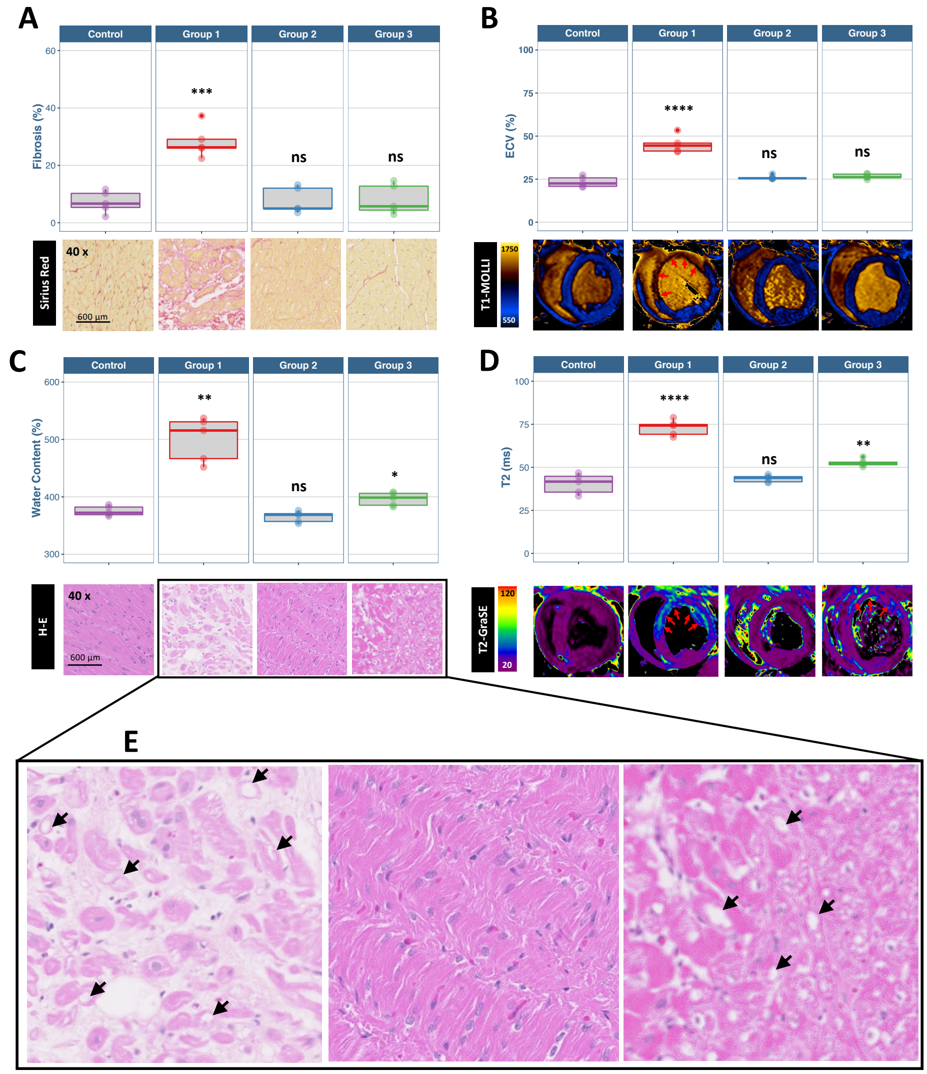

Figure 16: End follow-up ex-vivo and imaging studies of the infused area in each group.

(A) Fibrosis (%) in the infused area for each group at sacrifice. Representative images show SR staining.

(B) ECV (%) in the infused area for each group at sacrifice. Representative images show CMR native T1-MOLLI with a 550-1750 ms mask range. Red arrows mark areas with significantly increased signal.

(C) Water content (normalized to dry weight) in the infused area for each group at sacrifice. Representative HE images are shown. Black arrows mark intra-cardiomyocyte vacuolization.

(D) T2-GraSE mapping (ms) in the infused area for each group at sacrifice. Representative images show CMR T2-GraSE mapping with a 20-120 ms mask range. Red arrows mark areas with significantly increased signal.

Asterisks indicate statistically significant statistical differences compared with week 0 for each time point:* p <0.05, ** p>0.01, *** p>0.001; ns, non-significant.

(Picture adapted from Galán-Arriola et al [68]).

Structural myocardial changes: HE staining of Group-3 samples (harvested at week 6, after 3 doxorubicin doses) revealed cardiomyocyte vacuolization (**Figure 16, E**, left panel) with no other overt alteration to myocardial tissue structure; cardiomyocytes maintained their shape and there was no increase in extracellular space. Interestingly, at 16-week follow-up of animals receiving 3 doxorubicin doses (Group 2), samples showed no intra-cardiomyocyte vacuolization (Figure R.3E, right panel). Conversely, myocardial samples from Group 1 pigs (5 doxorubicin doses and 16-week follow-up) showed even larger intra-cardiomyocyte vacuolae and a disarrayed myocardial structure, with increased extracellular space and replacement fibrosis, suggestive of end-stage disease (**Figure 16, A and E** mid panel).

6.2 Objective 2: ***Effect of doxorubicin on cardiac microcirculation***

There were no casualties in any of the study groups. Doxorubicin administration was not associated with any adverse reaction during injection (i.e. no changes were noted in ECG or systolic arterial pressure during).

6.2.1 Effect on the microvasculature of an acute exposure to intracoronary doxorubicin

We have already reported in the previous objective that i.c injections of doxorubicin are not associated with any deterioration in LV systolic function until a certain cumulative dose is reached (i.e. after 4 biweekly 0.45 mg/Kg injections) [68]. In that original description of the model, the status of the vasculature during the subclinical stage of cardiotoxicity was not evaluated. In order to rule an acute deleterious effect that could arise from the local route of administration, we first wanted to study the acute effects of a single i.c doxorubicin injection. To this end, we evaluated in-vivo at rest (CMR-based absolute quantitative perfusion) and stressed (invasive CRF) microcirculation status before/after a single 0.45 mg/Kg doxorubicin i.c injection, as well as 48h and 2 weeks later (including histology at these time-points).

48 hours after a single i.c doxorubicin injection, CMR-based absolute quantitative perfusion and invasive CFR were not different from baseline ($199 \pm 40ml/100g/min$ vs 180 ± 29.3 for CMR-perfusion and 3.7 ± 1.22 vs 3.63 ± 0.45 for CRF at baseline and 48 hours respectively). 2 weeks after a single i.c doxorubicin injection, CMR-perfusion and CFR were again not different from baseline ($199ml/100g/min \pm 40$ vs 183 ± 49.2 for perfusion and 3.7 ± 1.22 vs 3.57 ± 0.9 for CRF at baseline and 2 weeks respectively) (**Figure 17, A and B**).

On histology, 48 hours and 2 weeks after a single i.c doxorubicin injection, a mild increase in the collagen content in the media layer of arteries of any size was the only structural abnormality observed. Arterioles from doxorubicin-treated pigs did not show any difference from control ones. **Figure 18, A**, pink and purple circles). Capillary density was not different in samples from pigs receiving one single i.c doxorubicin injection and controls at 48hours ($1470 \pm 310capillaries/mm2$ in controls vs. 1320 ± 259, p=0.1) nor at 2 weeks ($1470 \pm 310capillaries/mm^2$ vs. 1410 ± 227, p=1 for 2 weeks). **Figure 20, A and B**, pink and purple boxplots. In vivo and histological data in the remote region did not show any differences between animals receiving one single i.c injection of doxorubicin and controls (**Figure 19, B**).

No inflammatory component was found in any grade of lesion. Altogether, these data rule out an acute chemical damage induced by i.c doxorubicin injections.

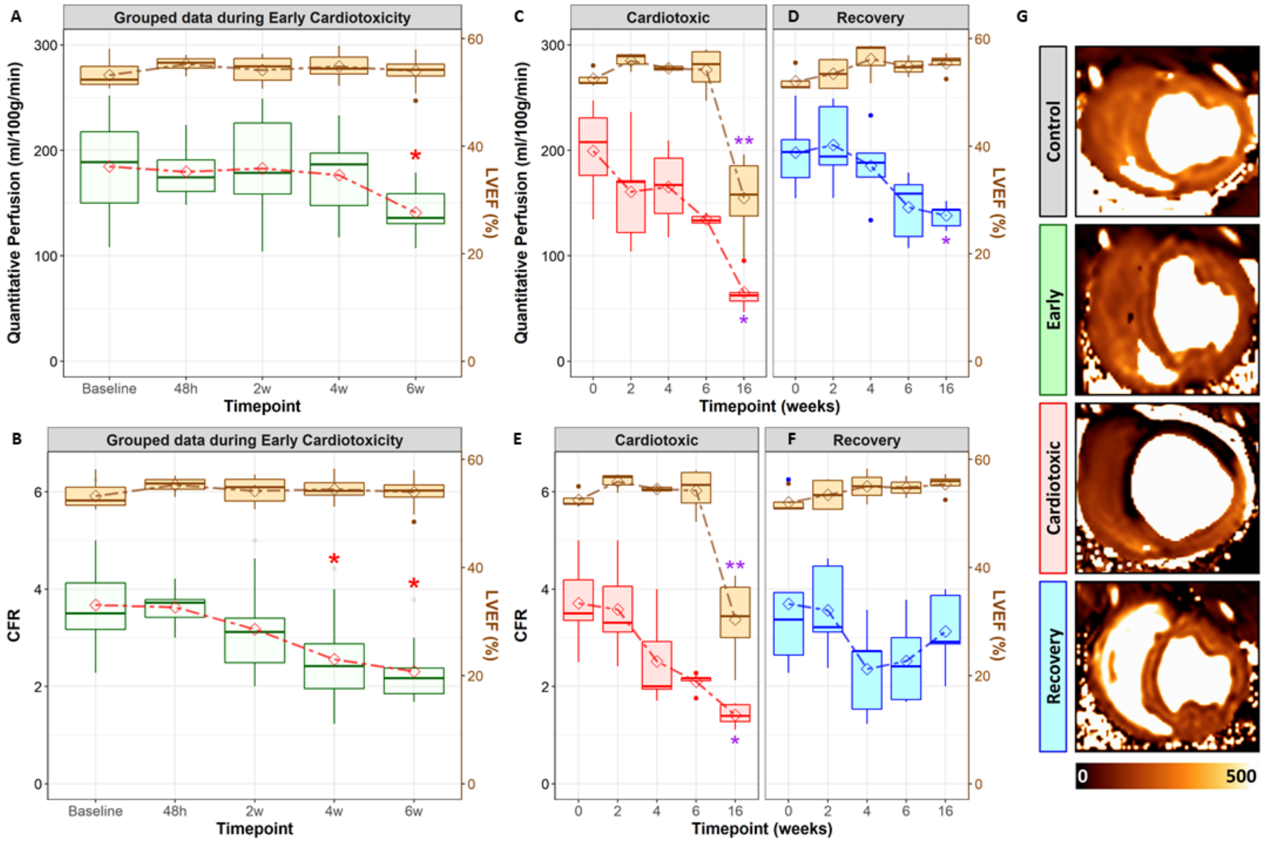

Figure 17: In-vivo functional microvascular assessment.

(A-B) Evolution over time from grouped data of Quantitative Perfusion, CFR and LVEF.

(C-F) Cardiotoxic and Recovery groups showed separately and followed in long-term until 16 weeks.

(G) Representative cardiac perfusion maps from Control, Early, Cardiotoxic and Recovery groups are shown in the left panel.

Asterisks indicate statistically significant statistical differences compared with week 0 for each time point:* p <0.05, ** p>0.01, *** p>0.001; ns, non-significant.

6.2.2 Trajectories of microcirculation status across anthracycline-induced cardiotoxicity stages

Early stages of (subclinical) cardiotoxicity:

As detailed before, from baseline to week 6 is the subclinical stage of cardiotoxicity in our model since no LV motion abnormalities are detected [68]. Given that all groups followed the shame study protocol until week 6 (including same anthracycline regime with doxorubicin injections on weeks 0, 2, and 4), CMR-based LVEF, CMR-based quantitative perfusion and invasive CRF data from all different groups were grouped.

As previous described [68], LVEF remained unchanged from baseline (pre-doxorubicin) to 6 weeks (i.e. 2 weeks after third dose), **Figure 17, A and B**, orange boxes. Conversely, CMR-based quantitative perfusion progressively declined, reaching significant differences compared to baseline by week 6 ($199 \pm 40ml/100g/min$ vs 141 ± 23.3 at baseline and after 3 biweekly doxorubicin doses respectively, p=0.012), **Figure 17, A**, green boxes. Functional evaluation of the microcirculation by invasive CFR showed a similar trend of progressive reduction across time. At 4 weeks the decline in CRF was already statistically significant ((3.7 ± 1.22 vs 2.44 ± 0.91 at baseline and after 2 biweekly doxorubicin doses respectively, p=0.03). At 6 weeks, CFR was even further reduced, **Figure 17, B**, green boxes (3.7 ± 1.22 vs 2.31 ± 0.65 at baseline and after 3 biweekly doxorubicin doses, p=0.04).

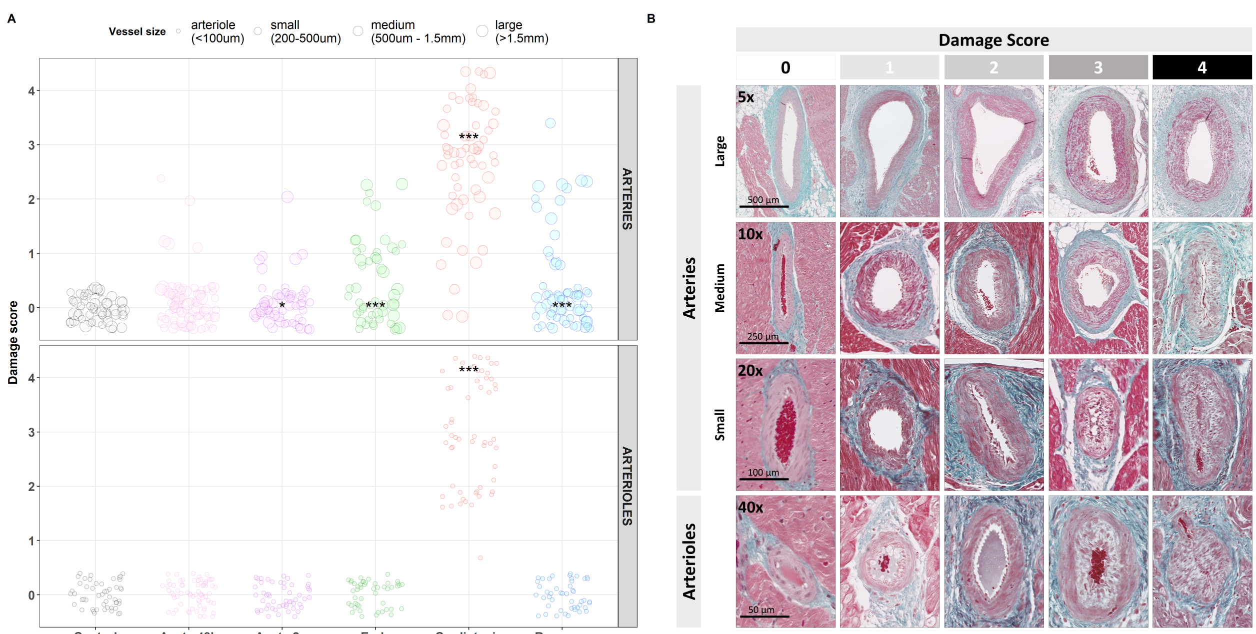

Figure 18: Histopathological findings regarding arterial niche.

(A) Dot plot representing each artery and arteriole and its associated damage score from all the animals divided by group.

(B) Representative images for each artery size and arteriole and their associated damage score with M staining (from 0 to 4).

Asterisks indicate statistically significant statistical differences compared with week 0 for each time point:* p <0.05, ** p>0.01, *** p>0.001; ns, non-significant.

Histological evaluation at 6 weeks (i.e. 2 weeks after the third biweekly doxorubicin injection) revealed structural alterations in arteries of all sizes (small, medium and large caliber); **Figure 18, A**, upper panel, green circles. Observed changes were mild but statistically significant compared to control arteries (p<0.001). Alterations included perivascular fibrosis, collagen infiltration in the media layer and mild vacuolization of smooth muscle cells (**Figure 18, B**). Capillary density quantification by CD31 immunohistochemistry at 6 weeks showed a non-significant decrease in the number of capillaries $(1090 \pm 344 capillaries/mm^2$ vs 1470 ± 310 in samples from doxorubicin-injected and controls respectively, p=0.43). **Figure 20, A and B** green boxplot and "early" labeled. Conversely, arterioles architecture was preserved at 6 weeks in animals injected with doxorubicin, **Figure 18, A and B**, lower panels.

In vivo (perfusion and CRF) trajectories and histology evaluation at 6 weeks in the remote region were overall attenuated in the remote than in the infused region (**Figure 19, A**).

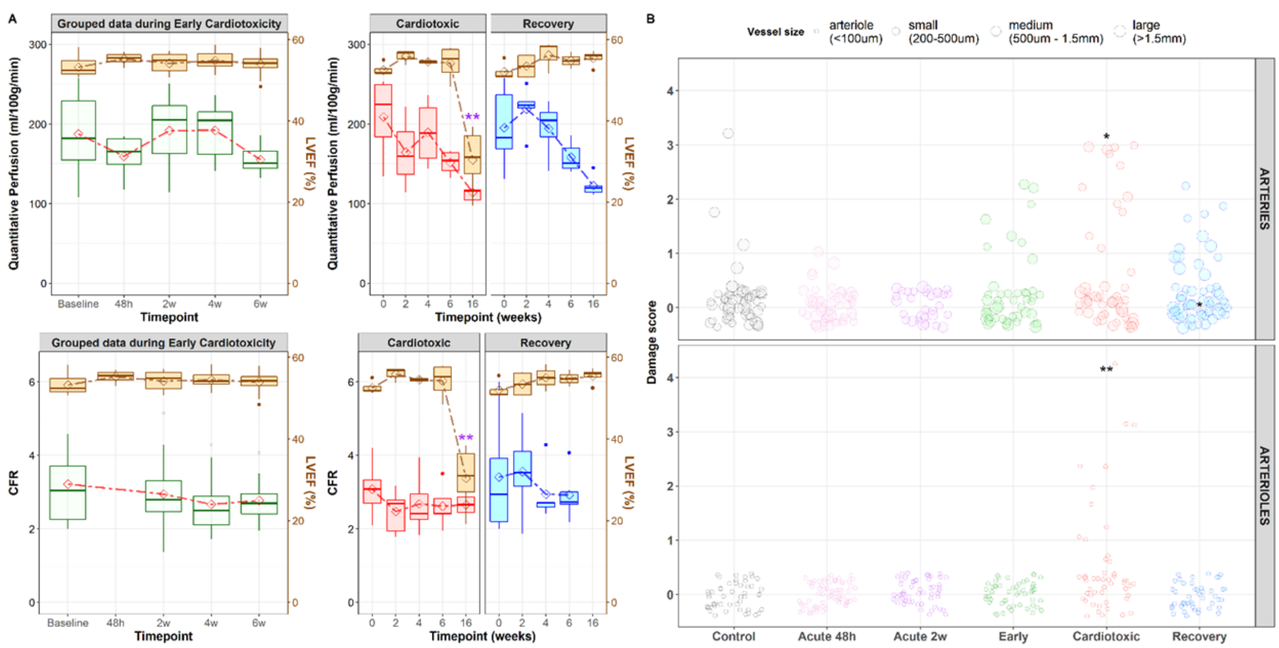

Figure 19: Functionally and anatomopathological data from the remote area.

(A) Quantitative perfusion and CFR values from grouped data during early cardiotoxicity development and from Cardiotoxic and Recovery groups in long-term.

(B) Individual damaged score from arteries of every size and arterioles in all the study groups.

Asterisks indicate statistically significant statistical differences compared with week 0 for each time point:* p <0.05, ** p>0.01, *** p>0.001; ns, non-significant.

Overt cardiotoxicity stages:

There was a significant decline in LVEF between 6 weeks and 16 weeks follow-up. At 16 weeks, there was a very severe LV systolic depression evidencing the overt cardiotoxicity after 5 biweekly doxorubicin injections ($52.5 \pm 1.5\%$ vs. 30.4 ± 7.7 at baseline and 16 weeks respectively, p=0.01). CMR-based quantitative perfusion, which was already reduced at 6 weeks, further and largely declined at week 16 ($135 \pm 4.9 ml/100g/min$ vs. 65.4 ± 18.2 at 6 and 16 weeks respectively, p=0.008, **Figure 17, C**, red boxes. Invasive functional evaluation of the microcirculation showed a similar pattern of progressive decline in CFR, reaching its lowest value at 16 weeks follow-up (2.1 ± 0.2 vs. 1.41 ± 0.23 at 6 and 16 weeks respectively, P=0.003), **Figure 17, E**, red boxes.

Histological evaluation at 16 weeks (i.e. 8 weeks after the fifth (last) biweekly doxorubicin injection) revealed a massive injury at arterial and arteriolar levels (p<0.001 compared with control group), **Figure 18, A**. Structural alterations in arteries of all sizes (small, medium and large caliber) and arterioles included moderate to severe tunica intima hyperplasia with luminal stenosis or massive loss of smooth muscle cells in tunica media with extracellular matrix replacement **Figure 18, B**. Capillary density evaluation showed a massive loss of capillaries at these late stages of cardiotoxicity ($1470 \pm 310 capillaries/mm2$ vs 394 ± 271 in controls vs 16 weeks, p<0.001). **Figure 20, A and B** red boxplot and "cardiotoxic" labeled.

In vivo (perfusion and CRF) trajectories and histology evaluation at 16 weeks in the remote region followed a same pattern than in the infused region (significant deterioration of structural and functional microvascular structure), albeit the effect size was attenuated (**Figure 19**).

6.2.3 Reversibility of anthracycline-induced microvascular alterations

Once cardiotoxicity is overt (i.e. clinical stage), the induced damage already passed a no-return point both in terms of LV systolic function and microvascular alterations, as seen in previous section. Here we wanted to explore the persistence or reversibility of the microvascular alterations (anatomical and functional) induced by doxorubicin at 6 weeks (i.e. in the subclinical stages of the disease). To this end, we evaluated microvascular trajectories and histological alterations long after completion of a three biweekly doxorubicin injections (i.e. subclinical cardiotoxicity protocol). Animals in the "recovery" group were followed up until week 16 (i.e. 12 weeks after last (third) i.c doxorubicin injection), and underwent serial in vivo microvascular evaluations (CMR-perfusion and invasive CFR), and histology evaluation at the end of the protocol.

LVEF was unaltered at 6 weeks, and remained the same at 16 weeks follow-up ($53.7 \pm 4.21\%$ vs. 57.1 ± 4.05 at baseline and 16 weeks respectively, p = 0.14). CMR-based quantitative perfusion was reduced at 6 weeks (described above), and remained reduced at 16 weeks ($146 \pm 31.5 ml/100g/min$ vs 138 ± 11.9 at 6 and 16 weeks respectively, p=0.63), **Figure 18, D**. A similar pattern was observed when CRF was evaluated invasively (3.52 ± 10.89 vs. 3.13 ± 0.82 at baseline and 16 weeks respectively, p=0.13), **Figure 18, F**.

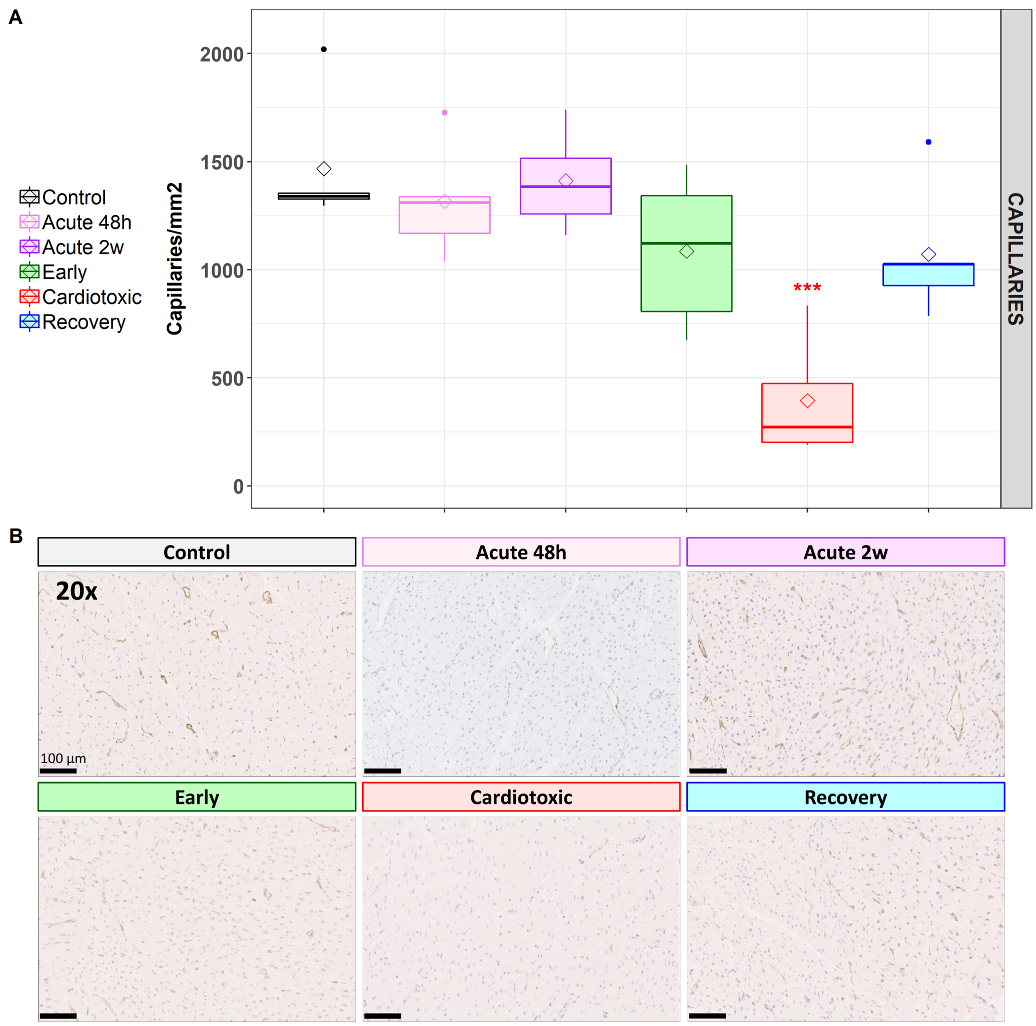

Figure 20: Capillary density in all groups.

(A) Boxplots for each study group indicating capillary density values.

(B) Representative CD31 staining images for each group.

Asterisks indicate statistically significant statistical differences compared with week 0 for each time point:* p <0.05, ** p>0.01, *** p>0.001; ns, non-significant.

Histological evaluation at the end of the 16 weeks protocol in the "recovery" group (3 biweekly doxorubicin injections followed-up until week 16) showed a similar pattern to that seen at 6 weeks (mild collagen infiltration and muscular vacuolization of the media layer of all-sized arteries without any visible damage on arterioles) (**Figure 18, A**, blue circles). Similar to what was seen at 6 weeks, capillary density was non-significantly reduced at 16 weeks ($1470 \pm 310 capillaries/mm^2$ in controls vs. 1070 ± 307, p=0.4), (**Figure 20, A and B**, blue boxplot). Data in remote myocardium showed a similar pattern but attenuated in its magnate (**Figure 19**).

6.3 Objective 3: *Vulnerability of the hypertrophied heart to anthracycline-induced cardiotoxicity*

6.3.1 Survival probability during anthracycline-induced cardiotoxicity development in animals with pressure afterload

For the mortality study, humanitarian sacrifice due to myelosuppression and other side effects of i.v anthracycline administration were considered as censored times. Similarly, peri-mortality secondary to aortic banding surgery complication was treated as well as censored event for the analysis. For this purpose, first 7 animals performed per group were included. Due to the mortality, individuals that died during this part of the experiment were replaced in order to maintain the calculated sample size for the main objective in this study (cardiotoxicity evidenced as significant differences in LVEF between groups). During the experiment, animals with aortic banding receiving doxorubicin treatment showed significant higher mortality than the rest of the groups (p=0.006): 1 animal was found dead during anthracycline treatment and 2 more in the next 3 months. Only 1 animal was to be sacrificed in both doxorubicin groups (Banding and No banding) because secondary deterioration due to anthracycline exposure. None of the animals died in both control groups (Banding and No banding). Kaplan-Meier curves and number at risk are represented in **Figure 21**. As is pointed before, new animals were enrolled because the mortality to complete the sample of 7 pigs per group: 1 new animal in No banding + doxo group and 6 in Banding + doxo group (3 also died during the experiments).

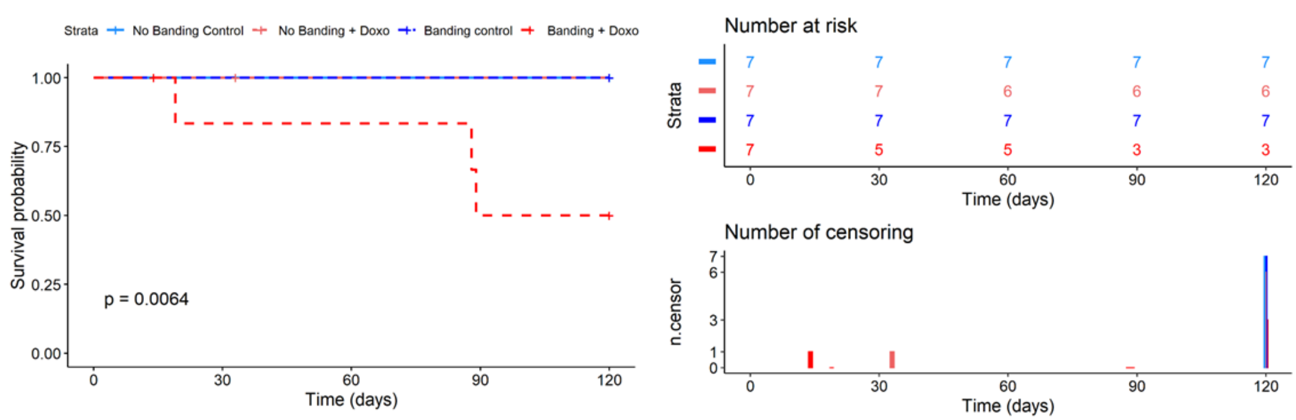

Figure 21: Kaplan-Meier survival curves with number at risk and number of censoring for all the groups.

6.3.2 Cardiac magnetic resonance evidences of cardiotoxicity development in animals with aortic banding surgery

For both CMR sequences, functional and mapping, two-way factorial ANOVA was performed taking in account doxorubicin administration but also aortic banding surgery effect in the several imaging parameters.

Functional cardiotoxicity development in animals with pressure overload:

All animals underwent aortic banding surgery developed pressure overload with hyperkinetic phenotype at 0 months ($76.6\% \pm 6.64$ in control and 77.3 ± 8.65 in doxo). Those individuals that received i.v doxorubicin started to decrease their LV function at the end of systemic anthracycline treatment ($68.7\% \pm 12.9$ at 1 month), suffering a detrimental dysfunction until the end of the study at 4 months ($46.9\% \pm 8.67$). Aversely, control animals with only aortic stenosis surgery, continued increasing their hyperkinetic profile; which resulted in cardiac hypertrophy at 4 months, and showed significant differences compared with Banding + doxo group ($84.0\% \pm 4.83$ vs 46.9 ± 8.67; p<0.001). (**Figure 22, A** "over time" plot, banding panel). "No banding" animals from both groups (doxo and control) started with the same LV function at time 0 ($58.6\% \pm 2.68$ in control and 57.6 ± 4.71 in doxo) with little changes over time until the end of the experiment at 4 months, but no significant differences between them ($64.2\% \pm 3.53$ in control vs 62.4 ± 3.61 in doxo; p=0.56). Considering the aortic banding surgery effect itself, differences were found in both groups, control animals ($64.2\% \pm 3.53$ in "no banding" vs 84.0 ± 4.83 in "banding"; p<0.001) and animals receiving systemic anthracyclines therapy ($62.4\% \pm 3.61$ in "no banding" vs 46.9 ± 8.67 in "banding"; p<0.001). (**Figure 22, A** "4 months" plot and **Figure 22, E**).

Indexed LV mass and volumes concordantly changed according LV function. LV mass differences were statistically significant at 4 months only in control animals developing cardiac hypertrophy after aortic banding surgery compared with "No banding" controls ($102g.indx. \pm 27.3$ vs 62 ± 12.0; p=0.03). However, no differences were found in the rest of comparisons, neither in doxo animals underwent surgery compared with "No banding" doxo pigs ($101g.indx. \pm 37.2$ vs 69.3 ± 6.89; p=0.07), nor in "No banding" animals ($62g.indx. \pm 12.0$ in control vs 69.3 ± 6.89 in doxo; p=1) nor "Banding" groups ($102g.indx. \pm 27.3$ in control vs 101 ± 37.2 in doxo; p=1) (**Figure 22, B and E**).

Indexed LV end-diastolic volumes did not show any statistical differences in any comparison: "Banding control" vs "Banding + doxo" ($69.4ml.indx. \pm 12.3$ vs 84.8 ± 19.5; p=0.32), "No Banding control" vs "No Banding + doxo" ($68.7ml.indx. \pm 14.4$ vs 76.5 ± 11.9; p=1), "Banding control" vs "No Banding control" ($69.4ml.indx. \pm 12.3$ vs 68.7 ± 14.4; p =1) and "Banding + doxo" vs "No banding + doxo" ($84.8ml.indx. \pm 19.5$ vs 76.5 ± 11.9; p=1). However, they were always higher in animals receiving anthracyclines and reaching the highest value in "Banding + doxo" pigs (**Figure 22, C and E**).

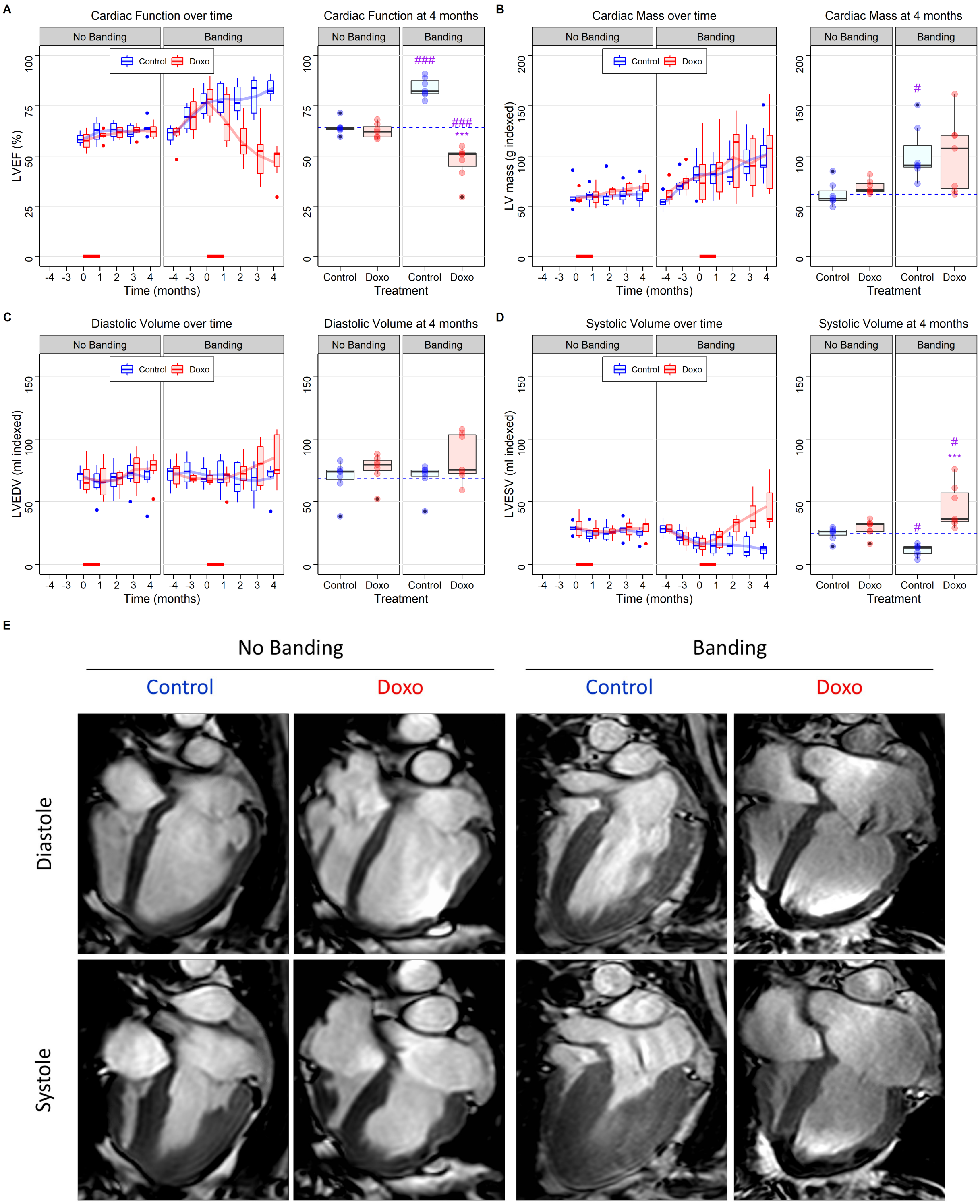

Figure 22: CMR functional parameters over time and at 4 months of study.

(A) LVEF data, (B) LV mass (indexed) data, (C) LVEDV (indexed) and (D) LVESV (indexed) data.

(E)Representative CMR CINE images for each group.

(#) represents differences between “No banding” and “Banding” groups (for controls and doxo) and (*) represents differences between “Control” and “Doxo” groups (for “Banding” and “No Banding”). */# for p < 0.05, **/## for p < 0.01 and ***/### for p < 0.001.

Indexed LV end-systolic volumes changed accordingly LVEF, showing statistically significant differences evaluating doxorubicin administration effect in operated animals ($11.5ml.indx. \pm 4.61$ in controls vs 46.2 ± 17.5 in doxo; p<0.001), but also banding effect itself in both doxorubicin administrated groups ($29.0ml.indx. \pm 6.57$ in “No Banding” vs 46.2 ± 17.5 in “Banding”; p=0.012). Differences were also identified in control animals underwent aortic banding surgery compared with “No Banding” control animals ($24.5ml.indx. \pm 5.19$ in “No Banding” vs 11.5 ± 4.61 in “Banding”; p=0.046) but not among “No Banding” groups ($24.5ml.indx. \pm 5.19$ in control vs 29.0 ± 6.57 in doxo; p=0.4) (**Figure 22, D and E**).

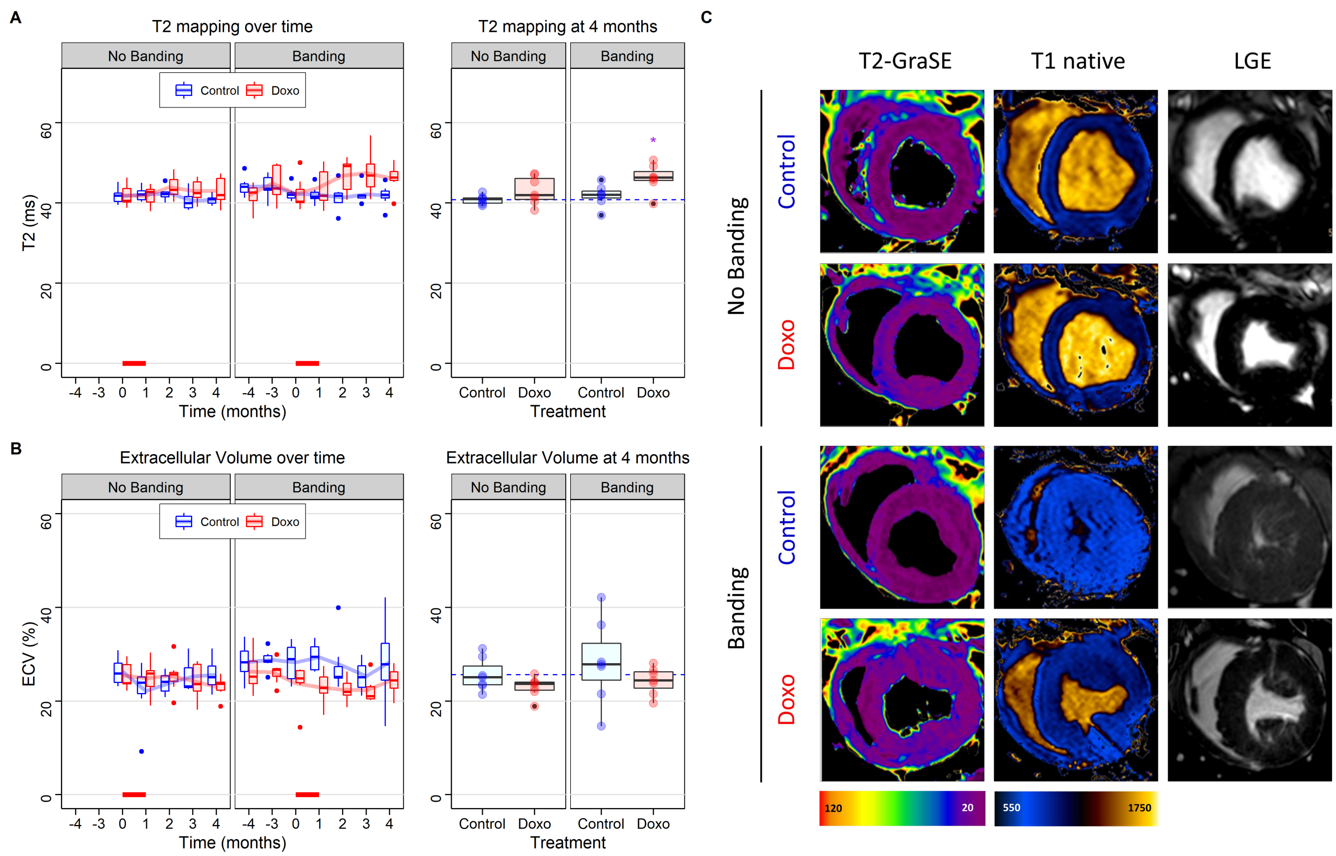

Figure 23: CMR mapping values over time and at 4 months.

(A) T2-GraSE mapping values.

(B) ECV mapping values.

(C) Representative short axis myocardial images by group for T2-GraSE, Native T1 and LGE.

(#) represents differences between “No banding” and “Banding” groups (for controls and doxo) and (*) represents differences between “Control” and “Doxo” groups (for “Banding” and “No Banding”). */# for p < 0.05, **/## for p < 0.01 and ***/### for p < 0.001.

Tissue in-vivo characterization of cardiotoxicity development in animals with pressure overload:

Firstly, T2-GraSE mapping were acquired and a septal ROI was traced in the anteroseptal wall. Only animals with aortic banding surgery that received anthracyclines showed increased T2 values in that area compared only with operated control animals ($41.8ms \pm 2.72$ in control vs 46.2 ± 17.5 in doxo; p=0.043). No differences were found in the rest of comparisons: "No Banding + doxo" vs "Banding + doxo" ($43.0ms \pm 3.52$ vs 46.2 ± 17.5; p=0.2), "No Banding control" vs "Banding control" ($40.8ms \pm 1.15$ vs 41.8 ± 2.72; p=0.88), nor "No Banding control" vs "No Banding + doxo" ($40.8ms \pm 1.15$ vs 43.0 ± 3.52; p=0.46) (**Figure 23, A and C**).

ECV maps did not show differences in any comparison: "Banding control" vs "Banding + doxo" ($28.3\% \pm 9.03$ vs 24.3 ± 2.97; p=0.70), "No Banding + doxo" vs "Banding + doxo" ($23.0\% \pm 2.17$ vs 24.3 ± 2.97; p=1), "No Banding control" vs "Banding control" ($25.6\% \pm 3.51$ vs 28.3 ± 9.03; p=1), nor "No Banding control" vs "No Banding + doxo" ($25.6\% \pm 3.51$ vs 23.0 ± 2.17; p=1) (**Figure 23, B and C**).

Ex-vivo evaluation of doxorubicin administration impact in cardiac tissue :

According to ECV mapping data, histological analysis revealed no changes in collagen fraction area in Sirius Red staining; with no differences between any comparison: "Banding control" vs "Banding + doxo" ($8.78\% \pm 2.05$ vs 12.1 ± 3.59; p=0.67), "No Banding + doxo" vs "Banding + doxo" ($11.5\% \pm 8.36$ vs 12.1 ± 3.59; p=0.82), "No banding control" vs "Banding control" ($16.0\% \pm 2.46$ vs 8.78 ± 2.05; p = 0.1), nor "No banding control" vs "No banding + doxo" ($16.0\% \pm 2.46$ vs 11.5 ± 8.36; p=0.67). Showing that no myocardial fibrosis is developed with aortic banding surgery nor anthracycline administration or combination (**Figure 24, A and B**).

Regarding histopathological analyses in H-E staining; while control animals (operated and non-operated) had a normal tissue composition with no changes nor alterations; animals that received low i.v regimes of systemic anthracyclines 4 months after aortic banding surgery developed doxorubicin-induced cardiotoxic anatomopathological findings. Those alterations consisted in severe intra-cardiomyocyte vacuolization, cardiac fiber disorganization in absence of any inflammatory infiltration. Animals with no banding in which the same regime of anthracyclines were administrated, developed a very mild version of anthracycline lesions with few vacuole formations and no additional structural changes (**Figure 24, C and D**).

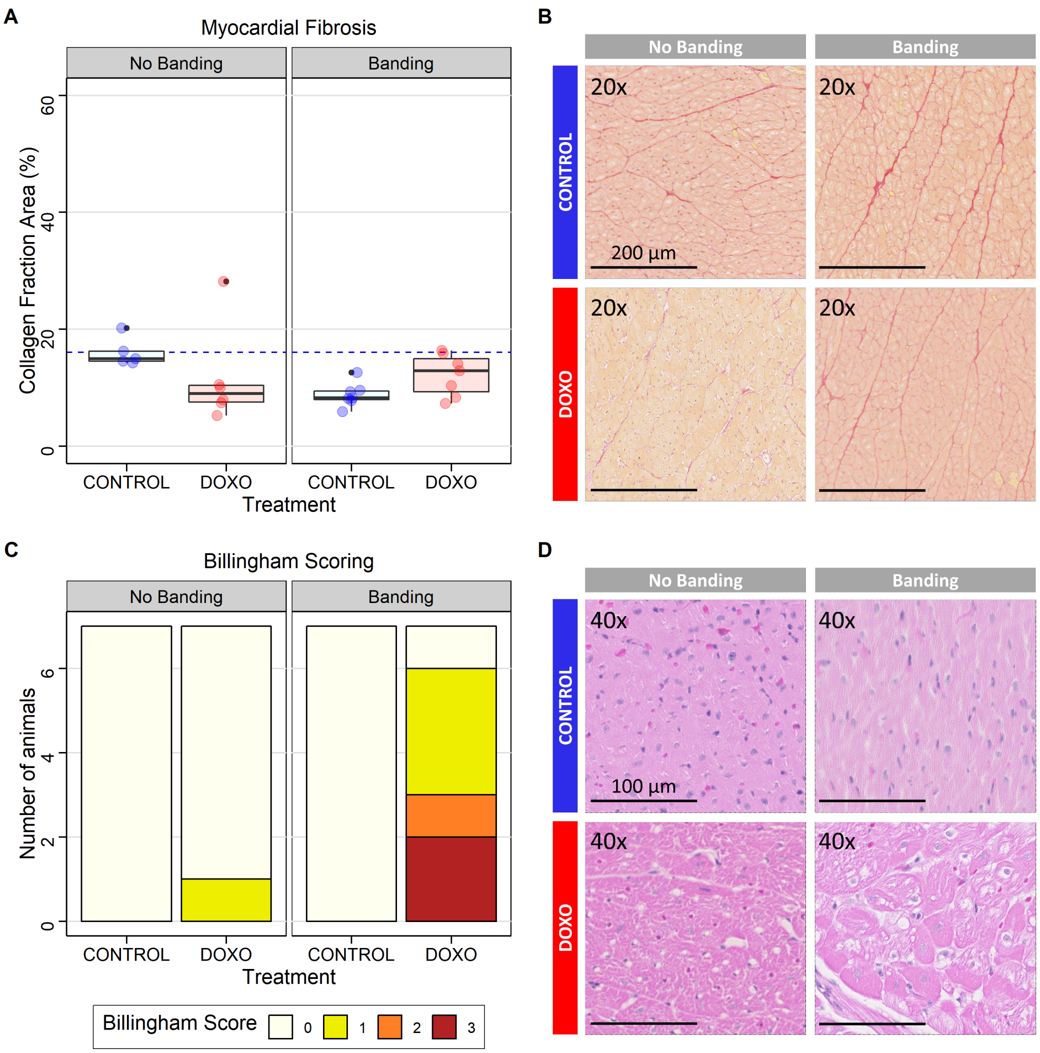

Figure 24: Ex vivo tissue characterization.

(A) Collagen Fraction Area in the LV anterior wall.

(B) Representative SR staining images from each group.

(C) Billingham score evaluation represented in stacked barplots.

(D) Representative HE intra-cardiomyocyte vacuolization from each group.

(#) represents differences between "No banding" and "Banding" groups (for controls and doxo) and (*) represents differences between "Control" and "Doxo" groups (for "Banding" and "No Banding"). */# for $p < 0.05$, **/## for $p < 0.01$ and ***/### for $p < 0.001$.

6.4 Objective 4: *Remote ischemic preconditioning and anthracycline-induced cardiotoxicity*

One pig of RIPC+DOXO Group died after the third anthracycline injection due to experimental procedure. This pig was replaced by another to maintain calculated sample size.

6.4.1 Effect of remote ischemic preconditioning in cardiac function during cardiotoxicity development

Animals underwent RIPC protocol before each doxorubicin administration showed a borderline statistically significant better LVEF at 16 weeks compared with DOXO group ($41.5\% \pm 9.1$ vs 32.5 ± 8.7; p=0.04). These differences can be observed at week 12, once cardiac dysfunction have already taken place ($43.2\% \pm 8.1$ vs 33.4 ± 9.1) and seem to be maintained until the end of the study (**Figure 25, A**).

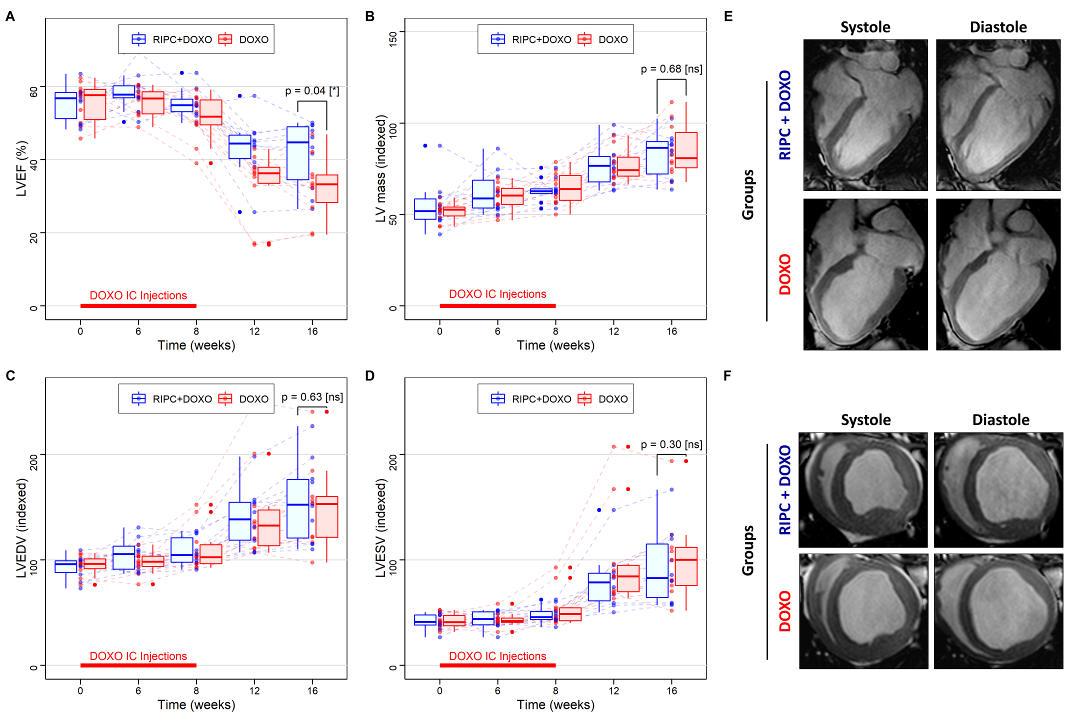

Figure 25: Effect of RIPC during ACT: functional serial evaluation by CMR.

(A) LVEF, (B) LV mass (indexed), (C) LVEDV (indexed) and (D) LVESV (indexed).

(E-F) Panels showing representative 4 chamber and short axis views from RIPC+DOXO and DOXO groups for systolic and diastolic phases. Asterisks indicate statistically significant differences comparing RIPC+DOXO vs DOXO group at 16 weeks: : ns p > 0.05, * p <0.05, ** p < 0.01 and *** p < 0.001.

This amelioration in LVEF was accompanied by lower LVEDV ($156.0 ml.indx. \pm 38.4$ vs 168.0 ± 69.7; p=0.63, **Figure 25, C, E and F**) and LVESV ($93.1 ml.indx. \pm 35.2$ vs 118.0 ± 64.3; p=0.30, **Figure 25, D, E and F**) in RIPC+DOXO group compared with DOXO group, but these differences were not statistically significant. Regarding LV mass values, once again, differences were not statistically significant between both groups ($82.9 ml.indx. \pm 12.4$ vs 85.4 ± 14.3; p=0.68, **Figure 25, B**).

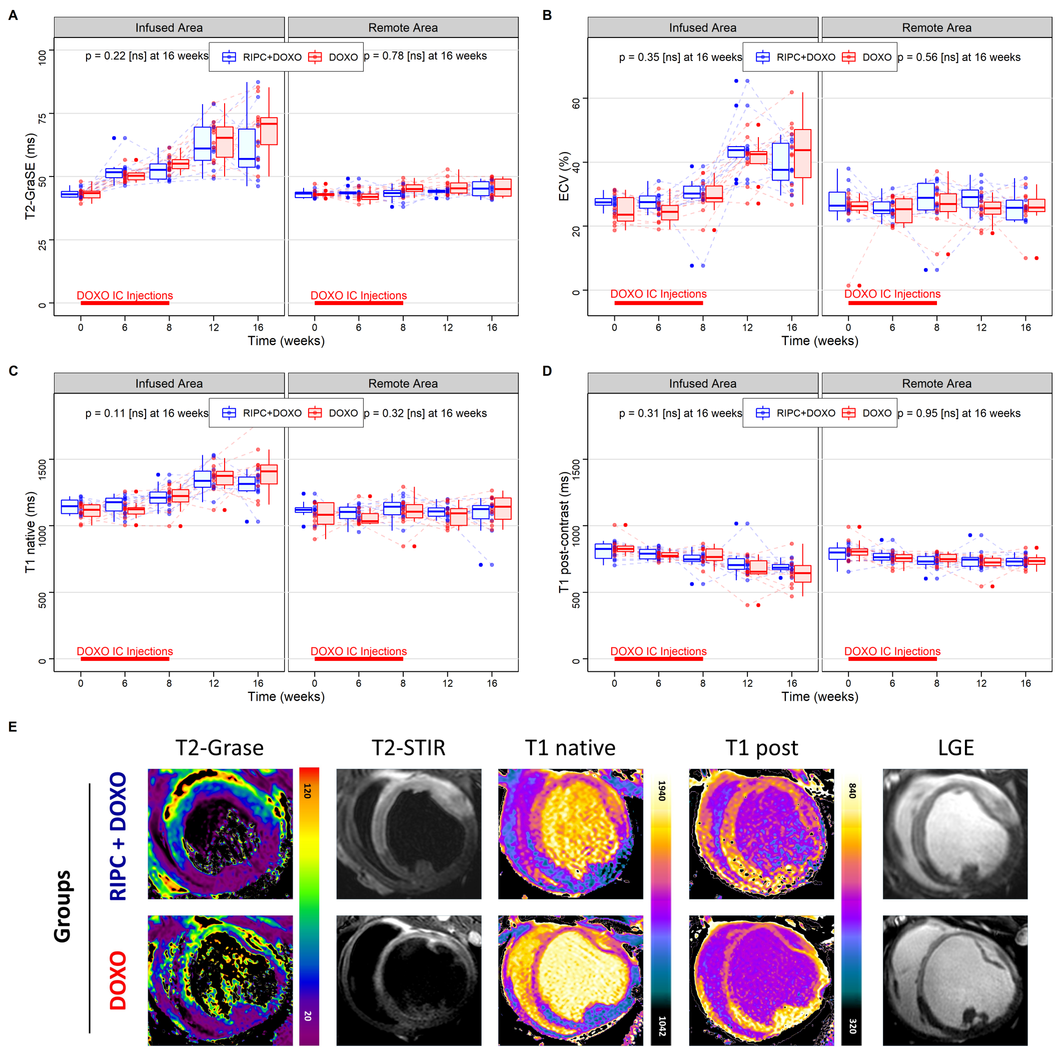

Figure 26: Effect of RIPC during ACT: mapping serial evaluation by CMR.

(A) T2-GraSE, (B) ECV, (C) T1-MOLLI native and (D) T1-MOLLI post-contrast values for infused and remote areas in both groups.
(E-F) Panels showing representative images of T2-GraSE, T2-STIR, T1 native and post contrast and Late Gadolinium Enhancement from RIPC+DOXO and DOXO groups.
Asterisks indicate statistically significant differences comparing RIPC+DOXO vs DOXO group at 16 weeks: : ns p > 0.05, * p <0.05, ** p < 0.01 and *** p < 0.001.

6.4.2 Effect of remote ischemic preconditioning in cardiac magnetic resonance tissue characterization during cardiotoxicity development

T2-GraSE mapping and water content analysis:

As we reported before [68], T2 elongation took place at early timepoint (6 weeks), during subclinical stages, and was maintained elevated in the Infused Area during anthracycline-induced cardiotoxicity development in both groups, RIPC+DOXO ($43.3ms \pm 1.8$ at basal vs 52.2 ± 5.2 at 6 weeks; p=0.008, vs 52.9 ± 4.4 at 8 weeks; p<0.001, vs 62.8 ± 9.3 at 12 weeks; p<0.001, vs 61.9 ± 13.8 at 16 weeks; p=0.01) and DOXO ($43.2ms \pm 2.4$ at basal vs 50.5 ± 2.6 at 6 weeks; p=0.001, vs 55.2 ± 3.2 at 8 weeks; p<0.001, vs 64.3 ± 8.7 at 12 weeks; p=0.001, vs 69.0 ± 11.1 at 16 weeks; p<0.001). At 16 weeks RIPC+DOXO group showed lower T2 values than DOXO group; however, these differences were not significant between them ($61.9ms \pm 13.8$ in RIPC+DOXO vs 69.0 ± 11.1 in DOXO; p=0.22, **Figure 26 A, and E**, left panel and first column). As we also reported before [68], no changes in Remote Areas were noticed in any of both groups (**Figure 26 A, and E**, first and second columns).

Ex-vivo tissue characterization revealed increase in water content in both groups with no differences between them ($83.0 \pm 1.2\%$ in RIPC+DOXO vs 82.9 ± 1.8 in DOXO; p=0.92, **Figure 27 A**). Classical doxorubicin-cardiotoxicity lesions consisted in muscle fibber disarray and intra-cardiomyocyte vacuolization could be observed in HE sections in both groups (**Figure 27 C**, upper panels).

T1-MOLLI native and post-contrast, ECV expansion and collagen content:

As in T2 assessment during anthracycline-induced cardiotoxicity development, T1 native and post-contrast, as well as, ECV result were equal as we previously reported [68].

T1 native started to increase once LVEF deterioration is already present, at 12 weeks, for both groups: RIPC+DOXO ($1150ms \pm 58$ at basal vs 1160 ± 71 at 6 weeks; p=1, vs 1220 ± 90 at 8 weeks; p=0.35, vs 1360 ± 112 at 12 weeks; p=0.01, vs 1300 ± 109 at 16 weeks; p=0.02), and DOXO ($1110ms \pm 63$ at basal vs 1120 ± 68 at 6 weeks; p=1, vs 1210 ± 98 at 8 weeks; p=0.23, vs 1350 ± 108 at 12 weeks; p=0.003, vs 1410 ± 108 at 16 weeks; p=0.01). At 16 weeks, RIPC+DOXO group showed lower T1-native values than DOXO group; however, these differences were not significant between them ($1300ms \pm 109$ in RIPC+DOXO vs 1410 ± 108 in DOXO; p=0.11, **Figure 26 C and E**, left panel and third column).

Similarly, T1 post-contrast started to significantly change once LVEF deterioration was already present, at 12-16 weeks, for both groups: RIPC+DOXO ($809ms \pm 64$ at basal vs 790 ± 43 at 6 weeks; p=1, vs 742 ± 74 at

8 weeks; p=0.4, vs 725 ± 116 at 12 weeks; p=1, vs 697 ± 42 at 16 weeks; p=0.003), and DOXO ($838ms \pm 66$ at basal vs 778 ± 30 at 6 weeks; p=0.21, vs 775 ± 62 at 8 weeks; p=0.13, vs 665 ± 109 at 12 weeks; p=0.02, vs 647 ± 114 at 16 weeks; p=0.008). At 16 weeks, RIPC+DOXO group showed higher T1 post-contrast values than DOXO group; however, these differences were not significant between them ($697ms \pm 42$ in RIPC+DOXO vs 647 ± 114 in DOXO; p=0.31, **Figure 26 D and E**, left panel and fourth column). As we also reported before(95), no changes in Remote Areas were noticed in any of both groups (**Figure 26 B-D and E**, right panel; and third, fourth and fifth columns).

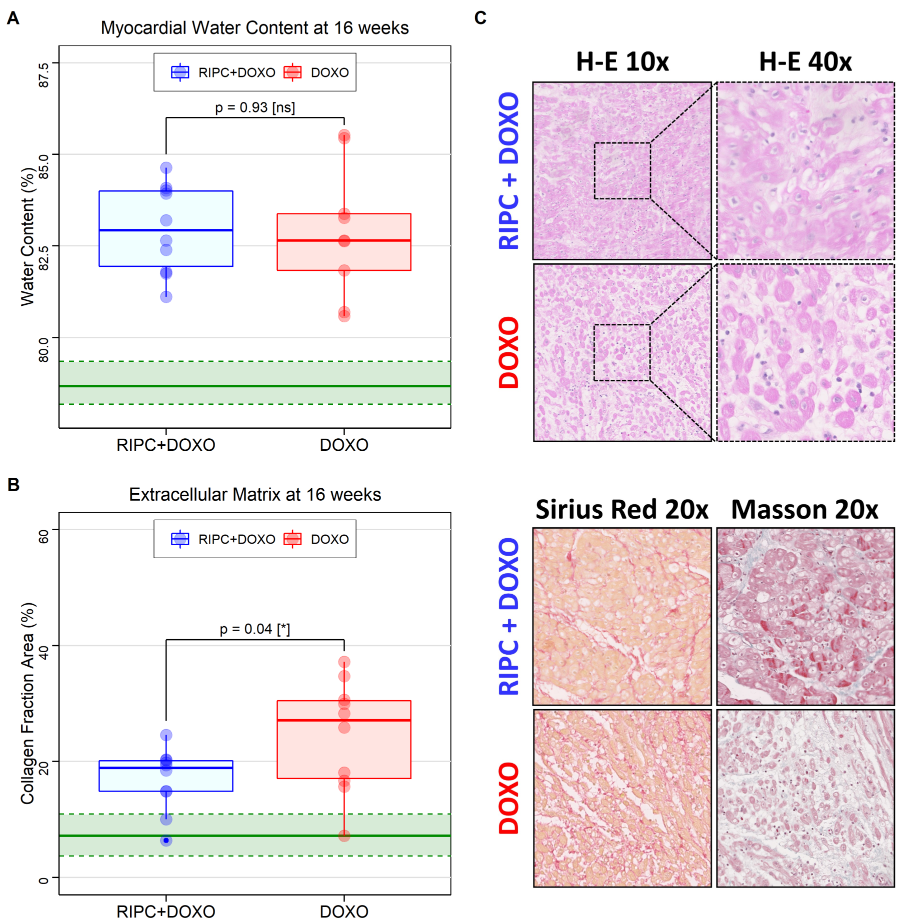

Figure 27: Effect of RIPC at late stages of anthracycline-induced cardiotoxicity: ex-vivo evaluation.

(A) Myocardial Water Content and (B) Collagen Fraction Area values in Infused Area for both groups at 16 weeks.

(C) Panels showing representative images HE (upper panels) or SR and M staining (lower panels) from RIPC+DOXO and DOXO groups. Asterisks indicate statistically significant differences comparing RIPC+DOXO vs DOXO group at 16 weeks: : ns p > 0.05, * p <0.05, ** p < 0.01 and *** p < 0.001.

For ECV results were pretty much the same, beginning to significantly change once LVEF deterioration is already present, at 12 weeks, for both groups: RIPC+DOXO ($27.5\% \pm 2.14$ at basal vs 27.8 ± 3.0 at 6 weeks; p=1, vs 29.1 ± 8.2 at 8 weeks; p=1, vs 45.1 ± 9.7 at 12 weeks; p=0.003, vs 39.3 ± 6.9 at 16 weeks; p=0.007), and DOXO ($24.8\% \pm 4.6$ at basal vs 24.6 ± 3.6 at 6 weeks; p=1, vs 29.4 ± 5.4 at 8 weeks; p=0.5, vs 41.0 ± 7.1 at 12 weeks; p=0.003, vs 43.2 ± 10.9 at 16 weeks; p=0.007). At 16 weeks, RIPC+DOXO group showed lower ECV values than DOXO group; however, these differences were not significant between them ($39.3\% \pm 6.9$ in RIPC+DOXO vs 43.2 ± 10.9 in DOXO; p=0.35, **Figure 26 B and E**, left panel and fifth column). As we also reported before [68], no changes in Remote Areas were noticed in any of both groups (**Figure 26 B-D and E**, right panel; and third, fourth and fifth columns). Nevertheless, borderline statistically significant differences were observed regarding collagen fraction area in the Sirius Red staining for the Infused Area; being the percentage of Collagen lower in the RIPC+DOXO group than in the DOXO group ($16.9\% \pm 5.4$ vs 24.4 ± 9.6; p=0.04, **Figure 27 B and C**, left panel and lower panel).

6.4.3 Effect of remote ischemic preconditioning in heart metabolism during cardiotoxicity development

In order to explore metabolic changes during and at late stages of anthracycline-induced cardiotoxicity, PET scans at baselines, 8 weeks (just before the last doxorubicin IC injection) at 16 weeks (before animal sacrifice) as well as mitochondrial TEM and WEB analysis at 16 weeks were performed in both groups.

FDG uptake during ACT development:

PET counts were measured in Infused and Remote areas and normalized by counts in pectoral muscle in order to reduce variability. In both groups, an increase in glucose uptake was notice in the Infused Area at 8 weeks during subclinical cardiotoxicity development, with no deterioration in LVEF nor T1 or ECV mapping (**Figure 28, A and C**). Despite of counts of radiotracer were lower for RIPC+DOXO group for both areas, differences were not statistically significant at 16 weeks in Infused (9.98 ± 2.95 vs 10.20 ± 8.65; p=0.93,**Figure 28, A and C**) and Remote area (6.28 ± 4.00 vs 10.30 ± 17.80; p=0.5, **Figure 28, B and C**).

Impact of RIPC in mitochondrial quality control:

Ex-vivo mitochondrial TEM analysis at 16 weeks revealed higher mitochondrial size in healthy control animals compared with RIPC+DOXO and DOXO animals, but mitochondria from RIPC-treated groups preserved their size more like healthy controls compared with DOXO individuals ($0.19 \mu m2 \pm 0.23$ vs 0.14 ± 0.19 [$median \pm IQR$]; p<0.001, **Figure 29, A**).

Density curves also pointed that area distribution shapes from RIPC+DOXO group were located between DOXO and healthy controls (**Figure 29, B**). Both groups treated with doxorubicin showed a greater number of mitochondria compared with healthy control but with no statistically significant differences between them ($291 mitochondria \pm 10$ vs 270 ± 80; p=0.70, **Figure 29, C**)

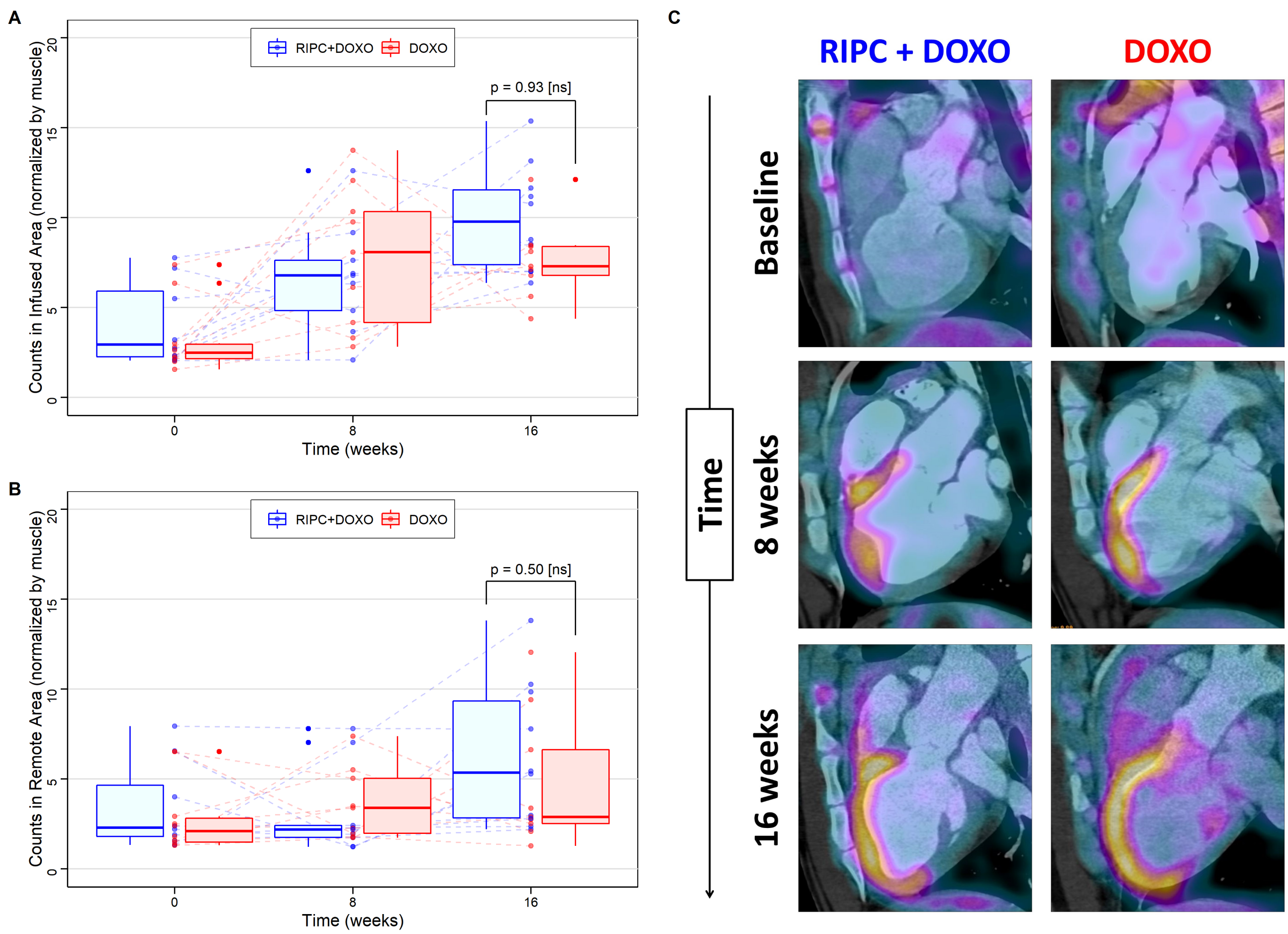

Figure 28: Effect of RIPC during ACT: glucose uptake serial evaluation by PET scan.

(A) Infused and (B) Remote for both groups over time.

(C) Panels showing representative images of PET-CT reconstructed studies from RIPC+DOXO and DOXO groups for each timepoint.

Asterisks indicate statistically significant differences comparing RIPC+DOXO vs DOXO group at 16 weeks: : ns p > 0.05, * p < 0.05, ** p < 0.01 and *** p < 0.001.

Regarding mitochondrial morphology evaluation, while healthy mitochondria presented a round shape with their cristae well defined, organelles from RIPC+DOXO group lose their shape and presented intra-matrix vacuolization. In the DOXO group, mitochondria shape was quite aberrant, elongated and irregular, their cristae were so affected and thickened, and their matrix was highly condensed (**Figure 29, D**).

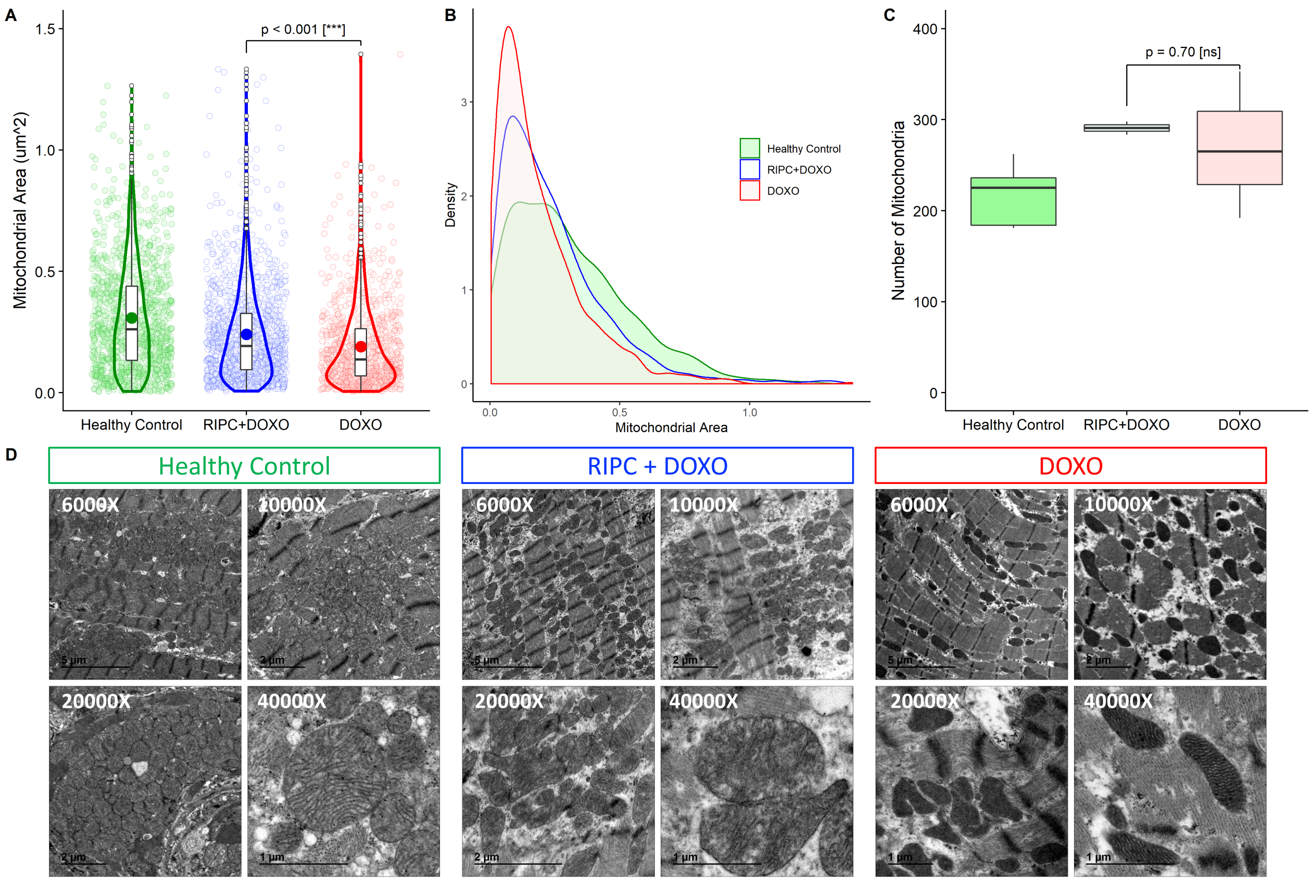

Figure 29: Effect of RIPC at late stages of ACT: Mitochondrial TEM evaluation.

(A) Mitochondrial Area for each mitochondrion in the Infused Area from each group.

(B) Density mitochondrial area distribution curves for each group.

(C) Number of mitochondria in the Infused Area from each group.

(D) Representative mitochondrial TEM images at 6000X, 10000X, 20000X and 40000X from each group.

Asterisks indicate statistically significant differences comparing RIPC+DOXO vs DOXO group at 16 weeks: : ns $p > 0.05$, * $p < 0.05$, ** $p < 0.01$ and *** $p < 0.001$.

7 Discussion

7.1 Objective 1: *Serial cardiac magnetic resonance for early detection of anthracycline-induced cardiotoxicity*

In a pig model of anthracycline-induced cardiotoxicity with serial multiparametric CMR evaluations, we demonstrate that T2 mapping abnormalities provide the earliest marker of subtle myocardial damage, with T2 relaxation times prolonged long before LV motion abnormalities were detected. At this early stage of cardiotoxicity, T1 relaxation times and ECV quantification were unaltered. Pathology evaluation upon T2 prolongation demonstrated an absolute increase in myocardial water content, correlating with vacuolae formation in preserved cardiomyocytes but with no concomitant fibrosis or increased extracellular space. These findings demonstrate that T2 relaxation-time prolongation in the presence of normal T1 mapping and ECV identifies intra-cardiomyocyte edema as the earliest anthracycline-induced cardiotoxic event. Our results further demonstrate that stopping doxorubicin administration upon detection of T2 relaxation-time prolongation prevents progression to myocardial dysfunction, with subsequent T2 normalization as a surrogate of cardiomyocyte vacuolae resolution (**Figure 30**).

These findings indicate that this marker of intra-cardiomyocyte edema appears at a reversible disease stage and thus has important clinical implications.

Previous CMR evaluations of anthracycline-induced cardiotoxicity have been performed in mice [78], rats [79], [80], and rabbits [65, 66]; however, ours is the first study to use the pig model with serial CMR evaluations. We chose the pig because of its anatomical and physiological similarity to humans (including heart rate and metabolism) and because the CMR protocols are the same as those used clinically. Our study is the most comprehensive to date, since it includes weekly multiparametric CMR evaluations over 4 months to cover all cardiotoxicity stages, from baseline to end-stage disease with overt LVEF deterioration. Following a modification of a published protocol in pigs [69, 70], doxorubicin was injected directly into the coronary arteries rather than intravenously. This approach achieves high local doxorubicin concentrations in the heart without exposing animals to undesired systemic adverse effects like myelosuppression, which would render the animals vulnerable to infection and thus potentially affect survival and even cardiac readouts. This approach is validated by the absence of casualties in our study.

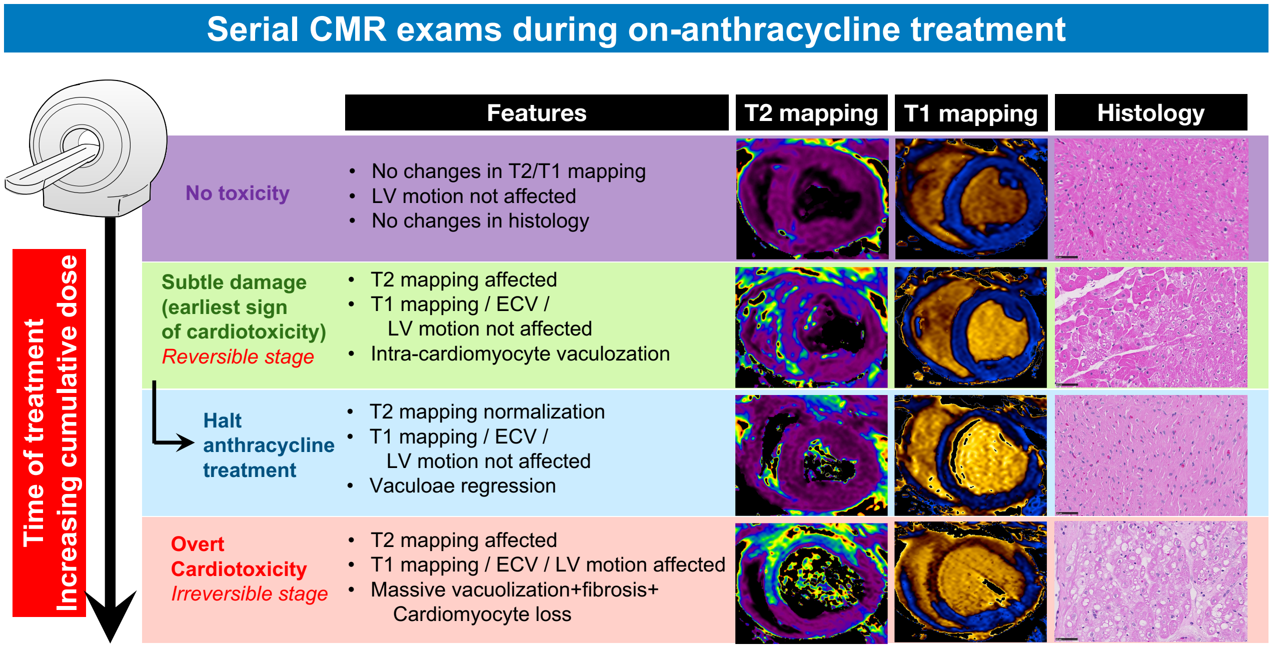

Figure 30: Summary Illustration for Objective 1.

Serial cardiac magnetic resonance (CMR) evaluations during on-(anthracycline)-treatment allows very early detection of subtle myocardial damage. Isolated T2 relaxation times prolongation (with normal T1, ECV, and LV motion) is able to identify intra-cardiomyocyte vacuolization, the earliest cardiotoxic event. Stopping anthracycline therapy at this early time point results in no progression to LV motion abnormalities and normalization of T2 values (corresponding to vacuolae regression). These phenomena support that T2 mapping identifies anthracycline-induces cardiotoxicity at a reversible stage of the disease. If anthracycline therapy is not halted, T1 mapping and ECV become pathological at a stage where LV motion is already deteriorated. Serial multiparametric CMR might serve to implement a personalized treatment approach for patients undergoing anthracycline therapy and prevent cardio-toxicity.

Current clinical approaches for the early detection of cardiotoxicity are based on deterioration of LV motion, detected as LVEF or global longitudinal strain [7,15]; however, these changes reflect profound damage to myocardial function and thus only become manifest at an advanced stage of the disease. Almost 90% of patients developing anthracycline-mediated LVEF deterioration never fully recover pre-treatment LVEF even with HF therapies [81].

The identification of T2 relaxation-time prolongation as a very early marker of reversible intra-cardiomyocyte vacuolization thus has important clinical implications. Serial T2 mapping might allow tailored anthracycline dose management, with patients showing no T2 mapping abnormalities perhaps able to receive further doses, even beyond currently accepted high cardiotoxicity limits, without increasing the risk of future LV dysfunction. This could be especially helpful for patients requiring high anthracycline doses to halt cancer progression. There is also potential to monitor and possibly modify anthracycline therapy in vulnerable populations, such as patients with pre-existing myocardial disease (we further explored this issue in Objective 3); pediatric or geriatric patients; smokers; obese or sedentary patients; patients consuming alcohol; or patients with hypertension, diabetes, or hypercholesterolemia [7].

The chemotherapy dose-management potential of serial T2 mapping is supported by the finding that cessation of doxorubicin therapy upon detection of T2 mapping abnormalities prevented progression to LV motion deterioration or fibrosis development and led to regression of cardiomyocyte vacuolae formation.

Another potential application of serial T2 mapping is decision making about heart failure therapy initiation (e.g. with beta-blockers and/or ACE-inhibitors). This is highly significant, since a major predictor of therapeutic myocardial recovery is the time elapsed between anthracycline therapy and cardiotoxicity diagnosis [82].

Cardinale et al. found that only 42% of patients with anthracycline-induced cardiotoxicity fully recovered LV function in response to heart failure therapy; in that study, the percentage of responders decreased progressively as the time from the end of anthracycline therapy to the start of heart failure treatment increased [82]. Therefore, early detection and prompt treatment of cardiotoxicity is crucial to ensuring substantial recovery of cardiac function. With current approaches (based on LVEF and global longitudinal strain), the mean interval from the end of anthracycline therapy to the detection of cardiotoxicity is 3.5 months [81]. The ability to identify patients at a much earlier stage would allow earlier initiation of heart failure therapy and thus prevent many cases of overt LV dysfunction.

T2 mapping is an accurate technique for the detection and quantification of myocardial edema [46]. We have previously used T2 mapping to characterize the edematous reaction of porcine [47–49] and human [50] myocardium to ischemia/reperfusion. T2 relaxation-time prolongation correlates with increased myocardial water content [46] but by itself does not differentiate between intracellular and extracellular edema. Our multiparametric approach, combining T2 mapping with T1 mapping and ECV quantification, here allowed us to define the spatial location of increased myocardial water. T2 mapping prolongation in the absence of T1 mapping or T1-based ECV changes is highly suggestive of intracellular edema formation. Intracellular vacuolization is an early change in the anthracycline-injured myocardium, identified as a pre-apoptotic phenomena in animal models and human biopsies [28–30, 83].

Our analysis records not only in-vivo changes in T2 mapping, but also the very early presence of intra-cardiomyocyte vacuolization, before the appearance of LV functional abnormalities. At the end of follow-up in animals undergoing the full doxorubicin protocol (5 biweekly injections and follow-up to 16 weeks), T2 relaxation times were even longer than at early stages and were accompanied by significant T1 relaxation-time prolongation, a significantly elevated T1-based ECV fraction, and patchy LGE. The pathological correlate at this end-stage of the disease was the presence of larger and more numerous intra-cardiomyocyte vacuoles accompanied by intense extracellular matrix remodeling and diffuse fibrosis.

Our results are in line with those reported by Farhad et al [78]. Using a mouse model of anthracycline-induced cardiotoxicity, these authors found that 5 weekly doxorubicin injections induced early prolongation of T2 relaxation times accompanied by intracellular vacuolization [78]. This study and ours confirm the feasibility of in-vivo non-invasive identification of vacuolae formation inside cardiomyocytes as a direct toxic effect of anthracyclines in 2 different species. However, Farhad et al. found that T2 mapping abnormalities were associated with concurrent T1 relaxation-time prolongation and expanded extracellular space on electron microscopy images, a finding not observed in our analysis until later disease stages. This indicates that we identified doxorubicin cardiotoxic effects at an earlier disease stage, when only intra-cardiomyocyte changes were present, with preservation of the extracellular space. Our weekly protocol was able to identify the onset of cardiac damage, whereas Farhad et al [78] performed the first scan at the end of the doxorubicin protocol, thus missing the earliest on-treatment tissue composition changes.

In another study, Hong et al [65] used a rabbit model of doxorubicin-induced cardiotoxicity to study the evolution of changes in T1 mapping and T1-based ECV, but did not include T2 mapping. These authors found that T1 relaxation-time prolongation occurred concurrently with ECV expansion at a time when LVEF had already deteriorated (albeit not significantly vs baseline). Histological evaluation revealed intra-cardiomyocyte vacuolization and interstitial fibrosis, indicating that this time point corresponds to more advanced disease stage than that identified by us.

To date, very few studies have used a serial multiparametric CMR strategy including T2 mapping in patients undergoing anthracycline therapy. Several authors have reported CMR findings in patients treated with anti-cancer therapies [54–57, 84, 85]. In some of these studies, increased ECV coincided with cardiac function deterioration. Few studies have reported serial CMR exams before and after anthracycline exposure, and in most of them CMR was performed only after completion of anthracycline administration, thus missing early changes occurring during treatment [86–88].

More recently, Schulz-Menger's group reported the findings of serial multiparametric CMR exams in a cohort of 30 sarcoma patients on high anthracycline regimes [89]. Patients underwent comprehensive T2/T1 mapping and ECV assessment before treatment, 48 hours after the first dose, and after finishing the anti-cancer therapy; 30% of patients developed cardiotoxicity. In contrast with our results, T2 mapping showed no differences between patients developing cardiotoxicity and those who did not, although both groups showed a non-significant trend toward increased T2 relaxation times over time. ECV did not change over time. Interestingly, patients who subsequently developed cardiotoxicity had significantly shortened T1 relaxation times 48 hours after the first dose. In our study, we observed no drop in T1 relaxation time after doxorubicin dosing; however, this might reflect the performance of CMR exams one week after dosing in our protocol and not after 48 hours as in the Muehelberg et al. study [89].

7.1.1 Study limitations

One potential limitation of the present study is the i.c doxorubicin administration route, contrasting the i.v route used in cancer patients. In the pig, the intravenous route requires very high doxorubicin doses that result in significant myelosuppresion and compromise the experimental setting [67]. The i.c approach in the pig model was described by Christiansen et al. and has been validated by several imaging approaches as a valid alternative [69]. Regarding statistical limitations, we used parametric test based on K-S normality test for small samples, which is not the optimal option. Another limitation involves the accessibility of CMR in daily clinical practice; our results suggest the window in which early changes take place is small and translation of serial multiparametric exams in cancer patients could be complex due to the variability of cardiotoxicity in humans.

7.2 Objective 2: ***Effect of doxorubicin on cardiac microcirculation***

In a pig model of anthracycline-induced cardiotoxicity, induced by serial biweekly i.c doxorubicin injections, we studied the trajectories of microvascular damage across different stages of the disease, from very acute to subclinical to overt myocardial damage. To this aim we used state-of-the art techniques to study in vivo myocardial perfusion (by CMR), and functional status of microcirculation (invasive CRF).

Main results of the present study are: 1) i.c injection of (0.45 mg/Kg) doxorubicin does not induce any acute injury in the microvasculature, ruling out an immediate chemical damage secondary to the route of administration. 2) Across the subclinical stage of cardiotoxicity (i.e. when no LV motion defects are still present), there is a progressive deterioration of rest (perfusion) and stressed (CRF) microcirculation. These in vivo deficits have an histological correlate in the form of mild alterations in arteries (slight to moderate tunica hyperplasia by myofibroblast proliferation and collagen accumulation). 3) The damage of the microcirculation seen in the subclinical stages is persistent in time (i.e. no recovery of microcirculation status is seen despite stopping the doxorubicin regime after "only" 3 injections. 4). At high cumulative doxorubicin dose (i.e. after 5 biweekly i.c injections), overt "clinical" cardiotoxicity is seen (severe LV motion deterioration) along with a massive and irreversible injury of the microcirculation at anatomical and functional status. **Figure 31** presents a general overview of these facts.

Our study clearly confirms that anthracyclines induce an irreversible damage in the myocardial microcirculation. These results might have an important clinical implications: given that cardiac microcirculation damage has been consistently associated with poor cardiovascular outcomes in patients with different conditions [90, 91]; the injury exerted by anthracyclines in this vascular compartment might be a significant contributor to the increased cardiovascular adverse outcomes seen in cancer survivors who received anthracyclines. Even those who did not developed clinical cardiotoxicity (LV motion abnormalities) [38, 92].

There is a growing interest in the impact of different cancer therapies and the vascular system [93, 94]. Most of the experimental evidences come from in vitro studies testing the vulnerability of endothelial and smooth muscle cells to a given cancer treatment. Endothelial cell damage upon the exposure to these agents is well known to be mediated by an increase in ROS production and a direct DNA damage. These pathophysiological pathways are similar to those described in cardiomyocytes [95, 96].

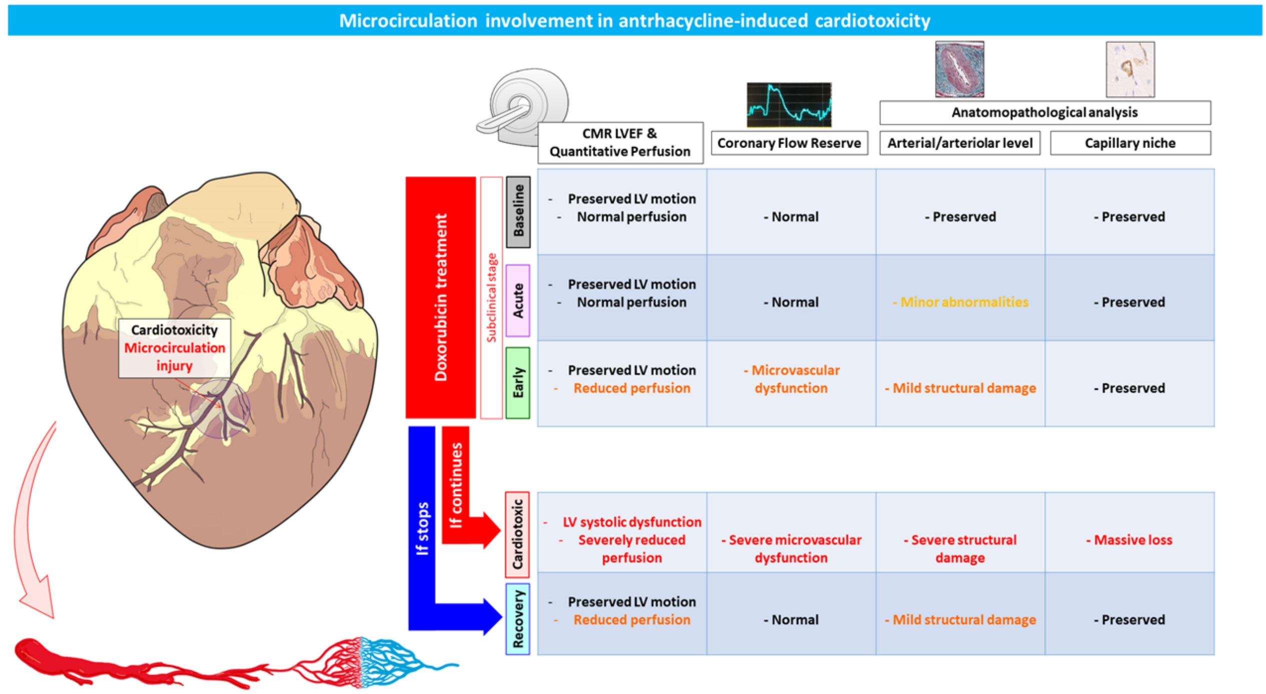

Figure 31: Summary Illustration for Objective 2.

Myocardial quantitative perfusion can detect early cardiotoxicity during anthracycline treatment. These defects correlate with anatomopathological findings. If chemotherapy continues, microvascular damage is exacerbated; but if stops, it is not recovered at all.

Murata and colleagues [34], described apoptotic changes and DNA fragmentation like in the previously studies examining isolated cells, but also functional disruption in term of vascular contractility with increasing doses of anthracyclines. Our study confirms the association between increasing cumulative doses and vascular damage in an in vivo setting.

There are previous in vivo experimental studies showing that anthracyclines exert a deleterious effect on the microcirculation of the heart and other organs [36, 37, 64, 95]. Eckman et al [37], used a rat model of doxorubicin intraperitoneal injections, demonstrating early coronary remodeling after high cumulative dose. Huang et al [36], explored the clinical implications of subtle cardiotoxic microvascular impairment in juvenile mice testing different injury scenarios in the adults (rapid HF development in a model of myocardial infarction and overt cardiotoxicity development when animals underwent over exercise training). Ours is the first large animal study to explore the impact of doxorubicin treatment in cardiac microcirculation. We chose the pig because it is one of the closest models to human cardiac anatomy and physiology, and because in vivo tools used in clinics to evaluate microcirculation (CMR and invasive coronary physiology catheters) can be used. The possibility of doing serial in vivo evaluations and thus study the entire cardiotoxic process from its subclinical to clinical stages in a model close to humans is a clear added value of our study.

In the clinical scenario, vascular injury associated with different anti-cancer interventions (including anthracyclines) has been studied extensively [38, 97, 98]. In fact, cardiac perfusion has been proposed previously as a potential means to study the adverse effects on the heart of chemotherapy [92].

Hardenbergh and collaborators [97], found visible perfusion defects using single photon emission computed tomography (SPECT) in approximately 60% of women with breast cancer treated with radiotherapy alone. Perfusion anomalies were defined in 100% of patients when radiotherapy was combined with doxorubicin. Gallucci and colleagues [38] used stress-SPECT in order to expose perfusion defects in breast cancer survivors. They found that 23.3% of the enrolled patients presented some grade of myocardial perfusion defect. In our study, we combined rest myocardial CMR-based quantitative perfusion with stress coronary physiology assessment, providing a comprehensive in-vivo evaluation of the microcirculation status from the structural and functional perspectives. Our work was consistent with previous human studies not only detecting microvascular injury in animals who developed LV systolic dysfunction, and more importantly show that even subclinical stages of cardiotoxicity are associated with irreversible microcirculation damage.

Regarding the acute impact of single doxorubicin administration, Laursen et al [99] used rest/stress Rubidium82 positron emission tomography (PET) myocardial perfusion imaging in 70 lymphoma patients before and after their first doxorubicin exposure. They found defects in myocardial perfusion reserve and stress myocardial perfusion but not at rest after just one cycle of anthracycline. Opposed to this Laursen et al [99], we did not find acute myocardial perfusion defects or CFR alterations after one single dose of doxorubicin, but on histology we observed a mild structural damage both 48h and 2 weeks after a single i.c doxorubicin injection.

In a long-term perspective, our study highlights that even in cases where no apparent anthracycline-induced cardiotoxicity is observed (no LV motion defects); microvasculature can suffer a significant and irreversible damage. These findings can have important clinical implications for cancer survivors who received anthracyclines, since it might partially explain the high risk of these to suffer adverse cardiovascular outcomes during their entire life. Given that microcirculation status can be assessed non-invasively by CMR [74], it might be used to stratify cardiovascular risk in cancer survivors who received anthracyclines.

7.2.1 Study limitations

This study has two main limitations. First, the use of i.c approach is controversial due to its potential direct effect on cardiac microvasculature by this administration route. We used this modified protocol [69, 70] because myelosuppression effects of doxorubicin are dramatic in pigs [67], compromising the experimental setting. To discard this possible caustic effect, we decided to add 2 new acute groups (at 48 hours and 2 weeks after 1 dose of intracoronary doxorubicin) in which the impact on cardiac perfusion and CFR was insignificant. Demonstrating that the cardiotoxic effect in the vasculature is also cumulative. Second, this study has several missing data regarding some time points for some of the groups and CFR assessment values in the remote areas. This is because Control, Early, Recovery and Cardiotoxic groups were performed for the previous T2-maping study and some of the variables were recorded as secondary endpoint, prioritizing the main goal of the study. However, all statistical analysis have been performed taking in account only groups with all complete data.

7.3 Objective 3: *Vulnerability of the hypertrophied heart to anthracycline-induced cardiotoxicity*

In this study, we demonstrated that very low dosage regimes of systemic i.v anthracyclines develop cardiotoxicity in a model of high left ventricle pressure overload. This doxorubicin-induced cardiotoxicity was characterized by a decline in the LVEF with mainly systolic dysfunction, elevation of T2 values with no expansion of extracellular volume and intra-cardiomyocyte vacuolization and fibber disruption with no fibrosis in the histology. These results contrast with the ones in the healthy non-operated animals that received the same regime of intravenous doxorubicin and were followed at the same time. In those pigs, no changes in cardiac function or cardiac volumes were noticed and anatomopathological evaluation only showed a mild subclinical affectation of myocardial tissue. Animals with aortic banding but not doxorubicin administration developed cardiac hypertrophy at the end of the study with no alterations in CMR mapping nor ex-vivo tissue lesions (**Figure 32**).

As we previously explained, the clinical evidence behind cardiovascular conditions such as hypertensive cardiomyopathy are risk factors for anthracycline-induced cardiotoxicity development in cancer patients is well known and have been profoundly reported [100–105]. The proportion of elderly patients with malignances such as lymphoma that suffer hypertension prior to treatment is also relevant [102].

Regarding animal studies that test cardiotoxic effect of doxorubicin in models with cardiac diseases, most of the work have been done in spontaneously hypertensive rats. Using a young mice model of occult cardiotoxicity; Matsumura et al [106], described that even subclinical low doses of anthracyclines were enough to increase susceptibility to suffer hypertension in the adulthood by angiotensin II-based treatment. In their case, animals that received chemotherapy were not able to develop cardiac hypertrophy in order to adapt their cardiovascular system to hypertension. Our approach is similar but the “damage hits” are reversed. We explored if this discrete doxorubicin posology could trigger overt cardiotoxicity after chronic left ventricular high-pressure overload development. Despite of they tested resveratrol as therapeutically strategy after defining the model; interestingly, we obtained similar results at that point.

Recently, Meléndez et al [107] tested the impact of systemic anthracyclines in spontaneously and normotensive rats using a similar regime to us. They described a deterioration in terms of collagen deposition in hypertensive animals compared with the healthy ones. Even though in our aortic banding model myocardial fibrosis and collagen related remodeling are not present, including the late stages of the follow up, we also found an exacerbated phenotype in animals that combined previous cardiac condition and doxorubicin administration.

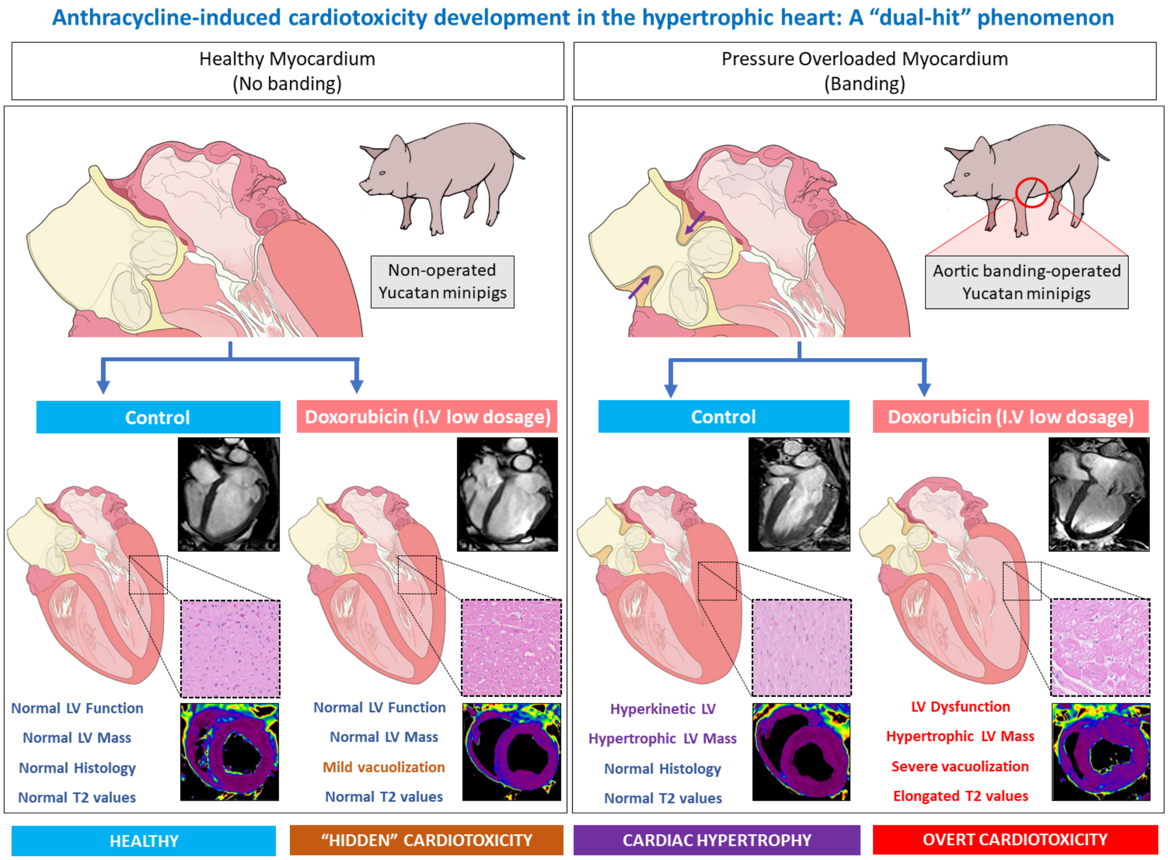

Figure 32: Summary Illustration for Objective 3.

Animals with aortic banding surgery that received low systemic regimes of doxorubicin developed overt cardiotoxicity while pigs, which just underwent surgery, resulted in cardiac hypertrophy. In the healthy scenario, individuals treated with the same regime of anthracyclines developed a subclinical "hidden" cardiotoxicity phenotype only evaluable in the anatomopathological analysis.

Large animal models of anthracycline-induced cardiomyopathy have been rarely utilized; and only one study used a mixed model of cardiotoxicity with pressure overload [108]. However, in this work, they tested pulmonary banding as a potential therapeutic strategy similar to the approach used in children with dilated cardiomyopathy. As in Matsumura article [106], doxorubicin is administrated before the second hit. Our research is pioneer in using pressure overload as first damage before anthracycline exposure. We also decide to use subclinical low regimes of administration due its harmful capacity [109, 110]; and trying to mimic as much as possible the current therapeutic guidelines in which cumulative doses are decreasing bellow classical cardiotoxic concentrations. For this purpose, we tested different systemic doxorubicin regimes to discard the most harmful due its dramatic and huge myelosuppression effect [67]. Moreover, we decided to use a protocol in which we reached proximately 220 mg/m2 of cumulative dose, less than the protocols that currently cancer patients receive in daily clinical practice.

Mixed models of cardiotoxicity are also important from a therapeutic point of view. At present, therapeutic approach of cancer patients treated with anthracyclines included a general battery of drugs used for cardiovascular diseases (including beta-blockers, ACE inhibitors, etc.): and patients diagnosed early improve with this general treatment [82]. Recent reports argue that patients with hypertension undergoing anthracycline chemotherapy could benefit from a more specific treatment focused in their hypertensive condition. However, they claim that long-term data from those patients as well as more experimental evidence of the additive effect in preexisting hypertension is needed for a better screening and therapeutic management [111]. Our findings showed that deterioration in cardiac function occurs very early after low doses of doxorubicin administration, and this is in consonance with new concept called “hidden cardiotoxicity” [112]; and remarks the importance of testing classical drugs in combined models of cardiovascular diseases. These results suggest that a careful follow-up using multiparametric imaging could be an interesting tool for individuals with a prior cardiac condition in treatment with anthracyclines. Similarly, this new mixed model could be used in order to test new potential targeted therapies in large-animal preclinical trials to prevent or revert cardiotoxicity.

We also observed a significant T2-mapping elongation in animals with aortic banding treated with low dose regimes of doxorubicin. These results agreed with our previous work searching early CMR markers of subclinical cardiotoxicity [68]. This elevation in T2 values correlates in histology with intra-cardiomyocyte vacuolization, a typical anatomopathological change in doxorubicin-induced cardiotoxicity. T2 changes and ex vivo myocardial vacuolization was also observed in the non-operated group that received the same anthracycline treatment. In this case, changes in T2 relaxation times were not significant and vacuolization was very mild compared with aortic banding animals. These findings prompt that prior cardiac pressure overload exacerbates classical doxorubicin myocardial damage, leading to overt left ventricular dysfunction. Regarding this, CMR could be an useful in vivo tissue characterization-screening tool to detect subclinical cardiotoxicity even with low cumulative doses in patients with cardiac comorbidities.

7.3.1 Study limitations

This study has two different potential limitations. Firstly, aortic banding surgical model of cardiac pressure overload does not reproduce the extra cardiac effects of systemic arterial hypertension. Secondly, we performed weekly our anthracycline systemic protocol, administrating the cumulative dose in 1 month. This differs from human chemotherapy protocols like R-CHOP in which doxorubicin is infused every 21 days, making the anticancer protocol longer than in our study. This might have impact in the timing of cardiotoxicity-development, making the evolution of disease slower in humans than in our model.

7.4 Objective 4: *Remote ischemic preconditioning and anthracycline-induced cardiotoxicity*

In this preclinical study, we tested the cardioprotective effect of RIPC before doxorubicin administration in a large-animal model of anthracycline-induced cardiotoxicity with positive results. RIPC ameliorates cardiac dysfunction at 16 weeks compared with control animals receiving the same doxorubicin regime. This amelioration was accompanied with smaller left ventricular volumes, lower T2-GraSE, T1 pre contrast and ECV mapping values and higher T1 post-contrast measurements measured in vivo by CMR. Regarding glucose uptake, interestingly, changes occurred during subclinical stage with no differences between treated and untreated animals in all the study. At the end of the study, in a late overt cardiotoxicity phase of the disease, animals treated by RIPC were characterized by less myocardial fibrosis, higher mitochondrial size and less damaged. All these results support the hypothesis that RIPC, a classically therapeutic approach for ischemia/reperfusion injury, has a positive impact in cardiotoxicity context; being its applicability more realistic due to the scheduled character of chemotherapy cycles (**Figure 33**).

ACT have been a major concern for cancer patient survivors since the beginning of its clinical use for a wide range of malignancies. Current therapeutically options include the classical HF treatment [7, 15], that have been demonstrated efficacy even with its implementation at early stages of the disease [81]. However, there is a lack of specific targeted drugs, being dexrazoxane, an iron chelator, the only one that has demonstrated its efficacy in the clinical setting [20, 60]. Nevertheless, last metanalysis studied suggests that the quality of the available evidence is not high for breast cancer patients, and the authors recommend new clinical trials before the systematic implementation of the drug in daily clinical practice [113]. Thus, research for the development of new therapeutically options for ACT is needed.

Ischemic Conditioning (IC) is a physical therapy consisting in repeated short periods of ischemia, - directly in the target organ (local) or in a remote one (remote) - that lead to protection against damage, mostly ischemia-reperfusion (I/R) injury [114]. Regarding myocardial infarction, IC have been classically tested in preclinical and clinical research in several ways: 1) prior to the damage (Preconditioning – IPC -) in animal studies with positive results [115] or 2) during or post ischemia; being this last version the option used in clinical trials, with neutral results [116]; making the translational potential of IPC limited due to the unpredictable nature of myocardial infarction.

In this regard, RIPC have been postulated as one of the most promising cardioprotective therapies for myocardial ischemia/reperfusion injury after the positive results in most of the animal preclinical trials [115]. Unfortunately, last clinical evidence from CONDI-2/ERIC-PPCI trial, found that RIPC did not improve any clinical outcome within

12 months after myocardial infarction [116]. One of the reasons for the therapeutic failure might be the necessity of applying the RIPC before the injury occurs. Regarding this, ACT could be a promising clinical scenario for RIPC application due to the protocoled nature of chemotherapy administration, allowing enforce RIPC before anthracyclines produced cardiotoxicity.

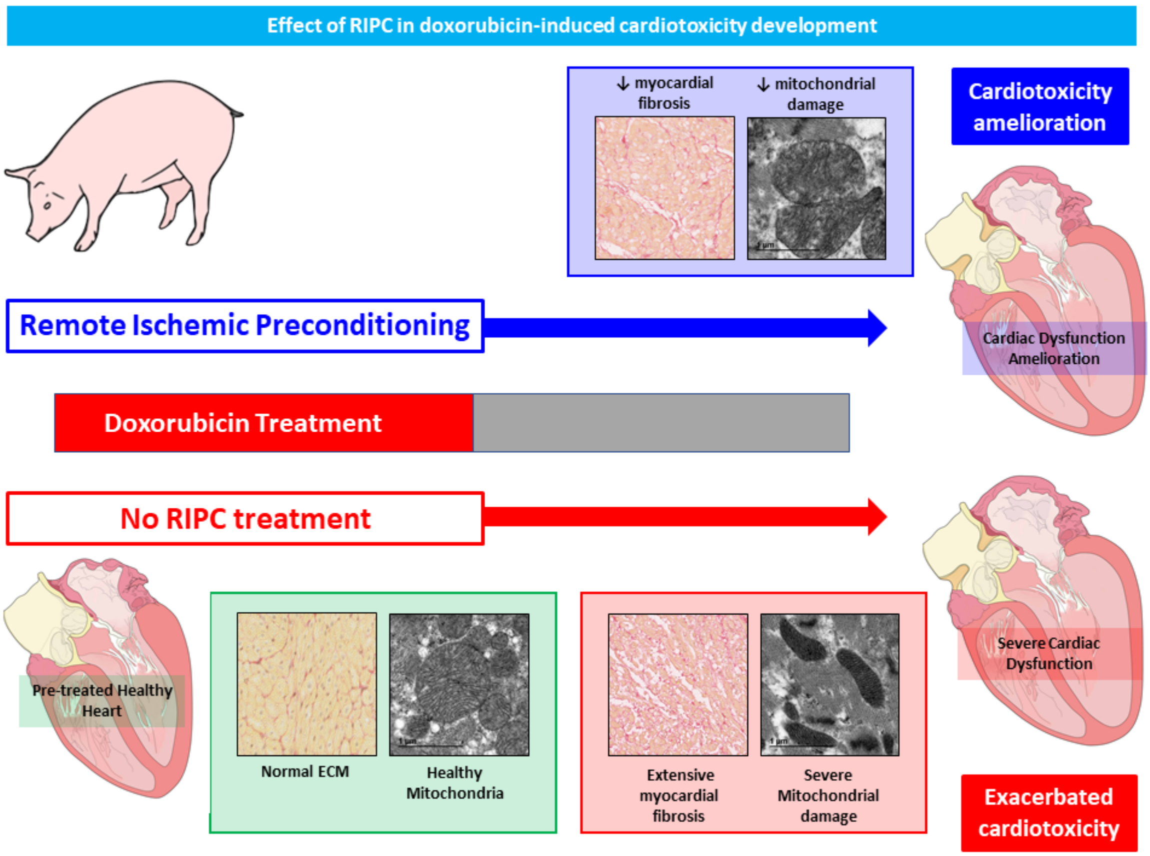

Figure 33: Summary Illustration for Objective 4.

Effect of RIPC during anthracycline-induced cardiotoxicity: Animals treated with RIPC before each doxorubicin administration showed better LVEF, less fibrosis and less mitochondrial damage compared with untreated animals receiving the same anthracycline regime.

RIPC have been poorly tested in cardio-oncology. Schjøtt et al [117] tested LIPC in isolated rat hearts before epirubicin administration, showing that cardiotoxic effect of the chemotherapy are attenuated and cardiac function improved after LIPC. Interestingly, they found lower levels of epirubicin in preconditioned myocardium than in controls, concluding that the cardioprotection effect of LIPC might acts through reducing anthracycline accumulation [117]. No more preclinical animal evidence of IPC effect in cardiotoxicity can be found in the literature. More recently, Maulik et al [118] tested IPC in cultured cardiomyocytes subjected to doxorubicin administration.

Their results were according preexisting animal study from Schjøtt [117]: cardiomyocytes pretreated with IPC were protected from doxorubicin-induced cell death. More importantly, IPC did not protect HeLa cells from cardiotoxicity, which is important to potential therapy testing in patients with malignancies.

Despite of the lack of experimental evidence regarding IPC potential in cardiotoxicity, two different clinical trials are being carried out but only one publish its design [119]. Chung et al [119] are testing 4 cycles of 5 minutes of RIPC at the upper limb before each cycle of chemotherapy in a general population of 128 oncology patients receiving anthracyclines. Li et al decided to test 3 cycles of 5 minutes of RIPC at the upper limb or the leg before each cycle in children from 4-18 years old undergoing anthracycline treatment. In both cases, primary endpoint is high sensitivity cardiac troponin T (hs-cTnT) after chemotherapy treatment finalization. Major Adverse Clinical Cardiovascular Events (MACCEs) and echocardiographic parameters are pointed as secondary outcomes. However, the status of both clinical trials is currently unknown. All these points explained before makes any potential preclinical/clinical evidence of RIPC effectiveness in the context of ACT most valuable.

In our study, we tested a similar RIPC protocol that in being used in both clinical trials, with 3 cycles of 5 minutes of ischemia and 5 of reperfusion in the pig's leg. We chose the leg, because is the most common used limb in the context of preclinical RIPC studies due mainly to the great amount of muscle in this area, given the relationship between the amount of muscle in ischemia and the level of achieved cardioprotection [120–122]. We present the first in-vivo demonstration that RIPC protect the heart against doxorubicin-induced cardiotoxicity, resulting in an improvement in LVEF. In our model this amelioration in cardiac function was accompanied by several (but not statistically significant) changes un in-vivo CMR tissue characterization, such, less T2, T1 native and ECV values and higher T1 post-contrast. It is very well reported that all these mapping parameters can be altered in patients developing chemotherapy-induced cardiotoxicity [54–57, 84–89, 107, 123, 124]. We also demonstrated these changes, being T2 mapping the early detector in absence of cardiac functional abnormalities in our model of li.cdoxorubicin cardiotoxicity [68]. Thus, changes in these tissue characterization-based techniques indicates less myocardial affectation during doxorubicin administration and at the end of the study. Regarding ex vivo evaluation at 16 weeks of cardiotoxicity evolution, despite water content analysis revealed no differences between treated and untreated groups, myocardial collagen content was lower in RIPC+DOXO than in DOXO group. This effect can be explained by SAFE and RISK cardioprotective pathways, being the cardiomyocytes from RIPC group more protected and dead and replace by collagen in the untreated DOXO group.

Regarding mitochondrial differences between all groups. It is very well know the role of mitochondrial damage during ACT [13, 18, 30, 83] as well as dynamic processes such as autophagy and mitophagy as response to the damage [125]. In TEM analysis, mitochondria from DOXO animals present several elongated, irregular and aberrant shapes with mitochondrial matrix hyper density, less size and increased cristae thickness, already described by others [18, 78]. In the case of RIPC+DOXO animals, mitochondrial size was higher compared with untreated animals, mitochondrial cristae also preserve their structure and intra-mitochondrial vacuolization can be observed as a previous stage of mitophagy.

7.4.1 Study limitations

This study has two main limitations. First, as in the case of Objective 1 and 2, the use of i.c approach is controversial due to its potential direct effect on cardiac microvasculature by this administration route. We used this modified protocol [69, 70], because myelosuppression effects of doxorubicin are dramatic in pigs [67], compromising the experimental setting. We also chose this setting in order to test RIPC in a very dramatic cardiotoxic scenario that we already deeply characterized. Second, despite of the availability of RIPC, we use a healthy pig model without any cancer disease. Maulik et al [118] tested the effect of IC on HeLa cells, but it are necessary further investigations testing the therapy in cardio-oncology mixed models in order to dismiss RIPC protective effect also in cancer cells.

8 Conclusions / Conclusiones

Objective 1: *Serial cardiac magnetic resonance (CMR) for early detection of anthracycline-induced cardiotoxicity (ACT)*

1 - In a large animal model of anthracycline-induced cardiotoxicity, we show that the earliest CMR on-treatment event is a prolongation of T2 relaxation time. T1 mapping and T1-based ECV are normal at this early time point and do not change until later in the cardiotoxic process.

2 - At this early stage, T2 mapping abnormalities correspond to intra-cardiomyocyte edema secondary to doxorubicin-induced vacuolization, unaccompanied by any extracellular alteration.

3 - Early identification of intra-cardiomyocyte edema from T2 mapping abnormalities has prognostic implications, since stopping doxorubicin treatment upon detection of this early CMR marker stops the progression of LV dysfunction and triggers regression of intra-cardiomyocyte vacuolization.

4- Serial multiparametric T2 mapping during treatment has the potential to support personalized anthracycline regimes.

Objective 2: *Effect of doxorubicin on cardiac microcirculation*

1 - In a large model of anthracycline-induced cardiotoxicity, we show that cardiac perfusion is a good CMR early marker for microvascular associated ACT.

2 - These changes concur with T2-mapping elevation and both occur in absence of abnormalities in LVEF or ECV.

3 - Moreover, in animals in which the infusion protocol is stopped, cardiac perfusion still detects abnormalities in microvascular function, again with no cardiac disfunction development and with T2 normalization.

4 - CFR seems not to be as sensitive as CMR quantitative perfusion to detect microvascular damage.

5 - Serial multiparametric studies during and post anthracycline treatment has the potential to support personalized medical handle not only in cancer patients receiving therapy, but also in long-term survivors.

Objective 3: *Vulnerability of the hypertrophied heart to anthracycline-induced cardiotoxicity (ACT)*

1 - In this experimental setting of large-animal model of anthracycline-induced cardiotoxicity, low doses of systemic anthracycline induce cardiotoxicity (characterized by the presence of LV dysfunction, elevation in T2 mapping values and an increase in the doxorubicin cardiotoxicity-related Billingham score in myocardial tissue) in the presence of left ventricular pressure overload secondary to aortic banding surgery.

2 - Cardiotoxicity remains “hidden” in healthy non-operated pigs with just a very mild vacuolization in the histology.

3 - These results might have important clinical implications in cancer patients with prior hypertensive/hypertrophic disease undergoing doxorubicin chemotherapy protocols.

Objective 4: *Remote ischemic preconditioning (RIPC) and anthracycline-induced cardiotoxicity (ACT)*

1 - In this study, we demonstrated that repeated RIPC protocols before doxorubicin administration exert a cardioprotective effect in long term. This amelioration in cardiotoxicity is characterized by better LVEF, less fibrosis and better mitochondrial quality.

2 - Glucose uptake measured by PET scan seems to be also a subclinical early detector for metabolic dysfunction in both group, RIPC and untreated animals receiving anthracyclines.

3 - Therefore, RIPC might be a good candidate for cardioprotective therapies against cardiotoxicity in patients' cohorts under anthracycline regimes and clinical trials are needed.

Objetivo 1: *Detección temprana de cardiotoxicidad por antraciclinas empleando la resonancia magnética cardiaca seriada*

1 - En este modelo de animal grande de cardiotoxicidad inducida por antraciclinas, demostramos que el marcador de resonancia magnética más precoz durante el tratamiento con el quimioterápico es la prolongación en los tiempos de relajación de T2, siendo los tiempos de relajación de T1 así como los mapas de volumen extracelular normales en este punto; no cambiando hasta fases avanzadas de la enfermedad

2 - En esta fase temprana, las anormalidades en el mapa de T2 corresponden a un edema intra-cardiomiocito secundario a la vacuolización inducida por la doxorubicina, no siendo acompañada por ninguna alteración extracelular.

3 - La identificación temprana de este edema intra-cardiomiocito utilizando el mapa de T2 tiene implicaciones prognósticas, ya que cesando el tratamiento con doxorubicina en el momento de la detección de la elevación del T2, hace que no se desarrolle cardiotoxicidad y desemboca en la normalización y regresión de la vacuolización intra-cardiomiocito.

4- El mapeo seriado multiparamétrico de T2 durante el tratamiento tiene el potencial de apoyar regimenes personalizados de antraciclinas.

Objetivo 2: *Efecto de la doxorrubicina en la microcirculación cardiaca*

1 - En nuestro modelo de animal grande de cardiotoxicidad inducida por antraciclinas, demostramos que la perfusión miocárdica es un buen marcador temprano para el daño microvascular asociado a cardiotoxicidad.

2 - Estos cambios concurren con los definidos por el T2 y ambos ocurren en ausencia de anormalidades en la función cardiaca o el volumen extracelular.

3 - En animales en los que la infusión de doxorrubicina es cesada, estos defectos en la perfusión permanecen a pesar del no desarrollo de cardiotoxicidad funcional y de la normalización del T2.

4 - El CFR parece no ser tan sensible como la perfusión cuantitativa por resonancia magnética para detectar este daño microvascular.

5 - La utilización de estudios de resonancia magnética cardiaca multiparamétrica durante y tras el tratamiento por antraciclinas tiene el potencial de personalizar el manejo del paciente, no sólo durante la quimioterapia, sino

también en supervivientes a largo plazo.

Objetivo 3: *Vulnerabilidad del corazón hipertrófico a la cardiotoxicidad por antraciclinas*

1 - En este escenario experimental de cardiotoxicidad inducida por antraciclinas en un modelo de animal grande, dosis bajas de doxorrubicina sistémicas inducen cardiotoxicidad (caracterizada por la presencia de disfunción de vertrículo derecho, elevación en el T2 y un incremento en la puntuación Billingham en el tejido miocárdico) en presencia de sobrecarga de volumen izquierda secundaria a una cirugía de banding aórtico.

2 - La cardiotoxicidad permanece "escondida" en animales sanos no operados con una vacuolización leve en la histología.

3 - Estos resultados tienen importantes implicaciones clínicas en pacientes oncológicos con enfermedad hipertensiva/hipertrófica previa sometidos a tratamientos con antraciclinas.

Objetivo 4: *Precondicionamiento isquémico remoto y cardiotoxicidad inducida por antraciclinas*

1 - En este estudio, demostramos que ciclos repetidos de precondicionamiento remoto antes de la administración de doxorrubicina tienen un efecto cardioprotector a largo plazo. Esta mejora en la cardiotoxicidad está caracterizada por una mejor función cardiaca izquierda, menos fibrosis miocárdica y una mejor calidad mitocondrial.

2 - La captación de glucosa medida por PET parece también indicar cambios subclínicos tempranos de disfunción metabólico en ambos grupos, tratados con precondicionamiento y no tratados.

3 - El precondicionamiento remoto podría ser un buen candidato de terapia cardioprotectora contra la cardiotoxicidad inducida por antraciclinas en cohortes de pacientes que reciban quimioterapia basada en antraciclinas. Se necesitan ensayos clínicos.

9 Bibliography

References

[1] Kimberly D Miller, Rebecca L Siegel, Chun Chieh Lin, Angela B Mariotto, Joan L Kramer, Julia H Rowland, Kevin D Stein, Rick Alteri, and Ahmedin Jemal. Cancer treatment and survivorship statistics, 2016. *CA: a cancer journal for clinicians*, 66(4):271–289, 2016.

[2] Michael S Ewer and Steven M Ewer. Cardiotoxicity of anticancer treatments. *Nature Reviews Cardiology*, 12(9):547, 2015.

[3] Maartje J Hooning, Akke Botma, Berthe MP Aleman, Margreet HA Baaijens, Harry Bartelink, Jan GM Klijn, Carolyn W Taylor, and Flora E Van Leeuwen. Long-term risk of cardiovascular disease in 10-year survivors of breast cancer. *Journal of the National Cancer Institute*, 99(5):365–375, 2007.

[4] Gregory T Armstrong, Vijaya M Joshi, Kirsten K Ness, Thomas H Marwick, Nan Zhang, DeoKumar Srivastava, Brian P Griffin, Richard A Grimm, James Thomas, Dermot Phelan, et al. Comprehensive echocardiographic detection of treatment-related cardiac dysfunction in adult survivors of childhood cancer: results from the st. jude lifetime cohort study. *Journal of the American College of Cardiology*, 65(23):2511–2522, 2015.

[5] Nadia Haddy, Stéphanie Diallo, Chiraz El-Fayech, Boris Schwartz, François Pein, Mike Hawkins, Cristina Veres, Odile Oberlin, Catherine Guibout, Hélène Pacquement, et al. Cardiac diseases following childhood cancer treatment: cohort study. *Circulation*, 133(1):31–38, 2016.

[6] Gregory T Armstrong, Kevin C Oeffinger, Yan Chen, Toana Kawashima, Yutaka Yasui, Wendy Leisenring, Marilyn Stovall, Eric J Chow, Charles A Sklar, Daniel A Mulrooney, et al. Modifiable risk factors and major cardiac events among adult survivors of childhood cancer. *Journal of Clinical Oncology*, 31(29):3673, 2013.

[7] Jose Luis Zamorano, Patrizio Lancellotti, Daniel Rodriguez Muñoz, Victor Aboyans, Riccardo Asteggiano, Maurizio Galderisi, Gilbert Habib, Daniel J Lenihan, Gregory YH Lip, Alexander R Lyon, et al. 2016 esc position paper on cancer treatments and cardiovascular toxicity developed under the auspices of the esc committee for practice guidelines: The task force for cancer treatments and cardiovascular toxicity of the european society of cardiology (esc). *European heart journal*, 37(36):2768–2801, 2016.

[8] Charlotte Tan, Hideko Tasaka, Kou-Ping Yu, M Lois Murphy, and David A Karnofsky. Daunomycin, an antitumor antibiotic, in the treatment of neoplastic disease. clinical evaluation with special reference to childhood leukemia. *Cancer*, 20(3):333–353, 1967.

[9] Daniela Cardinale, Maria T Sandri, Alessandro Colombo, Nicola Colombo, Marina Boeri, Giuseppina Lamantia, Maurizio Civelli, Fedro Peccatori, Giovanni Martinelli, Cesare Fiorentini, et al. Prognostic value of troponin i in cardiac risk stratification of cancer patients undergoing high-dose chemotherapy. *Circulation*, 109(22):2749–2754, 2004.

[10] O Hequet, QH Le, I Moullet, E Pauli, G Salles, D Espinouse, C Dumontet, C Thieblemont, P Arnaud, D Antal, et al. Subclinical late cardiomyopathy after doxorubicin therapy for lymphoma in adults. *Journal of clinical oncology*, 22(10):1864–1871, 2004.

[11] Eric Page, David Assouline, Odile Brun, David Coeffic, Daniele Fric, and Philippe Winckel. Cardiac dysfunction in clinical trials of trastuzumab. *Journal of clinical oncology: official journal of the American Society of Clinical Oncology*, 20(19):4119–author, 2002.

[12] Juan Carlos Plana, Maurizio Galderisi, Ana Barac, Michael S Ewer, Bonnie Ky, Marielle Scherrer-Crosbie, Javier Ganame, Igal A Sebag, Deborah A Agler, Luigi P Badano, et al. Expert consensus for multimodality imaging evaluation of adult patients during and after cancer therapy: a report from the american society of echocardiography and the european association of cardiovascular imaging. *European Heart Journal–Cardiovascular Imaging*, 15(10):1063–1093, 2014.

[13] Giorgio Minotti, Pierantonio Menna, Emanuela Salvatorelli, Gaetano Cairo, and Luca Gianni. Anthracyclines: molecular advances and pharmacologic developments in antitumor activity and cardiotoxicity. *Pharmacological reviews*, 56(2):185–229, 2004.

[14] Hui-Ming Chang, Rohit Moudgil, Tiziano Scarabelli, Tochukwu M Okwuosa, and Edward TH Yeh. Cardiovascular complications of cancer therapy: best practices in diagnosis, prevention, and management: part 1. *Journal of the American College of Cardiology*, 70(20):2536–2551, 2017.

[15] Teresa Lopez-Fernandez, Ana Martín García, Ana Santaballa Beltrán, Ángel Montero Luis, Ramón García Sanz, Pilar Mazón Ramos, Sonia Velasco del Castillo, Esteban Lopez de Sa Areses, Manuel Barreiro-Perez, Rocío Hinojar Baydes, et al. Cardio-onco-hematology in clinical practice. position paper and recommendations. *Revista Española de Cardiología (English Edition)*, 70(6):474–486, 2017.

[16] James C Wang. Cellular roles of dna topoisomerases: a molecular perspective. *Nature reviews Molecular cell biology*, 3(6):430, 2002.

[17] Giovanni Capranico, Stella Tinelli, Caroline A Austin, Mark L Fisher, and Franco Zunino. Different patterns of gene expression of topoisomerase ii isoforms in differentiated tissues during murine development. *Biochimica et Biophysica Acta (BBA)-Gene Structure and Expression*, 1132(1):43–48, 1992.

[18] Sui Zhang, Xiaobing Liu, Tasneem Bawa-Khalfe, Long-Sheng Lu, Yi Lisa Lyu, Leroy F Liu, and Edward TH Yeh. Identification of the molecular basis of doxorubicin-induced cardiotoxicity. *Nature medicine*, 18(11):1639, 2012.

[19] Virginia Shalkey Hahn, Daniel J Lenihan, and Bonnie Ky. Cancer therapy–induced cardiotoxicity: basic mechanisms and potential cardioprotective therapies. *Journal of the American Heart Association*, 3(2):e000665, 2014.

[20] Steven E Lipshultz, Nader Rifai, Virginia M Dalton, Donna E Levy, Lewis B Silverman, Stuart R Lipsitz, Steven D Colan, Barbara L Asselin, Ronald D Barr, Luis A Clavell, et al. The effect of dexrazoxane on myocardial injury in doxorubicin-treated children with acute lymphoblastic leukemia. *New England Journal of Medicine*, 351(2):145–153, 2004.

[21] Edward TH Yeh and Hui-Ming Chang. Oncocardiology—past, present, and future: a review. *JAMA cardiology*, 1(9):1066–1072, 2016.

[22] Dirk Lebrecht, Bernhard Setzer, Uwe-Peter Ketelsen, Jorg Haberstroh, and Ulrich A Walker. Time-dependent and tissue-specific accumulation of mtdna and respiratory chain defects in chronic doxorubicin cardiomyopathy. *Circulation*, 108(19):2423–2429, 2003.

[23] Neil Ashley and Joanna Poulton. Mitochondrial dna is a direct target of anti-cancer anthracycline drugs. *Biochemical and biophysical research communications*, 378(3):450–455, 2009.

[24] Hongliang Zhang, Juana M Barceló, Benson Lee, Glenda Kohlhagen, Drazen B Zimonjic, Nicholas C Popescu, and Yves Pommier. Human mitochondrial topoisomerase i. *Proceedings of the National Academy of Sciences*, 98(19):10608–10613, 2001.

[25] Robert L Low, Shayla Orton, and David B Friedman. A truncated form of dna topoisomerase iiβ associates with the mtdna genome in mammalian mitochondria. *European journal of biochemistry*, 270(20):4173–4186, 2003.

[26] Yong Wang, Yi Lisa Lyu, and James C Wang. Dual localization of human dna topoisomerase iiiα to mitochondria and nucleus. *Proceedings of the National Academy of Sciences*, 99(19):12114–12119, 2002.

[27] Salim Khiati, Ilaria Dalla Rosa, Carole Sourbier, Xuefei Ma, V Ashutosh Rao, Leonard M Neckers, Hongliang Zhang, and Yves Pommier. Mitochondrial topoisomerase i (top1mt) is a novel limiting factor of doxorubicin cardiotoxicity. *Clinical Cancer Research*, 20(18):4873–4881, 2014.

[28] L Maximilian Buja, Victor J Ferrans, Robert J Mayer, William C Roberts, and Edward S Henderson. Cardiac ultrastructural changes induced by daunorubicin therapy. *Cancer*, 32(4):771–788, 1973.

[29] Michael A Friedman, Marek J Bozdech, Margaret E Billingham, and Alan K Rider. Doxorubicin cardiotoxicity: serial endomyocardial biopsies and systolic time intervals. *Jama*, 240(15):1603–1606, 1978.

[30] Genzou Takemura and Hisayoshi Fujiwara. Doxorubicin-induced cardiomyopathy: from the cardiotoxic mechanisms to management. *Progress in cardiovascular diseases*, 49(5):330–352, 2007.

[31] Matthew B Wolf and John W Baynes. The anti-cancer drug, doxorubicin, causes oxidant stress-induced endothelial dysfunction. *Biochimica et Biophysica Acta (BBA)-General Subjects*, 1760(2):267–271, 2006.

[32] Aspasia Soultati, Giannis Mountzios, Chrysoula Avgerinou, George Papaxoinis, Dimitrios Pectasides, Meletios-Athanassios Dimopoulos, and Christos Papadimitriou. Endothelial vascular toxicity from chemotherapeutic agents: preclinical evidence and clinical implications. *Cancer treatment reviews*, 38(5):473–483, 2012.

[33] Tomasz Wojcik, Elzbieta Buczek, Katarzyna Majzner, Agnieszka Kolodziejczyk, Justyna Miszczyk, Patrycja Kaczara, Wojciech Kwiatek, Malgorzata Baranska, Marek Szymonski, and Stefan Chlopicki. Comparative endothelial profiling of doxorubicin and daunorubicin in cultured endothelial cells. *Toxicology In Vitro*, 29(3):512–521, 2015.

[34] Takahisa Murata, Hideyuki Yamawaki, Masatoshi Hori, Koichi Sato, Hiroshi Ozaki, and Hideaki Karaki. Chronic vascular toxicity of doxorubicin in an organ-cultured artery. *British journal of pharmacology*, 132(7):1365–1373, 2001.

[35] Anna Bielak-Zmijewska, Maciej Wnuk, Dorota Przybylska, Wioleta Grabowska, Anna Lewinska, Olga Alster, Zbigniew Korwek, Anna Cmoch, Aleksander Myszka, Slawomir Pikula, et al. A comparison of replicative senescence and doxorubicin-induced premature senescence of vascular smooth muscle cells isolated from human aorta. *Biogerontology*, 15(1):47–64, 2014.

[36] Chengqun Huang, Xiaoxue Zhang, Jennifer M Ramil, Shivaji Rikka, Lucy Kim, Youngil Lee, Natalie A Gude, Patricia A Thistlethwaite, Mark A Sussman, Roberta A Gottlieb, and Asa B Gustafsson. Juvenile exposure to anthracyclines impairs cardiac progenitor cell function and vascularization resulting in greater susceptibility to stress-induced myocardial injury in adult mice. *Circulation*, 121(5):675–683, Feb 2010.

[37] Delrae M Eckman, R Brandon Stacey, Robert Rowe, D Ralph, Nancy D Kock, David C Sane, Frank M Torti, Joseph Yeboah, Susan Workman, Kimberly S Lane, et al. Weekly doxorubicin increases coronary arteriolar wall and adventitial thickness. *PLoS One*, 8(2):e57554, 2013.

[38] G Gallucci, M Coccaro, G Storto, L Lapadula, A Tartarone, A Nappi, A Cammarota, C Buonerba, G Di Lorenzo, V Fusco, et al. The clinical impact of a cardiologic follow-up in breast cancer survivors: an observational study. *International journal of immunopathology and pharmacology*, 23(4):1221–1227, 2010.

[39] V Kirthi, C Schultz, and SW Davies. Cardiac imaging of trastuzumab-induced cardiomyopathy. *Eur J Heart Fail Suppl*, 10(Suppl 1):S18, 2011.

[40] Jun Zhang, John R Clark, Eugene H Herman, and Victor J Ferrans. Doxorubicin-induced apoptosis in spontaneously hypertensive rats: differential effects in heart, kidney and intestine, and inhibition by icrf-187. *Journal of molecular and cellular cardiology*, 28(9):1931–1943, 1996.

[41] Eugene H Herman, Antoine N El-Hage, Victor J Ferrans, and Bach Ardalan. Comparison of the severity of the chronic cardiotoxicity produced by doxorubicin in normotensive and hypertensive rats. *Toxicology and applied pharmacology*, 78(2):202–214, 1985.

[42] Eugene H Herman, Jun Zhang, Brian B Hasinoff, Khanh T Tran, Douglas P Chadwick, John R Clark Jr, and Victor J Ferrans. Comparison of the chronic toxicity of piroxantrone, losoxantrone and doxorubicin in spontaneously hypertensive rats. *Toxicology*, 128(1):35–52, 1998.

[43] Mehdi S Hazari, Najwa Haykal-Coates, Darrell W Winsett, Daniel L Costa, and Aimen K Farraj. Continuous electrocardiogram reveals differences in the short-term cardiotoxic response of wistar-kyoto and spontaneously hypertensive rats to doxorubicin. *Toxicological sciences*, 110(1):224–234, 2009.

[44] Leslie C Sharkey, M Judith Radin, Lois Heller, Lynette K Rogers, Anthony Tobias, Ilze Matise, Qi Wang, Fred S Apple, and Sylvia A McCune. Differential cardiotoxicity in response to chronic doxorubicin treatment in male spontaneous hypertension-heart failure (shhf), spontaneously hypertensive (shr), and wistar kyoto (wky) rats. *Toxicology and applied pharmacology*, 273(1):47–57, 2013.

[45] Alessia Pepe, Fausto Pizzino, Paola Gargiulo, Pasquale Perrone-Filardi, Christian Cadeddu, Donato Mele, Ines Monte, Giuseppina Novo, Concetta Zito, and Gianluca Di Bella. Cardiovascular imaging in the diagnosis and monitoring of cardiotoxicity: cardiovascular magnetic resonance and nuclear cardiology. *Journal of Cardiovascular Medicine*, 17(1):S45–S54, 2016.

[46] Rodrigo Fernández-Jiménez, Javier Sánchez-González, Jaume Aguero, María del Trigo, Carlos Galán-Arriola, Valentin Fuster, and Borja Ibáñez. Fast t2 gradient-spin-echo (t2-grase) mapping for myocardial edema quantification: first in vivo validation in a porcine model of ischemia/reperfusion. *Journal of Cardiovascular Magnetic Resonance*, 17(1):92, 2015.

[47] Rodrigo Fernández-Jiménez, Javier Sánchez-González, Jaume Agüero, Jaime García-Prieto, Gonzalo J López-Martín, José M García-Ruiz, Antonio Molina-Iracheta, Xavier Rosselló, Leticia Fernández-Friera, Gonzalo Pizarro, et al. Myocardial edema after ischemia/reperfusion is not stable and follows a bimodal pattern: imaging and histological tissue characterization. *Journal of the American College of Cardiology*, 65(4):315–323, 2015.

[48] Rodrigo Fernández-Jiménez, Jaime García-Prieto, Javier Sánchez-González, Jaume Agüero, Gonzalo J López-Martín, Carlos Galán-Arriola, Antonio Molina-Iracheta, Roisin Doohan, Valentin Fuster, and Borja Ibáñez. Pathophysiology underlying the bimodal edema phenomenon after myocardial ischemia/reperfusion. *Journal of the American College of Cardiology*, 66(7):816–828, 2015.

[49] Rodrigo Fernández-Jiménez, Carlos Galán-Arriola, Javier Sánchez-González, Jaume Agüero, Gonzalo J López-Martín, Sandra Gomez-Talavera, Jaime Garcia-Prieto, Austin Benn, Antonio Molina-Iracheta, Manuel Barreiro-Pérez, et al. Effect of ischemia duration and protective interventions on the temporal dynamics of tissue composition after myocardial infarction. *Circulation research*, 121(4):439–450, 2017.

[50] Rodrigo Fernández-Jiménez, Manuel Barreiro-Pérez, Ana Martin-García, Javier Sánchez-González, Jaume Agüero, Carlos Galán-Arriola, Jaime García-Prieto, Elena Díaz-Pelaez, Pedro Vara, Irene Martinez, et al. Dynamic edematous response of the human heart to myocardial infarction: implications for assessing myocardial area at risk and salvage. *Circulation*, 136(14):1288–1300, 2017.

[51] Andrew S Flett, Martin P Hayward, Michael T Ashworth, Michael S Hansen, Andrew M Taylor, Perry M Elliott, Christopher McGregor, and James C Moon. Equilibrium contrast cardiovascular magnetic resonance for the measurement of diffuse myocardial fibrosis: Preliminary validation in humans. *Circulation*, 122(2):138–144, 2010.

[52] Shiro Nakamori, Kaoru Dohi, Masaki Ishida, Yoshitaka Goto, Kyoko Imanaka-Yoshida, Taku Omori, Itaru Goto, Naoto Kumagai, Naoki Fujimoto, Yasutaka Ichikawa, et al. Native t1 mapping and extracellular volume mapping for the assessment of diffuse myocardial fibrosis in dilated cardiomyopathy. *JACC: Cardiovascular Imaging*, 11(1):48–59, 2018.

[53] Bharath Ambale-Venkatesh and Joao AC Lima. Cardiac mri: a central prognostic tool in myocardial fibrosis. *Nature Reviews Cardiology*, 12(1):18, 2015.

[54] Tomas G Neilan, Otavio R Coelho-Filho, Ravi V Shah, Jiazuo H Feng, Diego Pena-Herrera, Damien Mandry, Francois Pierre-Mongeon, Bobak Heydari, Sanjeev A Francis, Javid Moslehi, et al. Myocardial extracellular volume by cardiac magnetic resonance imaging in patients treated with anthracycline-based chemotherapy. *The American journal of cardiology*, 111(5):717–722, 2013.

[55] Olga H Toro-Salazar, Eileen Gillan, Michael T O'Loughlin, Georgine S Burke, Joanna Ferranti, Jeffrey Stainsby, Bruce Liang, Wojciech Mazur, Subha V Raman, and Kan N Hor. Occult cardiotoxicity in childhood cancer survivors exposed to anthracycline therapy. *Circulation: Cardiovascular Imaging*, 6(6):873–880, 2013.

[56] Kaisa Ylänen, Tuija Poutanen, Päivi Savikurki-Heikkilä, Irina Rinta-Kiikka, Anneli Eerola, and Kim Vettenranta. Cardiac magnetic resonance imaging in the evaluation of the late effects of anthracyclines among long-term survivors of childhood cancer. *Journal of the American College of Cardiology*, 61(14):1539–1547, 2013.

[57] Edythe B Tham, Mark J Haykowsky, Kelvin Chow, Maria Spavor, Sachie Kaneko, Nee S Khoo, Joseph J Pagano, Andrew S Mackie, and Richard B Thompson. Diffuse myocardial fibrosis by t 1-mapping in children with subclinical anthracycline cardiotoxicity: relationship to exercise capacity, cumulative dose and remodeling. *Journal of Cardiovascular Magnetic Resonance*, 15(1):48, 2013.

[58] Jennifer H Jordan, Ralph B D'Agostino Jr, Craig A Hamilton, Sujethra Vasu, Michael E Hall, Dalane W Kitzman, Vinay Thohan, Julia A Lawrence, Leslie R Ellis, Timothy L Lash, et al. Longitudinal assessment of concurrent changes in left ventricular ejection fraction and left ventricular myocardial tissue characteristics after administration of cardiotoxic chemotherapies using t1-weighted and t2-weighted cardiovascular magnetic resonance. *Circulation: Cardiovascular Imaging*, 7(6):872–879, 2014.

[59] Matteo Sarocchi, Matteo Bauckneht, Eleonora Arboscello, Selene Capitanio, Cecilia Marini, Silvia Morbelli, Maurizio Miglino, Angela Giovanna Congiu, Giorgio Ghigliotti, Manrico Balbi, et al. An increase in myocardial 18-fluorodeoxyglucose uptake is associated with left ventricular ejection fraction decline in hodgkin lymphoma patients treated with anthracycline. *Journal of translational medicine*, 16(1):295, 2018.

[60] Steven E Lipshultz, Rebecca E Scully, Stuart R Lipsitz, Stephen E Sallan, Lewis B Silverman, Tracie L Miller, Elly V Barry, Barbara L Asselin, Uma Athale, Luis A Clavell, et al. Assessment of dexrazoxane as a cardioprotectant in doxorubicin-treated children with high-risk acute lymphoblastic leukaemia: long-term follow-up of a prospective, randomised, multicentre trial. *The lancet oncology*, 11(10):950–961, 2010.

[61] Geeta Gulati, Siri Lagethon Heck, Anne Hansen Ree, Pavel Hoffmann, Jeanette Schulz-Menger, Morten W Fagerland, Berit Gravdehaug, Florian von Knobelsdorff-Brenkenhoff, Åse Bratland, Tryggve H Storås, et al. Prevention of cardiac dysfunction during adjuvant breast cancer therapy (prada): a $2\times$ 2 factorial, randomized, placebo-controlled, double-blind clinical trial of candesartan and metoprolol. *European heart journal*, 37(21):1671–1680, 2016.

[62] Kyung Ko, Yin Wang, Sivareddy Kotla, Yuka Fujii, Hang Thi Vu, Bhanu P Venkatesulu, Tamlyn N Thomas, Jan L Medina, Young Jin Gi, Megumi Hada, et al. Developing a reliable mouse model for cancer therapy-induced cardiovascular toxicity in cancer patients and survivors. *Frontiers in cardiovascular medicine*, 5:26, 2018.

[63] Nabil E Boutagy, Jing Wu, Zhengxi Cai, Wenjie Zhang, Carmen J Booth, Tassos C Kyriakides, Daniel Pfau, Tim Mulnix, Zhao Liu, Edward J Miller, et al. In vivo reactive oxygen species detection with a novel positron emission tomography tracer, 18f-dhmt, allows for early detection of anthracycline-induced cardiotoxicity in rodents. *JACC: Basic to Translational Science*, 3(3):378–390, 2018.

[64] Irit Ben Aharon, Hadas Bar Joseph, Moran Tzabari, Boris Shenkman, Nahid Farzam, Mattan Levi, Ruth Shalgi, Salomon M Stemmer, and Naphtali Savion. Doxorubicin-induced vascular toxicity–targeting potential pathways may reduce procoagulant activity. *PLoS One*, 8(9):e75157, 2013.

[65] Yoo Jin Hong, Heae Surng Park, Jeffrey Kihyun Park, Kyunghwa Han, Chul Hwan Park, Tai Kyung Kim, Sae Jong Yoo, Ji Yeon Lee, Pan Ki Kim, Jin Hur, et al. Early detection and serial monitoring of anthracycline-induced cardiotoxicity using t1-mapping cardiac magnetic resonance imaging: an animal study. *Scientific reports*, 7(1):2663, 2017.

[66] Yoo Jin Hong, Tai Kyung Kim, Donghyun Hong, Chul Hwan Park, Sae Jong Yoo, Mary Ellen Wickum, Jin Hur, Hye-Jeong Lee, Young Jin Kim, Young Joo Suh, et al. Myocardial characterization using dual-energy ct in doxorubicin-induced dcm: comparison with cmr t1-mapping and histology in a rabbit model. *JACC: Cardiovascular Imaging*, 9(7):836–845, 2016.

[67] JF Vleet Van, LA Greenwood, and VJ Ferrans. Pathologic features of adriamycin toxicosis in young pigs: nonskeletal lesions. *American journal of veterinary research*, 40(11):1537–1552, 1979.

[68] Carlos Galán-Arriola, Manuel Lobo, Jean Paul Vílchez-Tschischke, Gonzalo J López, Antonio de Molina-Iracheta, Claudia Pérez-Martínez, Jaume Agüero, Rodrigo Fernández-Jiménez, Ana Martín-García, Eduardo Oliver, et al. Serial magnetic resonance imaging to identify early stages of anthracycline-induced cardiotoxicity. *Journal of the American College of Cardiology*, 73(7):779–791, 2019.

[69] Stefan Christiansen, Alberto Perez-Bouza, Gereon Schälte, Ralf-Dieter Hilgers, and Rüdiger Autschbach. Selective left ventricular adriamycin-induced cardiomyopathy in the pig. *The Journal of Heart and Lung Transplantation*, 27(1):86–92, 2008.

[70] Andreas Goetzenich, Nima Hatam, Alma Zernecke, Christian Weber, Tanja Czarnotta, Rüdiger Autschbach, and Stefan Christiansen. Alteration of matrix metalloproteinases in selective left ventricular adriamycin-induced cardiomyopathy in the pig. *The Journal of Heart and Lung Transplantation*, 28(10):1087–1093, 2009.

[71] Ali Ayaon-Albarran, Rodrigo Fernandez-Jimenez, Jacobo Silva-Guisasola, Jaume Agüero, Javier Sanchez-Gonzalez, Carlos Galan-Arriola, Fernando Reguillo-Lacruz, Luis C Maroto Castellanos, and Borja Ibanez. Systolic flow displacement using 3d magnetic resonance imaging in an experimental model of ascending aorta aneurysm: impact of rheological factors. *European Journal of Cardio-Thoracic Surgery*, 50(4):685–692, 2016.

[72] Rodrigo Fernández-Jiménez, Jacobo Silva, Sara Martínez-Martínez, Mª Dolores López-Maderuelo, Mario Nuno-Ayala, José Manuel García-Ruiz, Ana García-Álvarez, Leticia Fernández-Friera, Tech Gonzalo Pizarro, Jaime García-Prieto, et al. Impact of left ventricular hypertrophy on troponin release during acute myocardial infarction: new insights from a comprehensive translational study. *Journal of the American Heart Association*, 4(1):e001218, 2015.

[73] Kiyotake Ishikawa, Jaume Aguero, Jae Gyun Oh, Nadjib Hammoudi, Lauren A. Fish, Lauren Leonardson, Belén Picatoste, Carlos G Santos-Gallego, Kenneth M. Fish, and Roger J Hajjar. Increased stiffness is the major early abnormality in a pig model of severe aortic stenosis and predisposes to congestive heart failure in the absence of systolic dysfunction. *Journal of the American Heart Association*, 4(5):e001925, 2015.

[74] Javier Sánchez-González, Rodrigo Fernandez-Jiménez, Nils D Nothnagel, Gonzalo López-Martín, Valentin Fuster, and Borja Ibañez. Optimization of dual-saturation single bolus acquisition for quantitative cardiac perfusion and myocardial blood flow maps. *Journal of Cardiovascular Magnetic Resonance*, 17(1):21, 2015.

[75] Awal M Hadi, Koen TB Mouchaers, Ingrid Schalij, Katrien Grunberg, Gerrit A Meijer, Anton Vonk-Noordegraaf, Willem J van der Laarse, and Jeroen AM Beliën. Rapid quantification of myocardial fibrosis: a new macro-based automated analysis. *Cellular oncology*, 34(4):343–354, 2011.

[76] ME Billingham, JW Mason, MR Bristow, and JR Daniels. Anthracycline cardiomyopathy monitored by morphologic changes. *Cancer treatment reports*, 62(6):865–872, 1978.

[77] Johannes Schindelin, Ignacio Arganda-Carreras, Erwin Frise, Verena Kaynig, Mark Longair, Tobias Pietzsch, Stephan Preibisch, Curtis Rueden, Stephan Saalfeld, Benjamin Schmid, et al. Fiji: an open-source platform for biological-image analysis. *Nature methods*, 9(7):676, 2012.

[78] Hoshang Farhad, Pedro V Staziaki, Daniel Addison, Otavio R Coelho-Filho, Ravi V Shah, Richard N Mitchell, Balint Szilveszter, Siddique A Abbasi, Raymond Y Kwong, Marielle Scherrer-Crosbie, et al. Characterization of the changes in cardiac structure and function in mice treated with anthracyclines using serial cardiac magnetic resonance imaging. *Circulation: Cardiovascular Imaging*, 9(12):e003584, 2016.

[79] Yves Cottin, Christophe Ribugt, Véronique Maupoil, Diane Godin, Laurent Arnould, François Brunotte, and Luc Rochette. Early incidence of adriamycin treatment on cardiac parameters in the rat. *Canadian journal of physiology and pharmacology*, 72(2):140–145, 1994.

[80] James C Lightfoot, Ralph B D'Agostino Jr, Craig A Hamilton, Jennifer Jordan, Frank M Torti, Nancy D Kock, James Jordan, Susan Workman, and W Gregory Hundley. Novel approach to early detection of doxorubicin cardiotoxicity by gadolinium-enhanced cardiovascular magnetic resonance imaging in an experimental model. *Circulation: Cardiovascular Imaging*, 3(5):550–558, 2010.

[81] Daniela Cardinale, Alessandro Colombo, Giulia Bacchiani, Ines Tedeschi, Carlo A Meroni, Fabrizio Veglia, Maurizio Civelli, Giuseppina Lamantia, Nicola Colombo, Giuseppe Curigliano, et al. Early detection of anthracycline cardiotoxicity and improvement with heart failure therapy. *Circulation*, 131(22):1981–1988, 2015.

[82] Daniela Cardinale, Alessandro Colombo, Giuseppina Lamantia, Nicola Colombo, Maurizio Civelli, Gaia De Giacomi, Mara Rubino, Fabrizio Veglia, Cesare Fiorentini, and Carlo M Cipolla. Anthracycline-induced cardiomyopathy: clinical relevance and response to pharmacologic therapy. *Journal of the American College of Cardiology*, 55(3):213–220, 2010.

[83] Maria A Mitry and John G Edwards. Doxorubicin induced heart failure: Phenotype and molecular mechanisms. *IJC heart & vasculature*, 10:17–24, 2016.

[84] Tomas G Neilan, Otavio R Coelho-Filho, Diego Pena-Herrera, Ravi V Shah, Michael Jerosch-Herold, Sanjeev A Francis, Javid Moslehi, and Raymond Y Kwong. Left ventricular mass in patients with a cardiomyopathy after treatment with anthracyclines. *The American journal of cardiology*, 110(11):1679–1686, 2012.

[85] Yiu-fai Cheung, Wendy Wai-man Lam, Janice Jing-Kun Ip, Daniel Ka-leung Cheuk, Frankie Wai-tsoi Cheng, Janet Yee-kwan Yang, Jeffrey Ping-wa Yau, Karin Ka-huen Ho, Chi-kong Li, Rever Chak-ho Li, et al. Myocardial iron load and fibrosis in long term survivors of childhood leukemia. *Pediatric blood & cancer*, 62(4):698–703, 2015.

[86] Brandon C Drafts, Katie M Twomley, Ralph D'Agostino, Julia Lawrence, Nancy Avis, Leslie R Ellis, Vinay Thohan, Jennifer Jordan, Susan A Melin, Frank M Torti, et al. Low to moderate dose anthracycline-based chemotherapy is associated with early noninvasive imaging evidence of subclinical cardiovascular disease. *JACC: Cardiovascular Imaging*, 6(8):877–885, 2013.

[87] Jennifer H Jordan, Sujethra Vasu, Timothy M Morgan, Ralph B D'Agostino Jr, Giselle C Meléndez, Craig A Hamilton, Andrew E Arai, Songtao Liu, Chia-Ying Liu, João AC Lima, et al. Anthracycline-associated t1 mapping characteristics are elevated independent of the presence of cardiovascular comorbidities in cancer survivors. *Circulation: Cardiovascular Imaging*, 9(8):e004325, 2016.

[88] Matthew A Lunning, Shelby Kutty, Eric T Rome, Ling Li, Asif Padiyath, Fausto Loberiza, Robert Gregory Bociek, Philip J Bierman, Julie M Vose, James O Armitage, et al. Cardiac magnetic resonance imaging for the assessment of the myocardium after doxorubicin-based chemotherapy. *American journal of clinical oncology*, 38(4):377–381, 2015.

[89] Fabian Muehlberg, Stephanie Funk, Leonora Zange, Florian von Knobelsdorff-Brenkenhoff, Edyta Blaszczyk, Alexander Schulz, Saeed Ghani, Annete Reichardt, Peter Reichardt, and Jeanette Schulz-Menger. Native myocardial t1 time can predict development of subsequent anthracycline-induced cardiomyopathy. *ESC heart failure*, 5(4):620–629, 2018.

[90] David D Gutterman, Dawid S Chabowski, Andrew O Kadlec, Matthew J Durand, Julie K Freed, Karima Ait-Aissa, and Andreas M Beyer. The human microcirculation: regulation of flow and beyond. *Circulation research*, 118(1):157–172, 2016.

[91] Viviany R Taqueti, Brendan M Everett, Venkatesh L Murthy, Mariya Gaber, Courtney R Foster, Jon Hainer, Ron Blankstein, Sharmila Dorbala, and Marcelo F Di Carli. Interaction of impaired coronary flow reserve and cardiomyocyte injury on adverse cardiovascular outcomes in patients without overt coronary artery disease. *Circulation*, 131(6):528–535, 2015.

[92] Amy A Kirkham, Sean A Virani, and Kristin L Campbell. The utility of cardiac stress testing for detection of cardiovascular disease in breast cancer survivors: a systematic review. *International journal of women's health*, 7:127, 2015.

[93] Albert Z Luu, Biswajit Chowdhury, Mohammed Al-Omran, Hwee Teoh, David A Hess, and Subodh Verma. Role of endothelium in doxorubicin-induced cardiomyopathy. *JACC: Basic to Translational Science*, 3(6):861–870, 2018.

[94] Umberto Campia, Javid J Moslehi, Laleh Amiri-Kordestani, Ana Barac, Joshua A Beckman, David D Chism, Paul Cohen, John D Groarke, Joerg Herrmann, Carolyn M Reilly, et al. Cardio-oncology: vascular and metabolic perspectives: a scientific statement from the american heart association. *Circulation*, 139(13):e579–e602, 2019.

[95] V Pavillard, D Kherfellah, S Richard, J Robert, and D Montaudon. Effects of the combination of camptothecin and doxorubicin or etoposide on rat glioma cells and camptothecin-resistant variants. *British journal of cancer*, 85(7):1077, 2001.

[96] Srigiridhar Kotamraju, Eugene A Konorev, Joy Joseph, and B Kalyanaraman. Doxorubicin-induced apoptosis in endothelial cells and cardiomyocytes is ameliorated by nitrone spin traps and ebselen role of reactive oxygen and nitrogen species. *Journal of biological chemistry*, 275(43):33585–33592, 2000.

[97] Patricia H Hardenbergh, Michael T Munley, Gunilla C Bentel, Ronit Kedem, Salvador Borges-Neto, Donna Hollis, Leonard R Prosnitz, and Lawrence B Marks. Cardiac perfusion changes in patients treated for breast cancer with radiation therapy and doxorubicin: preliminary results. *International Journal of Radiation Oncology* Biology* Physics*, 49(4):1023–1028, 2001.

[98] Narumol Chaosuwannakit, Ralph D'Agostino Jr, Craig A Hamilton, Kimberly S Lane, William O Ntim, Julia Lawrence, Susan A Melin, Leslie R Ellis, Frank M Torti, William C Little, et al. Aortic stiffness increases upon receipt of anthracycline chemotherapy. *Journal of Clinical Oncology*, 28(1):166, 2010.

[99] Adam Høgsbro Laursen, Marie Bayer Elming, Rasmus Sejersten Ripa, Philip Hasbak, Andreas Kjær, Lars Køber, Jacob Louis Marott, Jens Jakob Thune, and Martin Hutchings. Rubidium-82 positron emission tomography for detection of acute doxorubicin-induced cardiac effects in lymphoma patients. *Journal of Nuclear Cardiology*, pages 1–10, 2018.

[100] Mary C Pinder, Zhigang Duan, James S Goodwin, Gabriel N Hortobagyi, and Sharon H Giordano. Congestive heart failure in older women treated with adjuvant anthracycline chemotherapy for breast cancer. *Journal of Clinical Oncology*, 25(25):3808–3815, 2007.

[101] Elizabeth C Moser, Evert M Noordijk, Flora E van Leeuwen, Saskia le Cessie, Joke W Baars, José Thomas, Patrice Carde, Jacobus H Meerwaldt, Martine van Glabbeke, and Hanneke C Kluin-Nelemans. Long-term risk of cardiovascular disease after treatment for aggressive non-hodgkin lymphoma. *Blood*, 107(7):2912–2919, 2006.

[102] Dawn L Hershman, A Eisenberger, J Wang, J Jacobson, V Grann, R McBride, W Tsai, and A Neugut. Doxorubicin, cardiac risk factors and cardiac toxicity in elderly patients with diffuse b-cell non-hodgkin's lymphoma. *Journal of Clinical Oncology*, 25(18_suppl):9050–9050, 2007.

[103] Sebastian Szmit, Wojciech Jurczak, Jan Maciej Zaucha, Joanna Drozd-Sokołowska, Wojciech Spychałowicz, Monika Joks, Monika Długosz-Danecka, and Adam Torbicki. Pre-existing arterial hypertension as a risk factor for early left ventricular systolic dysfunction following (r)-chop chemotherapy in patients with lymphoma. *Journal of the American Society of Hypertension*, 8(11):791–799, 2014.

[104] Daniel D Von Hoff, Maxwell W Layard, PETER BASA, Hugh L Davis, Ann L Von Hoff, Marcel Rozencweig, and Franco M Muggia. Risk factors for doxorubicin-Induced congestive heart failure. *Annals of internal medicine*, 91(5):710–717, 1979.

[105] Manish Jain and Raymond R Townsend. Chemotherapy agents and hypertension: a focus on angiogenesis blockade. *Current hypertension reports*, 9(4):320–328, 2007.

[106] Nobutoshi Matsumura, Beshay N Zordoky, Ian M Robertson, Shereen M Hamza, Nirmal Parajuli, Carrie-Lynn M Soltys, Donna L Beker, Marianne K Grant, Maria Razzoli, Alessandro Bartolomucci, et al. Co-administration of resveratrol with doxorubicin in young mice attenuates detrimental late-occurring cardiovascular changes. *Cardiovascular research*, 114(10):1350–1359, 2018.

[107] Giselle C Meléndez, Jennifer H Jordan, Ralph B D'Agostino Jr, Edward J Lesnefsky, and W Gregory Hundley. Accelerated left ventricular interstitial collagen deposition after receiving doxorubicin in hypertension. *Journal of the American College of Cardiology*, 72(13):1555, 2018.

[108] Can Yerebakan, Johannes Boltze, Hatem Elmontaser, Uygar Yoruker, Heiner Latus, Markus Khalil, Stefan Ostermayer, Blanca Steinbrenner, Christian Apitz, Matthias Schneider, et al. Effects of pulmonary artery banding in doxorubicin-induced left ventricular cardiomyopathy. *The Journal of thoracic and cardiovascular surgery*, 157(6):2416–2428, 2019.

[109] Kasey Leger, Tamra Slone, Matthew Lemler, David Leonard, Cindy Cochran, W Paul Bowman, Lisa Bashore, and Naomi Winick. Subclinical cardiotoxicity in childhood cancer survivors exposed to very low dose anthracycline therapy. *Pediatric blood & cancer*, 62(1):123–127, 2015.

[110] Els Vandecruys, Veerle Mondelaers, Daniel De Wolf, Yves Benoit, and Bert Suys. Late cardiotoxicity after low dose of anthracycline therapy for acute lymphoblastic leukemia in childhood. *Journal of Cancer Survivorship*, 6(1):95–101, 2012.

[111] Robin K Kuriakose, Rakesh C Kukreja, and Lei Xi. Potential therapeutic strategies for hypertension-exacerbated cardiotoxicity of anticancer drugs. *Oxidative medicine and cellular longevity*, 2016, 2016.

[112] Péter Ferdinandy, István Baczkó, Péter Bencsik, Zoltán Giricz, Anikó Görbe, Pál Pacher, Zoltán V Varga, András Varró, and Rainer Schulz. Definition of hidden drug cardiotoxicity: paradigm change in cardiac safety testing and its clinical implications. *European heart journal*, 40(22):1771–1777, 2018.

[113] Ariane VS Macedo, Ludhmila A Hajjar, Alexander R Lyon, Bruno R Nascimento, Alessandro Putzu, Lorenzo Rossi, Rafael B Costa, Giovanni Landoni, Angélica Nogueira-Rodrigues, and Antonio LP Ribeiro. Efficacy of dexrazoxane in preventing anthracycline cardiotoxicity in breast cancer. *JACC CardioOncology*, 1(1):68–79, 2019.

[114] Derek J Hausenloy and Derek M Yellon. Ischaemic conditioning and reperfusion injury. *Nature Reviews Cardiology*, 13(4):193, 2016.

[115] Daniel I Bromage, Jack MJ Pickard, Xavier Rossello, Oliver J Ziff, Niall Burke, Derek M Yellon, and Sean M Davidson. Remote ischaemic conditioning reduces infarct size in animal in vivo models of ischaemia-reperfusion injury: a systematic review and meta-analysis. *Cardiovascular research*, 113(3):288–297, 2016.

[116] Derek J Hausenloy, Rajesh K Kharbanda, Ulla Kristine Møller, Manish Ramlall, Jens Aarøe, Robert Butler, Heerajnarain Bulluck, Tim Clayton, Ali Dana, Matthew Dodd, et al. Effect of remote ischaemic conditioning on clinical outcomes in patients with acute myocardial infarction (condi-2/eric-ppci): a single-blind randomised controlled trial. *The Lancet*, 2019.

[117] Jan Schjøtt, Hilde Olsen, Kirsti Berg, and Per Jynge. Pretreatment with ischaemia attenuates acute epirubicin-induced cardiotoxicity in isolated rat hearts. *Pharmacology & toxicology*, 78(6):381–386, 1996.

[118] Angshuman Maulik, Sean M Davidson, Izabela Piotrowska, Malcolm Walker, and Derek M Yellon. Ischaemic preconditioning protects cardiomyocytes from anthracycline-induced toxicity via the pi3k pathway. *Cardiovascular drugs and therapy*, 32(3):245–253, 2018.

[119] Robin Chung, Angshuman Maulik, Ashraf Hamarneh, Daniel Hochhauser, Derek J Hausenloy, J Malcolm Walker, and Derek M Yellon. Effect of remote ischaemic conditioning in oncology patients undergoing chemotherapy: Rationale and design of the eric-onc study—a single-center, blinded, randomized controlled trial. *Clinical cardiology*, 39(2):72–82, 2016.

[120] Nilgün Gedik, Marcus Krüger, Matthias Thielmann, Eva Kottenberg, Andreas Skyschally, Ulrich H Frey, Elke Cario, Jürgen Peters, Heinz Jakob, Gerd Heusch, et al. Proteomics/phosphoproteomics of left ventricular biopsies from patients with surgical coronary revascularization and pigs with coronary occlusion/reperfusion: remote ischemic preconditioning. *Scientific reports*, 7(1):7629, 2017.

[121] Helmut Raphael Lieder, Petra Kleinbongard, Andreas Skyschally, Helene Hagelschuer, William M Chilian, and Gerd Heusch. Vago-splenic axis in signal transduction of remote ischemic preconditioning in pigs and rats. *Circulation Research*, 123(10):1152–1163, 2018.

[122] Tamás Baranyai, Zoltán Giricz, Zoltán V Varga, Gábor Koncsos, Dominika Lukovic, András Makkos, Márta Sárközy, Noémi Pávó, András Jakab, Csilla Czimbalmos, et al. In vivo mri and ex vivo histological assessment of the cardioprotection induced by ischemic preconditioning, postconditioning and remote conditioning in a closed-chest porcine model of reperfused acute myocardial infarction: importance of microvasculature. *Journal of translational medicine*, 15(1):67, 2017.

[123] Jennifer H Jordan, Ryan M Todd, Sujethra Vasu, and W Gregory Hundley. Cardiovascular magnetic resonance in the oncology patient. *JACC: Cardiovascular Imaging*, 11(8):1150–1172, 2018.

[124] Olga H Toro-Salazar, Joanna Ferranti, Glenn S Slavin, and Kan N Hor. Cardiac magnetic resonance characteristics of acute anthracycline-induced cardiotoxicity. *Journal of Cardiovascular Magnetic Resonance*, 18(S1):P268, 2016.

[125] Navid Koleini and Elissavet Kardami. Autophagy and mitophagy in the context of doxorubicin-induced cardiotoxicity. *Oncotarget*, 8(28):46663, 2017.

10 Articles published during the thesis

As first author:

Galán-Arriola C, Sánchez-González J, Ibanez B. *Reply: CMR and Tissue Characterization: Don't Forget the Strain!* J Am Coll Cardiol. 2019 Jul 2;73(25):3360. doi: 10.1016/j.jacc.2019.04.037. PubMed PMID: 31248563.

Galán-Arriola C,, Lobo M, Vílchez-Tschischke JP, López GJ, de Molina-Iracheta A, Pérez-Martínez C, Agüero J, Fernández-Jiménez R, Martín-García A, Oliver E, Villena-Gutierrez R, Pizarro G, Sánchez PL, Fuster V, Sánchez-González J, Ibanez B. *Serial Magnetic Resonance Imaging to Identify Early Stages of Anthracycline-Induced Cardiotoxicity*. J Am Coll Cardiol. 2019 Feb 26;73(7):779-791. doi: 10.1016/j.jacc.2018.11.046. PubMed PMID: 30784671.

As co-author:

Orfany A, **Galán-Arriola C**,, Doulamis IP, Guariento A, Ramirez-Barbieri G, Moskowitzova K, Shin B, Blitzer D, Rogers C, Del Nido PJ, McCully JD. *Mitochondrial transplantation ameliorates acute limb ischemia*. J Vasc Surg. 2019 Jul 25. pii: S0741-5214(19)31188-7. doi: 10.1016/j.jvs.2019.03.079. [Epub ahead of print] PubMed PMID: 31353269.

Velasco C, Mota-Cobián A, Mota RA, Pellico J, Herranz F, **Galán-Arriola C**,, Ibáñez B, Ruiz-Cabello J, Mateo J, España S. *Quantitative assessment of myocardial blood flow and extracellular volume fraction using (68)Ga-DOTA-PET: A feasibility and validation study in large animals*. J Nucl Cardiol. 2019 Mar 29. doi: 10.1007/s12350-019-01694-z. [Epub ahead of print] PubMed PMID: 30927149.

Dorado B, Pløen GG, Barettino A, Macías A, Gonzalo P, Andrés-Manzano MJ, González-Gómez C, **Galán-Arriola C**,, Alfonso JM, Lobo M, López-Martín GJ, Molina A, Sánchez-Sánchez R, Gadea J, Sánchez-González J, Liu Y, Callesen H, Filgueiras-Rama D, Ibáñez B, Sørensen CB, Andrés V. *Generation and characterization of a novel knockin minipig model of Hutchinson-Gilford progeria syndrome*. Cell Discov. 2019 Mar 19;5:16. doi: 10.1038/s41421-019-0084-z. eCollection 2019. PubMed PMID: 30911407; PubMed Central PMCID: PMC6423020.

Torán JL, López JA, Gomes-Alves P, Aguilar S, Torroja C, Trevisan-Herraz M, Moscoso I, Sebastião MJ, Serra M, Brito C, Cruz FM, Sepúlveda JC, Abad JL, **Galán-Arriola C**,, Ibanez B, Martínez F, Fernández ME, Fernández-

Aviles F, Palacios I, R-Borlado L, Vázquez J, Alves PM, Bernad A. *Definition of a cell surface signature for human cardiac progenitor cells after comprehensive comparative transcriptomic and proteomic characterization*. Sci Rep. 2019 Mar 15;9(1):4647. doi: 10.1038/s41598-019-39571-x. PubMed PMID: 30874584; PubMed Central PMCID: PMC6420620.

Lee P, Quintanilla JG, Alfonso-Almazán JM, **Galán-Arriola C**,, Yan P, Sánchez-González J, Pérez-Castellano N, Pérez-Villacastín J, Ibañez B, Loew LM, Filgueiras-Rama D. *In vivo ratiometric optical mapping enables high-resolution cardiac electrophysiology in pig models*. Cardiovasc Res. 2019 Sep 1;115(11):1659-1671. doi: 10.1093/cvr/cvz039. PubMed PMID: 30753358; PubMed Central PMCID: PMC6704389.

Garcia-Lunar I, Pereda D, Santiago E, Solanes N, Nuche J, Ascaso M, Bobí J, Sierra F, Dantas AP, **Galán-Arriola C**,, San Antonio R, Sánchez-Quintana D, Sánchez-González J, Barberá JA, Rigol M, Fuster V, Ibáñez B, Sabaté M, García-Álvarez A. *Effect of pulmonary artery denervation in postcapillary pulmonary hypertension: results of a randomized controlled translational study*. Basic Res Cardiol. 2019 Jan 11;114(2):5. doi: 10.1007/s00395 018-0714-x. PubMed PMID: 30635778.

León DG, López-Yunta M, Alfonso-Almazán JM, Marina-Breysse M, Quintanilla JG, Sánchez-González J, **Galán-Arriola C**,, Castro-Núñez F, González-Ferrer JJ, Ibáñez B, Pérez-Villacastín J, Pérez-Castellano N, Fuster V, Jalife J, Vázquez M, Aguado-Sierra J, Filgueiras-Rama D. *Three-dimensional cardiac fibre disorganization as a novel parameter for ventricular arrhythmia stratification after myocardial infarction*. Europace. 2019 May 1;21(5):822-832. doi: 10.1093/europace/euy306. PubMed PMID: 30649290; PubMed Central PMCID: PMC6479517.

López-Yunta M, León DG, Alfonso-Almazán JM, Marina-Breysse M, Quintanilla JG, Sánchez-González J, **Galán-Arriola C**,, Cañadas-Godoy V, Enríquez-Vázquez D, Torres C, Ibáñez B, Pérez-Villacastín J, Pérez-Castellano N, Jalife J, Vázquez M, Aguado-Sierra J, Filgueiras-Rama D. *Implications of bipolar voltage mapping and magnetic resonance imaging resolution in biventricular scar characterization after myocardial infarction*. Europace. 2019 Jan 1;21(1):163-174. doi: 10.1093/europace/euy192. PubMed PMID: 30239689; PubMed Central PMCID: PMC6321957.

Rossello X, Piñero A, Fernández-Jiménez R, Sánchez-González J, Pizarro G, **Galán-Arriola C**,, Lobo-Gonzalez M, Vilchez JP, García-Prieto J, García-Ruiz JM, García-Álvarez A, Sanz-Rosa D, Ibanez B. *Mirabegron, a Clinically Approved B3 Adrenergic Receptor Agonist, Does Not Reduce Infarct Size in a Swine Model of Reperfused Myocardial Infarction*. J Cardiovasc Transl Res. 2018 Aug;11(4):310-318. doi: 10.1007/s12265-018-9819-8. Epub 2018 Aug 2. PubMed PMID: 30073540.

Alvino VV, Fernández-Jiménez R, Rodriguez-Arabaolaza I, Slater S, Mangialardi G, Avolio E, Spencer H, Culliford L, Hassan S, Sueiro Ballesteros L, Herman A, Ayaon-Albarrán A, **Galán-Arriola C**,, Sánchez-González J, Hennessey H, Delmege C, Ascione R, Emanueli C, Angelini GD, Ibanez B, Madeddu P. *Transplantation of Allogeneic Pericytes Improves Myocardial Vascularization and Reduces Interstitial Fibrosis in a Swine Model of Reperfused Acute Myocardial Infarction*. J Am Heart Assoc. 2018 Jan 22;7(2). pii: e006727. doi: 10.1161/JAHA.117.006727. PubMed PMID: 29358198; PubMed Central PMCID: PMC5850145.

Aguero J, **Galán-Arriola C**,, Fernandez-Jimenez R, Sanchez-Gonzalez J, Ajmone N, Delgado V, Solis J, Lopez GJ, de Molina-Iracheta A, Hajjar RJ, Bax JJ, Fuster V, Ibáñez B. *Atrial Infarction and Ischemic Mitral Regurgitation Contribute to Post-MI Remodeling of the Left Atrium*. J Am Coll Cardiol. 2017 Dec 12;70(23):2878-2889. doi: 10.1016/j.jacc.2017.10.013. PubMed PMID: 29216983.

Binek A, Fernández-Jiménez R, Jorge I, Camafeita E, López JA, Bagwan N, **Galán-Arriola C**,, Pun A, Agüero J, Fuster V, Ibanez B, Vázquez J. *Proteomic footprint of myocardial ischemia/reperfusion injury: Longitudinal study of the at-risk and remote regions in the pig model*. Sci Rep. 2017 Sep 27;7(1):12343. doi: 10.1038/s41598-017-11985-5. PubMed PMID: 28955040; PubMed Central PMCID: PMC5617837.

Fernández-Jiménez R, Barreiro-Pérez M, Martin-García A, Sánchez-González J, Agüero J, **Galán-Arriola C**,, García-Prieto J, Díaz-Pelaez E, Vara P, Martinez I, Zamarro I, Garde B, Sanz J, Fuster V, Sánchez PL, Ibanez B. *Dynamic Edematous Response of the Human Heart to Myocardial Infarction: Implications for Assessing Myocardial Area at Risk and Salvage*. Circulation. 2017 Oct 3;136(14):1288-1300. doi: 10.1161/CIRCULATIONAHA.116.025582. Epub 2017 Jul 7. PubMed PMID: 28687712; PubMed Central PMCID: PMC5625960.

Fernández-Jiménez R, **Galán-Arriola C**,, Sánchez-González J, Agüero J, López-Martín GJ, Gomez-Talavera S, Garcia-Prieto J, Benn A, Molina-Iracheta A, Barreiro-Pérez M, Martin-García A, García-Lunar I, Pizarro G, Sanz J, Sánchez PL, Fuster V, Ibanez B. *Effect of Ischemia Duration and Protective Interventions on the Temporal Dynamics of Tissue Composition After Myocardial Infarction*. Circ Res. 2017 Aug 4;121(4):439-450. doi: 10.1161/CIRCRESAHA.117.310901. Epub 2017 Jun 8. PubMed PMID: 28596216; PubMed Central PMCID: PMC5542781.

Bobi J, Solanes N, Fernández-Jiménez R, **Galán-Arriola C**,, Dantas AP, Fernández-Friera L, Gálvez-Montón C, Rigol-Monzó E, Agüero J, Ramírez J, Roqué M, Bayés-Genís A, Sánchez-González J, García-Álvarez A, Sabaté M, Roura S, Ibáñez B, Rigol M. *Intracoronary Administration of Allogeneic Adipose Tissue-Derived Mesenchymal Stem Cells Improves Myocardial Perfusion But Not Left Ventricle Function, in a Translational Model of Acute Myocardial Infarction*. J Am Heart Assoc. 2017 May 3;6(5). pii: e005771. doi: 10.1161/JAHA.117.005771.

PubMed PMID: 28468789; PubMed Central PMCID: PMC5524109.

García-Ruiz JM, **Galán-Arriola C**„ Fernández-Jiménez R, Aguero J, Sánchez-González J, García-Alvarez A, Nuno-Ayala M, Dubé GP, Zafirelis Z, López-Martín GJ, Bernal JA, Lara-Pezzi E, Fuster V, Ibáñez B. *Bloodless reperfusion with the oxygen carrier HBOC-201 in acute myocardial infarction: a novel platform for cardioprotective probes delivery*. Basic Res Cardiol. 2017 Mar;112(2):17. doi: 10.1007/s00395-017-0605-6. Epub 2017 Feb 10. PubMed PMID: 28188434.

Ayaon-Albarrán A, Fernandez-Jimenez R, Silva-Guisasola J, Agüero J, Sanchez-Gonzalez J, **Galán-Arriola C**„ Reguillo-Lacruz F, Maroto Castellanos LC, Ibanez B. *Systolic flow displacement using 3D magnetic resonance imaging in an experimental model of ascending aorta aneurysm: impact of rheological factors*. Eur J Cardiothorac Surg. 2016 Oct;50(4):685-692. Epub 2016 May 24. PubMed PMID: 27222592.

García-Ruiz JM, Fernández-Jiménez R, García-Alvarez A, Pizarro G, **Galán-Arriola C**„ Fernández-Friera L, Mateos A, Nuno-Ayala M, Aguero J, Sánchez-González J, García-Prieto J, López-Melgar B, Martínez-Tenorio P, López-Martín GJ, Macías A, Pérez-Asenjo B, Cabrera JA, Fernández-Ortiz A, Fuster V, Ibáñez B. I*mpact of the Timing of Metoprolol Administration During STEMI on Infarct Size and Ventricular Function*. J Am Coll Cardiol. 2016 May 10;67(18):2093-2104. doi: 10.1016/j.jacc.2016.02.050. Epub 2016 Apr 3. PubMed PMID: 27052688.

Fernández-Jiménez R, Sánchez-González J, Aguero J, Del Trigo M, **Galán-Arriola C**, Fuster V, Ibáñez B. *Fast T2 gradient-spin-echo (T2-GraSE) mapping for myocardial edema quantification: first in vivo validation in a porcine model of ischemia/reperfusion*. J Cardiovasc Magn Reson. 2015 Nov 4;17:92. doi: 10.1186/s12968-015-0199-9. PubMed PMID: 26538198; PubMed Central PMCID: PMC4634909.

Fernández-Jiménez R, García-Prieto J, Sánchez-González J, Agüero J, López-Martín GJ, **Galán-Arriola C**„ Molina-Iracheta A, Doohan R, Fuster V, Ibáñez B. *Pathophysiology Underlying the Bimodal Edema Phenomenon After Myocardial Ischemia/Reperfusion*. J Am Coll Cardiol. 2015 Aug 18;66(7):816-828. doi: 10.1016/j.jacc.2015.06.023. PubMed PMID: 26271065.

11 Supplementary material

	Group 1 (5 doses – 16 weeks)				Group 2 (3 doses – 16 weeks)				Group 3 (3 doses – 6 weeks)			
Week	LVEF (%)	T2 (ms)	T1 (ms)	ECV (%)	LVEF (%)	T2 (ms)	T1 (ms)	ECV (%)	LVEF (%)	T2 (ms)	T1 (ms)	ECV (%)
0	55.35±3.84	45.22±0.47	1087±101.1	26.03±4.3	56.56±3.53	45.58±0.6	1029±41.2	26.08±3.33	56.2±2.8	45.76±2.52	1075±47.5	29.09±1.78
1	54.05±0.56	45.37±0.25	1062±21.9	30.65±1.3	54.9±5.23	45.84±1.31	1040±37	28.91±0.51	55.68±2.41	46.86±2.3	1037±22.4	30.48±1.22
2	57.65±2.85	45.22±1.01	1048±30.2	26.2±3.44	55.41±5.15	46.1±0.6	1034±33.5	27.69±1.94	55.73±3.82	44.76±2.12	1003±23.4	30.25±3.91
3	58.23±2.5	46.97±1.47	1020±29.7	27.89±2.28	56.46±5.65	44.7±1.88	1040±35.8	28.23±1.76	55.19±4.87	46.14±3.87	1015±37	28.45±2.19
4	56.61±2.94	47.22±2.97	1032±40.7	28.04±1.46	57.48±3.3	46.04±2.39	1043±28.3	28.6±0.99	54.23±2.35	44.96±2.65	1017±64.3	28.7±2.17
5	55.47±3.74	47.83±3.33	1071±39.6	28.72±0.98	59.26±3.45	45.58±1.7	1036±63.3	26.31±1.96	53.06±2.17	48.56±4.35	1019±26.7	29.4±1.92
6	55.2±4.41	52.02±1.4	1067±25.9	28.12±1.34	57.94±4.53	51.6±0.82	1023±68.6	26.35±3.39	53.27±1.96	52.6±2.18	1010±27.3	26.62±1.46
7	57.1±3.33	54±1.87	1020±61	28.56±2.84	58.43±3.12	45.52±1.26	979±55.6	27.15±2.08				
8	52.46±5.98	55.58±4.24	1085±99.75	30.4±4.8	57.79±3.61	44.38±2.94	1045±36.3	28.49±1.05				
9	48.97±2.76	58.17±5.36	1085±96	30.25±1.18	59.51±2.86	44.1±2.28	1016±20.6	26.73±1.21				
10	42.7±6.36	58.24±4.13	1088±34.2	37.05±7.45	60.04±3.17	45.1±1.79	1032±51.6	28.26±1.68				
11	41.14±3.47	61.77±4.06	1149±84.9	37.49±4.43	60.08±2.47	45.22±0.89	1031±25.9	26.59±3.2				
12	32.93±5.83	66.94±4.16	1220±58.6	41±5.35	58.86±3.14	43.14±2.93	1000±52	24.86±3.2				
13	34.79±0.96	68.26±3.81	1169±6.4	41.25±4.84	58.3±2.57	44.46±1.59	992±51.9	27.17±2				
14	30.34±7.55	70.78±5.79	1315±53.3	41.34±1.34	57.27±2.17	44.66±0.68	1112±89.7	25.19±3.1				
15	34.62±2.07	73.17±4.5	1293±109	40.62±1.07	59.19±3.23	45.34±1.3	1082±45.1	25.94±0.99				
16	30.38±7.71	72.96±4.6	1329±81.3	45.22±5.04	57.05±4.05	44.78±1.43	1088±60.7	25.95±1.73				

Table 2: Summary data for Objective 1.

	Baseline					10 minutes	48 hours	2 weeks			
	Acute 48h (n=5)	Acute 2w (n=5)	Early (n=5)	Cardiotoxic (n=5)	Recovery (n=5)	Acute 48h (n=5)	Acute 48h (n=5)	Acute 2w (n=5)	Early (n=5)	Cardiotoxic (n=5)	Recovery (n=5)
LVEF											
Mean (SD)	NA (NA)	58.8 (5.63)	56.2 (2.80)	52.5 (1.50)	53.7 (4.21)	NA (NA)	NA (NA)	60.8 (7.69)	55.7 (3.82)	57.6 (2.85)	55.4 (5.15)
Median [Min, Max]	NA [NA, NA]	60.0 [52.0, 65.0]	56.2 [52.4, 59.5]	51.8 [51.3, 55.0]	51.0 [50.7, 60.3]	NA [NA, NA]	NA [NA, NA]	63.0 [51.0, 70.0]	54.8 [52.3, 62.0]	57.2 [53.8, 61.5]	56.0 [50.7, 63.2]
Missing	5 (100%)	0 (0%)	0 (0%)	0 (0%)	0 (0%)	5 (100%)	5 (100%)	0 (0%)	0 (0%)	0 (0%)	0 (0%)
Quantitative Perfusion (ml/100g/min)											
Mean (SD)	NA (NA)	172 (47.1)	NA (NA)	199 (49.2)	198 (37.1)	NA (NA)	180 (29.3)	NA (NA)	NA (NA)	161 (51.5)	205 (39.6)
Median [Min, Max]	NA [NA, NA]	183 [108, 233]	NA [NA, NA]	208 [135, 247]	198 [155, 252]	NA [NA, NA]	175 [148, 224]	NA [NA, NA]	NA [NA, NA]	170 [104, 236]	194 [155, 249]
Missing	5 (100%)	0 (0%)	5 (100%)	1 (20.0%)	0 (0%)	5 (100%)	0 (0%)	5 (100%)	5 (100%)	0 (0%)	0 (0%)
CFR											
Mean (SD)	3.78 (0.466)	3.83 (0.428)	3.36 (0.913)	3.71 (0.939)	3.69 (1.57)	4.06 (0.640)	3.63 (0.451)	3.07 (0.457)	2.49 (0.361)	3.58 (0.987)	3.56 (0.961)
Median [Min, Max]	4.00 [3.26, 4.23]	3.80 [3.17, 4.30]	3.07 [2.71, 4.94]	3.50 [2.50, 5.00]	3.38 [2.28, 6.25]	3.88 [3.39, 5.00]	3.72 [3.00, 4.21]	3.18 [2.50, 3.68]	2.44 [2.00, 3.00]	3.31 [2.41, 5.00]	3.21 [2.38, 4.63]
Missing	0 (0%)	0 (0%)	0 (0%)	0 (0%)	0 (0%)	0 (0%)	0 (0%)	0 (0%)	0 (0%)	0 (0%)	0 (0%)

	4 weeks			6 weeks			16 weeks	
	Early (n=5)	Cardiotoxic (n=5)	Recovery (n=5)	Early (n=5)	Cardiotoxic (n=5)	Recovery (n=5)	Cardiotoxic (n=5)	Recovery (n=5)
LVEF								
Mean (SD)	54.2 (2.35)	56.6 (2.94)	57.5 (3.30)	53.3 (1.96)	55.2 (4.41)	57.9 (4.53)	30.4 (7.70)	57.1 (4.05)
Median [Min, Max]	53.5 [51.2, 57.3]	55.3 [53.9, 60.3]	58.6 [51.7, 60.0]	54.1 [49.8, 54.4]	57.4 [48.4, 59.1]	56.9 [52.9, 63.2]	31.0 [19.2, 38.4]	56.1 [52.5, 63.6]
Missing	0 (0%)	0 (0%)	0 (0%)	0 (0%)	0 (0%)	0 (0%)	0 (0%)	0 (0%)
Quantitative Perfusion (ml/100g/min)								
Mean (SD)	NA (NA)	165 (40.9)	185 (36.1)	NA (NA)	135 (4.90)	146 (31.5)	65.4 (18.2)	138 (11.9)
Median [Min, Max]	NA [NA, NA]	167 [117, 210]	188 [134, 233]	NA [NA, NA]	133 [131, 141]	159 [107, 179]	62.4 [46.8, 95.4]	144 [124, 152]
Missing	5 (100%)	1 (20.0%)	0 (0%)	5 (100%)	1 (20.0%)	0 (0%)	0 (0%)	0 (0%)
CFR								
Mean (SD)	2.87 (1.04)	2.51 (0.951)	2.36 (0.962)	NA (NA)	2.10 (0.198)	2.52 (0.888)	1.41 (0.230)	3.13 (0.821)
Median [Min, Max]	2.42 [2.22, 4.42]	2.00 [1.71, 4.00]	2.73 [1.23, 3.57]	NA [NA, NA]	2.17 [1.76, 2.27]	2.41 [1.68, 3.78]	1.40 [1.11, 1.65]	2.92 [2.00, 4.00]
Missing	1 (20.0%)	0 (0%)	0 (0%)	5 (100%)	0 (0%)	0 (0%)	0 (0%)	0 (0%)

Table 3: Summary data for Objective 2 - Infused Area.

	Baseline					10 minutes	48 hours	2 weeks			
	Acute 48h (n=5)	Acute 2w (n=5)	Early (n=5)	Cardiotoxic (n=5)	Recovery (n=5)	Acute 48h (n=5)	Acute 48h (n=5)	Acute 2w (n=5)	Early (n=5)	Cardiotoxic (n=5)	Recovery (n=5)
LVEF											
Mean (SD)	NA (NA)	58.8 (5.63)	56.2 (2.80)	52.5 (1.50)	53.7 (4.21)	NA (NA)	NA (NA)	60.8 (7.69)	55.7 (3.82)	57.6 (2.85)	55.4 (5.15)
Median [Min, Max]	NA [NA, NA]	60.0 [52.0, 65.0]	56.2 [52.4, 59.5]	51.8 [51.3, 55.0]	51.0 [50.7, 60.3]	NA [NA, NA]	NA [NA, NA]	63.0 [51.0, 70.0]	54.8 [52.3, 62.0]	57.2 [53.8, 61.5]	56.0 [50.7, 63.2]
Missing	5 (100%)	0 (0%)	0 (0%)	0 (0%)	0 (0%)	5 (100%)	5 (100%)	0 (0%)	0 (0%)	0 (0%)	0 (0%)
Quantitative Perfusion											
Mean (SD)	NA (NA)	163 (36.4)	NA (NA)	209 (55.3)	195 (51.5)	NA (NA)	159 (27.2)	NA (NA)	NA (NA)	165 (42.4)	219 (28.8)
Median [Min, Max]	NA [NA, NA]	169 [108, 205]	NA [NA, NA]	224 [134, 253]	183 [131, 258]	NA [NA, NA]	165 [118, 184]	NA [NA, NA]	NA [NA, NA]	160 [114, 221]	223 [172, 251]
Missing	5 (100%)	0 (0%)	5 (100%)	1 (20.0%)	0 (0%)	5 (100%)	0 (0%)	5 (100%)	5 (100%)	0 (0%)	0 (0%)
CFR											
Mean (SD)	NA (NA)	3.13 (0.700)	3.25 (1.14)	3.08 (0.783)	3.41 (1.63)	NA (NA)	NA (NA)	3.32 (0.649)	2.42 (0.691)	2.47 (0.590)	3.56 (1.20)
Median [Min, Max]	NA [NA, NA]	3.60 [2.07, 3.64]	3.00 [2.12, 4.58]	3.08 [2.09, 4.20]	2.93 [2.00, 6.00]	NA [NA, NA]	NA [NA, NA]	3.16 [2.73, 4.28]	2.53 [1.37, 3.24]	2.69 [1.78, 3.17]	3.53 [1.88, 5.14]
Missing	5 (100%)	0 (0%)	0 (0%)	0 (0%)	0 (0%)	5 (100%)	5 (100%)	0 (0%)	0 (0%)	0 (0%)	0 (0%)

	4 weeks			6 weeks			16 weeks	
	Early (n=5)	Cardiotoxic (n=5)	Recovery (n=5)	Early (n=5)	Cardiotoxic (n=5)	Recovery (n=5)	Cardiotoxic (n=5)	Recovery (n=5)
LVEF								
Mean (SD)	54.2 (2.35)	56.6 (2.94)	57.5 (3.30)	53.3 (1.96)	55.2 (4.41)	57.9 (4.53)	30.4 (7.70)	57.1 (4.05)
Median [Min, Max]	53.5 [51.2, 57.3]	55.3 [53.9, 60.3]	58.6 [51.7, 60.0]	54.1 [49.8, 54.4]	57.4 [48.4, 59.1]	56.9 [52.9, 63.2]	31.0 [19.2, 38.4]	56.1 [52.5, 63.6]
Missing	0 (0%)	0 (0%)	0 (0%)	0 (0%)	0 (0%)	0 (0%)	0 (0%)	0 (0%)
Quantitative Perfusion								
Mean (SD)	NA (NA)	189 (43.4)	194 (34.0)	NA (NA)	152 (16.0)	158 (19.1)	114 (9.95)	122 (13.4)
Median [Min, Max]	NA [NA, NA]	188 [144, 236]	205 [141, 228]	NA [NA, NA]	154 [132, 166]	151 [140, 186]	116 [104, 128]	120 [111, 145]
Missing	5 (100%)	1 (20.0%)	0 (0%)	5 (100%)	1 (20.0%)	0 (0%)	0 (0%)	0 (0%)
CFR								
Mean (SD)	2.31 (0.784)	2.68 (0.811)	2.94 (0.761)	NA (NA)	2.62 (0.584)	2.93 (0.702)	2.66 (0.605)	NA (NA)
Median [Min, Max]	2.03 [1.71, 3.46]	2.41 [1.83, 3.94]	2.71 [2.42, 4.29]	NA [NA, NA]	2.42 [1.94, 3.50]	2.72 [2.18, 4.07]	2.66 [2.23, 3.08]	NA [NA, NA]
Missing	1 (20.0%)	0 (0%)	0 (0%)	5 (100%)	0 (0%)	0 (0%)	3 (60.0%)	5 (100%)

Table 4: Summary data for Objective 2 - Remote Area.

	-4		-3		0				1			
	Banding CONTROL (n=7)	Banding + DOXO (n=7)	Banding CONTROL (n=7)	Banding + DOXO (n=7)	No banding CONTROL (n=7)	No Banding + DOXO (n=7)	Banding CONTROL (n=7)	Banding + DOXO (n=7)	No banding CONTROL (n=7)	No Banding + DOXO (n=7)	Banding CONTROL (n=7)	Banding + DOXO (n=7)
LVEF (%)												
Mean (SD)	60.9 (3.87)	60.5 (5.68)	69.0 (6.13)	70.2 (9.46)	58.6 (2.68)	57.6 (4.71)	76.6 (6.64)	77.3 (8.65)	62.3 (5.47)	60.0 (2.61)	78.5 (7.87)	68.7 (12.9)
Median [Min, Max]	61.6 [55.6, 65.2]	62.2 [48.3, 64.4]	69.4 [61.4, 76.4]	69.3 [58.3, 83.8]	58.2 [54.9, 62.7]	57.5 [51.3, 64.1]	76.5 [68.5, 86.3]	78.2 [66.7, 89.9]	63.0 [54.4, 69.3]	60.0 [55.2, 63.8]	76.9 [69.9, 87.2]	65.7 [54.4, 84.3]
LV mass (mg indexed)												
Mean (SD)	54.6 (6.96)	62.3 (9.93)	71.8 (9.81)	74.3 (11.9)	59.7 (12.3)	58.0 (5.90)	82.0 (16.8)	79.3 (29.5)	60.5 (7.97)	59.9 (9.67)	81.2 (16.4)	85.4 (27.7)
Median [Min, Max]	54.4 [44.1, 67.0]	59.2 [51.6, 81.3]	70.1 [61.2, 91.8]	73.4 [60.5, 96.7]	56.5 [46.8, 85.8]	56.2 [53.2, 70.6]	81.3 [55.1, 108]	73.0 [53.1, 133]	61.1 [49.0, 74.5]	59.5 [47.7, 76.4]	81.8 [55.2, 104]	87.7 [56.7, 137]
LVEDV (ml indexed)												
Mean (SD)	71.7 (9.13)	73.0 (9.98)	74.1 (10.7)	68.6 (2.90)	70.1 (5.91)	69.0 (13.2)	71.0 (9.42)	68.3 (4.93)	65.1 (11.6)	66.7 (14.4)	71.7 (13.1)	67.8 (9.26)
Median [Min, Max]	74.2 [56.6, 83.9]	76.7 [61.2, 88.2]	74.0 [60.6, 89.9]	67.8 [65.0, 72.1]	72.1 [60.5, 78.9]	65.1 [56.6, 90.1]	68.0 [59.6, 85.2]	66.8 [63.1, 75.5]	65.9 [43.5, 79.4]	65.4 [50.0, 88.1]	67.4 [51.2, 87.9]	71.4 [49.7, 78.0]
LVESV (ml indexed)												
Mean (SD)	28.3 (5.64)	28.5 (3.27)	23.1 (6.03)	20.5 (7.04)	29.1 (3.93)	29.6 (8.62)	16.9 (6.31)	15.6 (6.29)	24.5 (6.17)	26.5 (5.15)	16.2 (8.21)	20.5 (7.34)
Median [Min, Max]	28.6 [20.1, 36.9]	27.9 [24.4, 32.2]	21.6 [15.6, 32.2]	20.1 [10.9, 30.1]	29.2 [22.5, 35.6]	27.9 [21.0, 43.9]	15.0 [9.34, 26.1]	14.3 [6.55, 23.2]	22.4 [17.7, 36.2]	26.7 [20.0, 35.4]	15.0 [6.60, 26.4]	21.9 [12.2, 29.3]
T2-GraSE (ms)												
Mean (SD)	44.1 (2.49)	41.8 (3.06)	44.2 (2.88)	45.0 (4.52)	41.7 (1.96)	41.9 (3.03)	42.3 (1.91)	42.2 (4.05)	42.1 (1.76)	41.8 (2.56)	42.0 (2.11)	43.8 (4.87)
Median [Min, Max]	44.0 [41.3, 48.6]	42.6 [36.1, 45.1]	43.5 [39.2, 47.6]	43.6 [38.6, 49.8]	41.8 [39.5, 45.2]	40.5 [38.8, 46.3]	42.0 [40.4, 46.1]	40.3 [38.4, 50.0]	42.1 [40.3, 45.0]	42.7 [37.9, 44.7]	41.5 [39.2, 45.9]	41.8 [38.0, 50.3]
Extracellular Volume (%)												
Mean (SD)	28.4 (3.81)	26.3 (4.29)	28.8 (2.17)	26.2 (2.46)	26.3 (2.86)	25.5 (2.81)	28.2 (4.12)	23.8 (4.34)	22.1 (6.15)	24.9 (3.60)	29.4 (2.91)	23.0 (3.39)
Median [Min, Max]	28.3 [22.7, 33.7]	25.2 [21.1, 33.5]	28.6 [25.1, 32.3]	26.6 [22.2, 29.9]	25.9 [23.2, 30.8]	23.8 [22.2, 29.5]	28.9 [23.1, 33.2]	24.8 [14.4, 26.7]	23.9 [9.21, 28.1]	25.8 [19.0, 30.3]	29.4 [26.3, 33.5]	22.8 [17.0, 27.5]
Missing	0 (0%)	0 (0%)	0 (0%)	0 (0%)	0 (0%)	0 (0%)	0 (0%)	0 (0%)	0 (0%)	0 (0%)	0 (0%)	0 (0%)
T1 native (ms)												
Mean (SD)	1060 (31.5)	1080 (43.1)	1050 (62.6)	1060 (45.0)	1110 (95.7)	1080 (50.1)	1010 (39.9)	1070 (90.2)	1040 (56.3)	1060 (53.5)	982 (52.1)	1050 (41.6)
Median [Min, Max]	1050 [1010, 1120]	1080 [1020, 1160]	1060 [956, 1150]	1050 [1010, 1140]	1060 [1030, 1290]	1080 [1000, 1140]	1020 [947, 1060]	1090 [924, 1210]	1060 [925, 1100]	1040 [1010, 1160]	1000 [900, 1040]	1040 [998, 1130]
T1 post-contrast (ms)												
Mean (SD)	609 (72.3)	636 (70.3)	608 (44.7)	620 (50.3)	694 (124)	624 (66.0)	614 (48.0)	592 (52.3)	608 (89.5)	580 (40.0)	577 (47.1)	540 (73.7)
Median [Min, Max]	592 [525, 728]	629 [543, 737]	604 [533, 672]	598 [573, 693]	632 [563, 834]	616 [538, 722]	626 [549, 692]	607 [518, 647]	597 [506, 792]	576 [528, 626]	574 [498, 648]	552 [423, 659]
Missing	0 (0%)	0 (0%)	0 (0%)	0 (0%)	0 (0%)	0 (0%)	0 (0%)	0 (0%)	0 (0%)	0 (0%)	0 (0%)	0 (0%)

	2				3				4			
	No banding CONTROL (n=7)	No Banding + DOXO (n=7)	Banding CONTROL (n=7)	Banding + DOXO (n=7)	No banding CONTROL (n=7)	No Banding + DOXO (n=7)	Banding CONTROL (n=7)	Banding + DOXO (n=7)	No banding CONTROL (n=7)	No Banding + DOXO (n=7)	Banding CONTROL (n=7)	Banding + DOXO (n=7)
LVEF (%)												
Mean (SD)	63.0 (4.08)	61.5 (2.80)	78.1 (8.01)	57.5 (11.1)	61.9 (3.83)	62.7 (3.05)	80.0 (9.43)	50.7 (13.2)	64.2 (3.53)	62.4 (3.61)	84.0 (4.83)	46.9 (8.67)
Median [Min, Max]	63.2 [57.5, 68.0]	61.8 [57.8, 64.6]	76.4 [67.9, 89.0]	55.3 [43.5, 74.1]	60.7 [56.0, 66.2]	62.9 [56.9, 66.4]	84.0 [68.1, 89.7]	52.7 [34.5, 73.9]	63.8 [59.6, 71.4]	62.2 [58.5, 68.2]	82.3 [77.5, 91.0]	50.9 [29.5, 54.9]
LV mass (mg indexed)												
Mean (SD)	60.0 (13.8)	64.3 (4.66)	87.1 (17.5)	98.7 (35.4)	61.7 (9.14)	66.7 (6.44)	96.2 (20.1)	92.3 (26.5)	62.0 (12.0)	69.3 (6.89)	102 (27.3)	101 (37.2)
Median [Min, Max]	56.0 [50.7, 89.8]	66.8 [56.7, 69.2]	79.1 [71.4, 116]	114 [52.6, 145]	60.1 [51.7, 78.3]	65.3 [59.4, 74.3]	89.6 [75.3, 132]	90.1 [59.4, 121]	57.8 [49.2, 84.9]	66.2 [62.6, 81.7]	90.5 [72.6, 151]	108 [61.8, 162]
LVEDV (ml indexed)												
Mean (SD)	67.9 (10.9)	67.1 (8.33)	67.7 (13.8)	73.3 (10.8)	72.3 (12.6)	75.6 (15.2)	66.8 (13.6)	79.3 (17.7)	68.7 (14.4)	76.5 (11.9)	69.4 (12.3)	84.8 (19.5)
Median [Min, Max]	69.6 [50.6, 84.8]	68.8 [52.4, 75.0]	63.8 [49.5, 82.3]	72.3 [59.6, 91.7]	72.7 [50.0, 88.3]	80.5 [54.4, 94.3]	69.2 [44.7, 82.3]	80.3 [59.5, 102]	73.9 [38.4, 82.8]	79.6 [52.1, 88.0]	73.9 [42.2, 78.2]	75.3 [59.1, 108]
LVESV (ml indexed)												
Mean (SD)	25.4 (6.41)	25.9 (4.06)	15.6 (8.14)	30.8 (7.78)	27.7 (6.55)	28.3 (6.71)	14.2 (8.86)	38.9 (14.2)	24.5 (5.19)	29.0 (6.57)	11.5 (4.61)	46.2 (17.5)
Median [Min, Max]	24.2 [18.6, 36.0]	25.8 [18.7, 31.2]	14.6 [6.59, 25.9]	33.7 [18.7, 39.5]	28.7 [16.9, 38.9]	30.0 [18.8, 36.6]	10.1 [5.51, 26.3]	34.8 [24.0, 62.3]	26.1 [14.3, 29.6]	32.0 [16.6, 36.5]	13.3 [3.82, 17.0]	36.2 [28.9, 75.9]
T2-GraSE (ms)												
Mean (SD)	42.3 (1.71)	44.0 (2.84)	41.4 (3.25)	46.8 (4.31)	40.5 (2.41)	43.0 (2.77)	42.1 (2.20)	47.4 (5.44)	40.8 (1.15)	43.0 (3.52)	41.8 (2.72)	46.2 (3.45)
Median [Min, Max]	42.2 [40.1, 45.5]	43.2 [40.3, 48.4]	41.8 [36.1, 46.8]	49.2 [40.8, 51.4]	39.9 [38.3, 44.9]	42.4 [39.0, 46.5]	41.8 [39.8, 46.8]	46.8 [40.9, 56.8]	40.9 [39.3, 42.7]	41.9 [38.1, 47.3]	42.0 [36.9, 45.7]	46.3 [39.8, 50.7]
Extracellular Volume (%)												
Mean (SD)	23.8 (2.23)	25.4 (3.64)	27.5 (5.80)	22.4 (2.47)	25.3 (3.36)	24.3 (3.91)	25.3 (3.80)	22.3 (2.71)	25.6 (3.51)	23.0 (2.17)	28.3 (9.03)	24.3 (2.97)
Median [Min, Max]	24.1 [20.8, 26.9]	25.7 [19.6, 31.6]	25.2 [23.0, 39.9]	22.0 [18.7, 26.3]	23.1 [22.5, 31.2]	23.6 [18.1, 28.5]	25.1 [21.2, 29.9]	21.0 [20.3, 27.8]	25.1 [21.4, 31.2]	23.7 [18.9, 25.8]	27.8 [14.6, 42.1]	24.4 [19.5, 28.1]
Missing	0 (0%)	0 (0%)	0 (0%)	0 (0%)	0 (0%)	0 (0%)	3 (42.9%)	0 (0%)	0 (0%)	0 (0%)	0 (0%)	0 (0%)
T1 native (ms)												
Mean (SD)	1070 (30.7)	1060 (75.7)	979 (33.4)	1030 (47.4)	1050 (49.4)	1060 (62.0)	942 (59.9)	1080 (113)	1020 (71.2)	1040 (46.5)	936 (90.0)	1030 (48.9)
Median [Min, Max]	1070 [1040, 1130]	1030 [967, 1140]	984 [908, 1010]	1020 [978, 1090]	1060 [961, 1110]	1060 [989, 1180]	950 [862, 1030]	1060 [927, 1280]	999 [938, 1150]	1040 [995, 1140]	993 [774, 1010]	1020 [973, 1120]
T1 post-contrast (ms)												
Mean (SD)	590 (42.0)	627 (66.5)	566 (53.0)	569 (77.3)	547 (52.4)	634 (35.9)	546 (56.7)	591 (83.2)	537 (29.4)	602 (24.8)	540 (35.9)	540 (58.9)
Median [Min, Max]	594 [544, 663]	602 [568, 740]	568 [462, 625]	554 [451, 688]	535 [459, 616]	626 [580, 678]	566 [462, 589]	564 [512, 769]	544 [482, 566]	608 [550, 629]	529 [494, 602]	521 [466, 634]
Missing	0 (0%)	0 (0%)	0 (0%)	0 (0%)	0 (0%)	0 (0%)	3 (42.9%)	0 (0%)	0 (0%)	0 (0%)	0 (0%)	0 (0%)

Table 5: Summary data for Objective 3.

	0			6			8		
	RIPC (n=10)	No RIPC (n=10)	Control (n=10)	RIPC (n=10)	No RIPC (n=10)	Control (n=10)	RIPC (n=10)	No RIPC (n=10)	Control (n=10)
LVEF (%)									
Mean (SD)	55.5 (4.91)	55.6 (5.64)	56.9 (4.30)	58.5 (5.24)	55.7 (3.93)	64.1 (6.24)	55.5 (3.91)	51.3 (6.41)	61.8 (4.61)
Median [Min, Max]	56.8 [48.3, 63.5]	57.6 [45.8, 62.4]	56.1 [50.9, 64.0]	57.8 [50.3, 69.4]	56.8 [48.8, 60.5]	65.1 [52.7, 74.3]	54.9 [50.1, 63.7]	51.8 [39.0, 59.1]	62.6 [55.0, 72.0]
LV mass (mg indexed)									
Mean (SD)	55.0 (13.3)	51.5 (5.06)	74.4 (9.28)	62.1 (11.8)	59.3 (7.59)	51.3 (5.43)	63.2 (6.26)	64.5 (9.18)	54.7 (4.55)
Median [Min, Max]	51.9 [39.1, 87.6]	52.7 [43.4, 59.3]	71.8 [64.1, 97.4]	58.7 [49.9, 86.1]	60.4 [46.8, 69.9]	50.2 [43.0, 60.2]	62.8 [53.3, 75.6]	63.9 [49.9, 78.7]	54.1 [49.2, 64.0]
LVEDV (ml indexed)									
Mean (SD)	93.2 (10.9)	94.8 (9.47)	92.7 (10.3)	105 (15.0)	97.6 (10.5)	92.3 (10.2)	108 (13.4)	110 (21.5)	98.9 (9.82)
Median [Min, Max]	96.1 [73.0, 109]	96.2 [76.5, 106]	91.3 [79.7, 111]	106 [86.8, 131]	98.2 [76.9, 115]	88.0 [83.9, 113]	105 [90.9, 127]	103 [92.5, 152]	100 [83.2, 112]
LVESV (ml indexed)									
Mean (SD)	41.6 (7.76)	42.2 (7.16)	40.2 (7.40)	43.5 (8.22)	43.3 (6.98)	33.6 (9.32)	48.2 (8.09)	54.9 (18.3)	37.8 (6.17)
Median [Min, Max]	41.2 [26.7, 50.6]	41.0 [31.6, 52.5]	40.1 [30.8, 54.6]	43.9 [26.6, 52.4]	42.0 [31.7, 58.6]	31.0 [22.3, 53.4]	45.8 [36.2, 62.5]	48.7 [40.0, 92.8]	37.9 [28.6, 48.1]
T2-GraSE (ms)									
Mean (SD)	43.3 (1.79)	43.2 (2.43)	43.6 (1.72)	52.2 (5.19)	50.5 (2.60)	44.6 (1.84)	52.9 (4.41)	55.2 (3.16)	43.8 (2.60)
Median [Min, Max]	43.0 [41.6, 46.6]	43.5 [39.2, 48.1]	43.6 [39.8, 45.7]	51.8 [46.4, 65.2]	50.3 [47.6, 56.6]	43.6 [43.1, 48.6]	52.7 [48.0, 61.5]	55.1 [50.5, 61.4]	43.5 [40.9, 49.5]
T1 native (ms)									
Mean (SD)	1150 (57.9)	1110 (63.1)	1160 (66.7)	1160 (71.0)	1120 (67.8)	1220 (59.3)	1220 (89.8)	1210 (98.2)	1150 (35.6)
Median [Min, Max]	1150 [1070, 1220]	1120 [1000, 1170]	1130 [1100, 1300]	1180 [1030, 1240]	1120 [1000, 1260]	1230 [1120, 1310]	1210 [1090, 1380]	1220 [996, 1320]	1140 [1120, 1230]
T1 post-contrast (ms)									
Mean (SD)	809 (63.7)	838 (65.6)	807 (62.8)	790 (43.1)	778 (30.4)	817 (214)	742 (73.5)	775 (61.8)	776 (34.0)
Median [Min, Max]	826 [703, 886]	827 [772, 1010]	801 [684, 905]	791 [733, 850]	774 [722, 832]	756 [680, 1420]	747 [562, 841]	766 [656, 865]	776 [726, 819]
Extracellular Volume (%)									
Mean (SD)	27.5 (2.14)	24.8 (4.58)	27.5 (4.64)	27.8 (2.99)	24.6 (3.64)	30.3 (13.3)	29.1 (8.18)	29.4 (5.37)	27.3 (2.59)
Median [Min, Max]	27.4 [24.0, 31.3]	23.6 [18.7, 31.3]	27.0 [18.4, 35.1]	27.5 [23.5, 34.1]	24.5 [19.0, 31.7]	34.6 [-6.86, 37.8]	30.2 [7.63, 38.7]	28.8 [18.8, 36.7]	26.7 [24.2, 33.1]

	8			12			16	
	RIPC (n=10)	No RIPC (n=10)	Control (n=10)	RIPC (n=10)	No RIPC (n=10)	Control (n=10)	RIPC (n=10)	No RIPC (n=10)
LVEF (%)								
Mean (SD)	55.5 (3.91)	51.3 (6.41)	61.8 (4.61)	43.2 (8.12)	33.4 (9.10)	65.5 (3.10)	41.5 (9.09)	32.5 (8.70)
Median [Min, Max]	54.9 [50.1, 63.7]	51.8 [39.0, 59.1]	62.6 [55.0, 72.0]	44.4 [25.7, 57.4]	36.3 [16.7, 43.0]	65.7 [60.8, 70.7]	44.7 [26.5, 50.1]	33.2 [19.5, 46.9]
LV mass (mg indexed)								
Mean (SD)	63.2 (6.26)	64.5 (9.18)	54.7 (4.55)	77.2 (12.1)	77.2 (8.79)	58.9 (5.41)	82.9 (12.4)	85.4 (14.3)
Median [Min, Max]	62.8 [53.3, 75.6]	63.9 [49.9, 78.7]	54.1 [49.2, 64.0]	76.6 [63.2, 99.0]	74.3 [66.3, 93.2]	59.0 [48.4, 66.0]	86.4 [63.6, 102]	80.8 [67.7, 112]
LVEDV (ml indexed)								
Mean (SD)	108 (13.4)	110 (21.5)	98.9 (9.82)	139 (28.2)	145 (45.9)	101 (10.6)	156 (38.4)	168 (69.7)
Median [Min, Max]	105 [90.9, 127]	103 [92.5, 152]	100 [83.2, 112]	138 [107, 198]	132 [107, 250]	103 [83.4, 117]	152 [110, 227]	155 [97.6, 329]
LVESV (ml indexed)								
Mean (SD)	48.2 (8.09)	54.9 (18.3)	37.8 (6.17)	80.6 (27.7)	100 (48.0)	35.0 (6.40)	93.1 (35.2)	118 (64.3)
Median [Min, Max]	45.8 [36.2, 62.5]	48.7 [40.0, 92.8]	37.9 [28.6, 48.1]	78.7 [50.3, 147]	84.5 [63.4, 207]	33.7 [26.8, 45.9]	82.9 [57.4, 167]	104 [51.8, 264]
T2-GraSE (ms)								
Mean (SD)	52.9 (4.41)	55.2 (3.16)	43.8 (2.60)	62.8 (9.32)	64.3 (8.70)	42.0 (1.71)	61.9 (13.8)	69.0 (11.1)
Median [Min, Max]	52.7 [48.0, 61.5]	55.1 [50.5, 61.4]	43.5 [40.9, 49.5]	61.1 [49.2, 78.6]	65.4 [50.0, 79.0]	41.7 [39.9, 45.6]	57.0 [46.2, 87.3]	70.8 [50.0, 85.3]
T1 native (ms)								
Mean (SD)	1220 (89.8)	1210 (98.2)	1150 (35.6)	1360 (112)	1350 (108)	1120 (38.6)	1300 (109)	1410 (180)
Median [Min, Max]	1210 [1090, 1380]	1220 [996, 1320]	1140 [1120, 1230]	1340 [1180, 1530]	1370 [1120, 1510]	1110 [1080, 1220]	1310 [1030, 1420]	1410 [1160, 1770]
T1 post-contrast (ms)								
Mean (SD)	742 (73.5)	775 (61.8)	776 (34.0)	725 (116)	665 (109)	759 (38.8)	687 (42.2)	647 (114)
Median [Min, Max]	747 [562, 841]	766 [656, 865]	776 [726, 819]	705 [591, 1020]	655 [403, 784]	766 [689, 805]	685 [608, 762]	644 [470, 865]
Extracellular Volume (%)								
Mean (SD)	29.1 (8.18)	29.4 (5.37)	27.3 (2.59)	45.1 (9.69)	41.0 (7.06)	26.3 (5.71)	39.3 (6.92)	43.2 (10.9)
Median [Min, Max]	30.2 [7.63, 38.7]	28.8 [18.8, 36.7]	26.7 [24.2, 33.1]	43.7 [33.3, 65.4]	42.5 [27.1, 51.7]	25.6 [17.2, 39.6]	37.6 [29.6, 48.6]	43.7 [26.7, 61.9]

Table 6: Summary data for Objective 4.